UFL/COEL-90/008

SOME FIELD OBSERVATIONS ON BOTTOM MUD MOTION DUE TO WAVES

by

Ashish J. Mehta
Feng Jiang

Sponsors:

South Florida Water Management District (SFWMD)
West Palm Beach, Florida

U.S. Army Engineer
Waterways Experiment Station (WES)
Vicksburg, Mississippi

October, 1990

REPORT DOCUMENTATION PAGE

1. Report No.	2.	3. Recipient's Accession No.
UFL/COEL-90/008		

4. Title and Subtitle	5. Report Date
SOME FIELD OBSERVATIONS ON BOTTOM MUD MOTION DUE TO WAVES	October, 1990
	6.

7. Author(s)	8. Performing Organization Report No.
Ashish J. Mehta Feng Jiang	UFL/COEL-90/008

9. Performing Organization Name and Address	10. Project/Task/Work Unit No.
Coastal and Oceanographic Engineering Department University of Florida 336 Weil Hall Gainesville, FL 32611	Task 4.4b*
	11. Contract or Grant No. DACW39-89-M-4639**
12. Sponsoring Organization Name and Address	13. Type of Report
South Florida Water Management District (SFWMD) West Palm Beach, Florida U.S. Army Engineer Waterways Experiment Station (WES) Vicksburg, Mississippi	Final
	14.

15. Supplementary Notes

*Lake Okeechobee Phosphorus Dynamics Study (SFWMD)
**Monitoring Fluid Mud Generation (WES)

16. Abstract (Synopsis)

The behavior of soft mud under progressive, non-breaking wave action has been briefly examined in the vicinity of the Okeechobee Waterway, Florida. The main objective was to demonstrate in the field that under wave conditions that are too mild to cause significant particle-by-particle resuspension, soft mud layers on the order of 20 cm thickness can undergo measurable oscillations induced by wave loading. Among other matters, such a motion may have implications for the rates of diffusive exchange of nutrients and contaminants between the bottom and the water column, and the formation and upward transport of gas bubbles, which are ubiquious in the mud in the study area. Continued mud motion can also retain the mud in a fluidized state, thereby enhancing its availability for resuspension during episodic events.

The chosen field site was in the shallow littoral margin of Lake Okeechobee, where the water depth was on the order of 1.5 m over a 0.5 m thick muddy substrate. During two experiments the water waves, induced orbital velocities in the water column and corresponding accelerations within the bottom mud layer were measured. In addition, bottom density profiles were obtained. A simple, two-layered wave

- Continued -

17. Originator's Key Words		18. Availability Statement
Fine sediment	Sedimentation	
Mud motion	Surf beat	
Okeechobee Waterway	Water quality	Available
Resuspension	Waves	

19. U. S. Security Classif. of the Report	20. U. S. Security Classif. of This Page	21. No. of Pages	22. Price
Unclassified	Unclassified	76	

propagation model which considers the water column to be inviscid and the mud layer to be a high viscosity fluid has been used to aid in data interpretation. Prior evidence indicates that 5-20 cm thick bottom surficial mud layer, which is rich in organic content (40% by weight), persists in the fluidized state over much of the area of the lake consisting of muddy bottom. In the first test in which wind wave frequency was on the order of 0.4 Hz and significant wave height around 10 cm, wave coherent mud motion was measured 20 cm below the mud-water interface, where the mud density was 1.18 gm/cm^3. In the second test similar motion occurred 5 cm below the interface.

Given the wave energy spectrum, the wave model approximately simulates both the water velocity spectrum as well as the mud acceleration spectrum, and highlights the fact that wave attenuation is strongly frequency dependent. Deviations between prediction and measurement are pronounced in the high frequency range of mud accelerations wherein the shallow water assumption inherent in the model breaks down. The muddy bottom causes waves to attenuate much more significantly than what would occur over a hard bottom. Model results indicate wave damping coefficients on the order of 0.005 m^{-1} in the shallow areas. These high values (compared with $\sim 10^{-5}$ m^{-1} over rigid beds) may explain why the waves arriving at the test site were only a quarter as high as those that might be expected if the lake bottom were wholly rigid.

A low frequency, long wave signature (e.g. at about 0.04 Hz in the first test), was characteristic of measured spectra. This signal was enhanced in the mud relative to the forcing signal (at 0.4 Hz) due to the dependence of wave attenuation on frequency, and led to horizontal mud displacements (twice the amplitude) on the order of 2 mm at 20 cm depth in the first test and 5 cm in the second. Since the dominant seiching frequency in the lake is around 10^{-4} Hz, a different cause must be found for the occurrence of the long wave. Although an unambiguous causative mechanism is not entirely apparent, it is suggested that the long wave signal is akin to surf beat characteristic of water level fluctuations at open coasts. The compliant bottom allows for the signal to be transmitted into the muddy substrate. This wave causes the mud to oscillate very slowly, thereby contributing to its mobility.

UFL/COEL-90/008

SOME FIELD OBSERVATIONS ON BOTTOM MUD MOTION DUE TO WAVES

Ashish J. Mehta
Feng Jiang

Coastal and Oceanographic Engineering Department
University of Florida
Gainesville, FL 32611

October, 1990

ACKNOWLEDGEMENT

This work was supported by the South Florida Water Management District (SFWMD), West Palm Beach, as a part of the Lake Okeechobee Phosphorus Dynamics Study (Task 4.4b), and by the U.S. Army Engineer Waterways Experiment Station (WES), Vicksburg, MS (Contract DACW39-89-M-4639 titled Monitoring Fluid Mud Generation). Thanks are due to Brad Jones and Dave Soballe of SFWMD and Allen Teeter of WES for project management assistance. Participation by Sidney Schofield, Nana Parchure and Kyu-Nam Hwang in different phases of the study is acknowledged.

TABLE OF CONTENTS

LIST OF TABLES

LIST OF FIGURES

SYNOPSIS

The behavior of soft mud under progressive, non-breaking wave action has been briefly examined in the vicinity of the Okeechobee Waterway, Florida. The main objective was to demonstrate in the field that under wave conditions that are too mild to cause significant particle-by-particle resuspension, soft mud layers on the order of 20 cm thickness can undergo measurable oscillations induced by wave loading. Among other matters, such a motion may have implications for the rates of diffusive exchange of nutrients and contaminants between the bottom and the water column, and the formation and upward transport of gas bubbles, which are ubiquious in the mud in the study area. Continued mud motion can also retain the mud in a fluidized state, thereby enhancing its availability for resuspension during episodic events.

The chosen field site was in the shallow littoral margin of Lake Okeechobee, where the water depth was on the order of 1.5 m over a 0.5 m thick muddy substrate. During two experiments the water waves, induced orbital velocities in the water column and corresponding accelerations within the bottom mud layer were measured. In addition, bottom density profiles were obtained. A simple, two-layered wave propagation model which considers the water column to be inviscid and the mud layer to be a high viscosity fluid has been used to aid in data interpretation. Prior evidence indicates that 5-20 cm thick bottom surficial mud layer, which is rich in organic content (40% by weight), persists in the fluidized state over much of the area of the lake consisting of muddy bottom. In the first test in which wind wave frequency was on the order of 0.4 Hz and significant wave height around 10 cm, wave coherent mud motion was measured 20 cm below the mud-water interface, where the mud density was 1.18 gm/cm^3. In the second test similar motion occurred 5 cm below the interface.

Given the wave energy spectrum, the wave model approximately simulates both the water velocity spectrum as well as the mud

acceleration spectrum, and highlights the fact that wave attenuation is strongly frequency dependent. Deviations between prediction and measurement are pronounced in the high frequency range of mud accelerations wherein the shallow water assumption inherent in the model breaks down. The muddy bottom causes waves to attenuate much more significantly than what would occur over a hard bottom. Model results indicate wave damping coefficients on the order of 0.005 m^{-1} in the shallow areas. These high values (compared with ~10^{-5} m^{-1} over rigid beds) may explain why the waves arriving at the test site were only a quarter as high as those that might be expected if the lake bottom were wholly rigid.

A low frequency, long wave signature (e.g. at about 0.04 Hz in the first test), was characteristic of measured spectra. This signal was enhanced in the mud relative to the forcing signal (at 0.4 Hz) due to the dependence of wave attenuation on frequency, and led to horizontal mud displacements (twice the amplitude) on the order of 2 mm at 20 cm depth in the first test and 5 cm in the second. Since the dominant seiching frequency in the lake is around 10^{-4} Hz, a different cause must be found for the occurrence of the long wave. Although an unambiguous causative mechanism is not entirely apparent, it is suggested that the long wave signal is akin to surf beat characteristic of water level fluctuations at open coasts. The compliant bottom allows for the signal to be transmitted into the muddy substrate. This wave causes the mud to oscillate very slowly, thereby contributing to its mobility.

SOME FIELD OBSERVATIONS ON BOTTOM MUD MOTION DUE TO WAVES

I. INTRODUCTION

It is generally well recognized that in shallow, episodic coastal or lacustrine environments with muddy beds, reworking of mud by waves causes the bottom to become loose, with looseness persisting as long as waves continue and thereafter, until the bottom material dewaters sufficiently to lead to hardening under calm conditions. Laboratory evidence shows that waves cause the mud bed to fluidize under cyclic loading, which breaks up the structural matrix of the bed held together by cohesive, inter-particle bonds. Furthermore, fluidization may occur without much entrainment of sediment in the water column, in which case no significant change in the bottom mud density occurs either (Ross and Mehta, 1990). In the limiting case of no resuspension (i.e. particle-by-particle erosion of the mud interface and upward entrainment of the eroded particulate matter), and therefore no density change of the bottom material, measurement of sediment concentration at different elevations would yield no evidence of the change of state of the mud from a cohesive bed to a fluid-supported slurry. Yet this change of state has obvious implications in bottom boundary layer related phenomena, including for example: 1) the availability of fluidized mud for potential resuspension by current or strong wave action, and 2) possible change in the effective permeability or resistance to diffusion, leading to corresponding changes in the exchange of nutrients or contaminants between the bottom and the water column. It is therefore relevant to examine the issue of mud motion by waves in terms of the nature of motion that results from wave action, and mud properties that influence the results. In this study the problem was examined from the following physical perspective.

II. A PHYSICAL PERSPECTIVE

A simple physical perspective is chosen to deal with a rather complex problem which is characterized by time-dependent changes in mud properties with continued wave action. Although

such changes have been tracked to some extent in laboratory experiments, field evidence is scarce due to evident problems in deploying requisite transducers. Furthermore, the basis for any theoretical examination of the time-variability of such properties as mud shear strength and rheology is presently inadequate. In treating the problem these limitations impose certain operational limitations in data gathering and analytic constraints in data analysis, which must be borne in mind as in the case of the following development.

In the way of a general description of the problem, it is instructive to consider Fig. 1, in which sediment density (ρ) profile and the horizontal component of the wave-induced velocity amplitude (u_m) in the water column and bottom mud are depicted in a somewhat idealized manner. With regard to the density profile, the important feature to recognize is the characteristic horizontal layering of the system. In the upper water column, in which pressure and inertia forces are dominant in governing water motion and the flow may be treated as essentially irrotational (ignoring the relatively thin wave boundary layer ref.), the sediment concentration tends to be typically low, say on the order of 0.1 g/l or less. Thus the suspension density is close to that of water. The lower boundary of the layer is characterized by a rather significant gradient in concentration, or lutocline, below which the concentrations of the fluidized mud are considerably higher, on the order of 10 to 200 g/l (density range: 1.01 to 1.12 g/cm^3 in fresh water).

Below fluidized mud is the cohesive bed having yet higher concentrations. Laboratory observations by Maa (1986) and Ross (1988), and theoretical work by Foda (1989) show that the wave orbits can penetrate the bed, thereby leading to elastic deformations of the bed. Under continued wave loading such deformations, coupled with a buildup of excess pore pressure, can cause fluidization, and this is in fact one way by which the thickness of the fluidized layer increases, starting, say, from a two-layered system of a porous solid bed and a clear water column at incipient wave motion (Ross and Mehta, 1990).

Recognizing that, due to the generally low rates of upward mass diffusion above the wave boundary layer, and therefore low observed concentrations of suspended sediment over most of the water column, the problem of mud motion by waves can be conveniently considered to be practically uncomplicated by the effects of particle-by-particle resuspension or entrainment (van Rijn, 1985; Maa and Mehta, 1987). In fact, laboratory observations as well as field data analysis show that wave conditions required to generate measurable bottom motion can be quite moderate compared with conditions required to cause significant particulate resuspension (Maa, 1986; Suhayda, 1986; Ross, 1988). Accordingly, the following simple system is considered.

A two-layered, water-fluid mud system forced by a progressive, non-breaking surface wave of periodicity specified by frequency, σ, is depicted in Fig. 2. As far as wave dynamics is concerned we will restrict the problem to one of long waves, which would therefore be applicable to very shallow coastal or lacustrine water bodies, or to the margins of deeper ones where wave action often matters the most. In the case of a rigid bottom, the shallow water condition is considered to be satisfied when $H\sigma^2/g < 0.1$, where H is water depth and g is acceleration due to gravity. For a given σ, this relationship specifies H such that for shallow water condition to hold, the actual depth must be equal to or less than that value of H. When the bottom is non-rigid the maximum water depth to which shallow water condition is satisfied will be somewhat larger, inasmuch as the wave length will be greater than in the rigid bottom case.

The upper water layer of thickness H_1 and density ρ_1 is considered to be inviscid, which is not unreasonable in comparison with the highly viscous lower, compliant layer of fluidized mud considered to be homogeneous and having a thickness H_2, density ρ_2 and dynamic viscosity μ. Physical scale arguments presented by Foda (1989) suggest that viscous dissipation in the bed may be restricted to a relatively thin boundary layer just below the mud-water interface. In the present case, however,

energy dissipation is assumed to be distributed over the entire lower (fluidized mud) layer. Beneath this layer is the bed, which is assumed to be rigid for the present purposes.

The surficial and interfacial variations about their respective mean values are $\eta_1(x,t)$ and $\eta_2(x,t)$. The amplitude of the simple harmonic surface wave is assumed to be small enough to conform to linear theory, as also the response of the mud layer. Accordingly, the relevant governing equations of motion and continuity can be written for the two layers as (Gade, 1958):

Upper layer:

$$\frac{\partial u_1}{\partial t} + g \frac{\partial \eta_1}{\partial x} = 0 \tag{1}$$

$$\frac{\partial}{\partial t} (\eta_1 - \eta_2) + H_1 \frac{\partial u_1}{\partial x} = 0 \tag{2}$$

Lower layer:

$$\frac{\partial u_2}{\partial t} + rg \frac{\partial \eta_2}{\partial x} + (1-r)\, g \frac{\partial \eta_1}{\partial x} = \nu \frac{\partial^2 u_2}{\partial z^2} \tag{3}$$

$$\int_0^h \frac{\partial u_2}{\partial x}\, dz + \frac{\partial \eta_2}{\partial t} = 0 \tag{4}$$

where $u_1(x,t)$ and $u_2(x,z,t)$ are the wave velocities, $h = H_2 + \eta_1$, $r = (\rho_2 - \rho_1)/\rho_2$ and $\nu = \mu/\rho_2$, is the kinematic viscosity of mud. Considering the fact that the fluid domain is bounded between $z = 0$ and $H_1 + H_2$, is infinite in extent in the $\pm x$ direction, the lower layer is viscous, and the solution sought is harmonic, the following boundary conditions are imposed:

$$\eta_1(0,t) = a_0 \cos\sigma t \tag{5a}$$

$$u_1(\infty,t),\ u_2(\infty,z,t),\ \eta_1(\infty,t) \text{ and } \eta_2(\infty,t) \to 0 \tag{5b}$$

$$u_2(x,0,t) = 0 \tag{5c}$$

$$\partial u_2(x,H_2,t)/\partial z = 0 \tag{5d}$$

where a_0 is the surface wave amplitude at x = 0. Eq. 5a specifies the surface wave form (progressive, simple harmonic), Eq. 5b represents the fact that due to viscous dissipation, all motion must cease at infinite distance, Eq. 5c is the no-slip bottom boundary condition, and Eq. 5d states that because the upper layer fluid is inviscid, there can be no stress at the interface.

In order to generalize the solution of Eqs. 1 through 4 and the boundary conditions (Eq. 5), the following convenient dimensionless quantities are introduced: $\tilde{u}_1 = u_1/\sigma H_1$, $\tilde{u}_2 = u_2/\sigma H_1$, $\tilde{\eta}_1 = \eta_1/H_1$, $\tilde{\eta}_2 = \eta_2/H_1$, $\tilde{H}_2 = H_2/H_1$, $\tilde{h} = \tilde{H}_2 + \tilde{\eta}_2$, $\tilde{t} = \sigma t$, $\tilde{k} = kH_1$ (where k is the wave number), $\tilde{x} = x/H_1$, and $\tilde{z} = z/H_1$. Thus Eqs. 1 through 4 become:

Upper layer:

$$\frac{\partial \tilde{u}_1}{\partial \tilde{t}} + \frac{1}{F_r^2}\frac{\partial \tilde{\eta}_1}{\partial \tilde{x}} = 0 \tag{6}$$

$$\frac{\partial}{\partial \tilde{t}}(\tilde{\eta}_1 - \tilde{\eta}_2) + \frac{\partial \tilde{u}_1}{\partial \tilde{x}} = 0 \tag{7}$$

Lower layer:

$$\frac{\partial \tilde{u}_2}{\partial \tilde{t}} + \frac{r}{F_r^2}\frac{\partial \tilde{\eta}_2}{\partial \tilde{x}} + \frac{1-r}{F_r^2}\frac{\partial \tilde{\eta}_1}{\partial \tilde{x}} = \frac{1}{Re}\frac{\partial^2 \tilde{u}_2}{\partial \tilde{z}^2} \tag{8}$$

$$\int_0^{\tilde{h}} \frac{\partial \tilde{u}_2}{\partial \tilde{x}}\, d\tilde{z} + \frac{\partial \tilde{\eta}_2}{\partial \tilde{t}} = 0 \tag{9}$$

where $F_r = \sigma(H_1/g)^{1/2}$ is the wave Froude number and $Re = \sigma H_1^2/\nu$ is the wave Reynolds number. Note that σH_1 is the characteristic shallow water velocity associated with wave motion. Note further

that the dimensionless surface slope term in Eq. 6, as well as the interfacial and surface slope terms in Eq. 8 are scaled by $1/F_r^2$, while the dissipation term in Eq. 8 is scaled by 1/Re. Consider a typical set of characteristic values including σ = 1 rad/s, H_1 = 1 m, $\nu = 10^{-3}$ m^2/s, and r = 0.1. This yields F_r = 0.32 and Re = 10^3. Thus the coefficient multipliers of the above four dimensionless terms will be 9.8, 1, 8.8 and 0.001, respectively. It is thus seen that the multiplier of the dissipation term is much smaller than those of the surface and interfacial gradient terms, particularly the former. Yet, of course, dissipation plays an critical role in the problem in terms of wave damping and a significant boundary layer effect within the mud. Note also that at such a low value of the wave Reynolds number, fluid mud motion is wholly laminar (Maa and Mehta, 1987).

The normalized boundary conditions are expressed as:

$$\tilde{\eta}_1(0,\tilde{t}) = A\cos\tilde{t} \tag{10a}$$

$$\tilde{u}_1(\infty,\tilde{t}),\ \tilde{u}_2(\infty,\tilde{z},\tilde{t}),\ \tilde{\eta}_1(\infty,\tilde{t}) \text{ and } \tilde{\eta}_2(\infty,\tilde{t}) \to 0 \tag{10b}$$

$$\tilde{u}_2 = 0 \tag{10c}$$

$$\partial\tilde{u}_2/\partial\tilde{z} = 0 \tag{10d}$$

where $A = a_0/H_1$ is the normalized wave amplitude. Note that by virtue of the assumption of rotationality in the lower layer only, and the shallow water wave condition, only $\tilde{u}_2$ can vary with z. The solution of Eqs. 6 through 9 with these boundary conditions is straightforward, and is given in Appendix D. Results relevant to the experiments conducted are presented later. While the solution is inherently simplistic, it served as a useful framework for guiding the interpretation of date which were obtained via field tower deployment in Lake Okeechobee. This large and shallow water body in the south-central part of Florida is well suited to studying wave-mud interaction, as noted in the next section.

The overall objective of the field investigation was to record oscillatory motion of fluidized mud in response to wind-generated waves at a shallow site with a muddy substrate. The field site and the experiments are noted below.

III. FIELD SITE

The main requirements for the field site were: 1) wave-dominated environment, 2) shallow water, and 3) a soft muddy bottom with sizeable thickness of fluidized mud. These conditions are approximately met in the southeastern part of Lake Okeechobee close to the shoreline (~1 km offshore) in the vicinity of the Okeechobee Waterway, a part of the Intracoastal Waterway system.

Fig. 3a shows depths in this rather shallow lake, and Fig. 3b shows the bottom mud thickness. Depths in Fig. 3a may be considered to be relative to the top of the mud. The depth datum is 3.81 m above NGVD, but the actual water level in the lake is subject to significant variation imposed by the inflows and outflows which are controlled. Thus, for example, during a field excursion to collect bottom sediment samples in March, 1988 (Hwang, 1989) the actual water level was about 1.2 m higher than the datum.

The variation of water level implies the likelihood of a corresponding variation in the mud bottom area which is influenced by wave action. Assuming typical storm-induced wave characteristics and their erodibility potential as represented by the critical shear stress for erosion, a water depth of 3.4 m can be calculated (see Appendix A) as the critical depth such that the bottom will erode only if the actual depth is equal to or less than this critical depth. Based on this criterion, Fig. 4 shows the lake area influenced by waves at different water levels (arbitrarily selected to be -1.0 m to +1.5 m relative to datum). It is observed that when the lake level is less than 0.5 m below datum, the entire mud bottom area of 528 sq. km is subject to wave action. On the other hand, when the level is, for example, 1.5 m above the datum, the affected area is reduced to 48 sq. km. The shape of the curve further implies that the bottom area influenced by wave action is most sensitive to water level in the

range from 0 to 1.0 m. Notwithstanding evident limitations in constructing this relationship which, for example, does not account for changes in wave conditions themselves at a given water level, this "mean" description does indicate a significant dependence of the bottom area acted on by the waves at different water depths. In turn this strong dependence suggests that seasonal water level variation in this lake is likely to be a major factor in affecting bottom resuspension and bottom mud motion characteristics.

During the field deployments, the wave conditions may be characterized as having been mild, with significant wave heights on the order of 10 cm or less and periods on the order of 2-3 s. While such waves did generate horizontal motions within the bottom mud under close to shallow water conditions, it can be shown that the maximum bottom stresses would be quite small, insufficient to cause measurable resuspension (Hwang, 1989). Therefore, under the given wave conditions, the assumption of zero resuspension in the theoretical approach was met adequately. When storm waves do occur, the top ~5 cm thick layer of the bottom mud tends to dilate due to upward diffusion of sediment to ~10 cm. Above this dilated layer, upward sediment mass transport tends to be comparatively very small, but the presence of the dilated layer does tend to complicate the near-bed processes as far as sediment motion is concerned (Hwang, 1989).

Two additional features of this mud bottom environment are noteworthy relative to the problem under consideration. Firstly, the mud throughout includes about 40 % (by weight) material that is essentially of organic origin and, as a result, the "granular" density of the composite material is 2.14 g/cm^3, which is less than that for clays for example (~2.65 g/cm^3) (Hwang, 1989). Secondly, the top 5 to 20 cm of the mud has negligible (vane shear) strength and is believed to be in a fluidized state (Kirby et al., 1989; Hwang, 1989). This state is brought about partly by the occasionally significant wave action, but it is believed that an additional noteworthy factor is the presence of the high fraction of organic material which, presumably by virtue of

having an open and comparatively strong aggregate structure of floral origin, prevents rapid dewatering of wave-suspended surficial deposits even during calms. Hence a bed is not formed easily in the top layer, although 10 to 20 cm below mud surface, self-weight does seem to lead to crushing of the aggregates and consolidation of the deposit. The outcome is a comparatively uniform density below the top fluidized layer.

IV. EXPERIMENTS

In order to achieve the study objective it was necessary to obtain the time-series of water level, the corresponding wave orbital velocities in the water column and induced orbital velocities in the mud. Water level was measure with a subsurface mounted pressure gage (Transmetrics, Model P21LA). Water motion was measured by an electromagnetic (EM) meter (Marsch-McBirney, Model 521). The EM meter has been used previously with a reasonable degree of success in the fluid mud environment to measure tide-induced flows having sediment concentrations up to about 400 g/l, i.e. 1.27 g/cm^3 (Kendrick and Derbyshire, 1985). In this study however it was decided to measure wave-induced accelerations instead, in order to obviate likely problems in interpreting EM meter data in the presence of high concentration sediment. The use of accelerometer for such a purpose has been reported previously (Tubman and Suhayda, 1976). A biaxial accelerometer was used in the present study (Entran, Model EGA2-C-5DY).

Two field tests were carried out at the selected nearshore site (Fig. 3a) using a tower shown in Figs. 5 and 6. The site was in the proximity of the "Green 17" channel marker. At this site, often prevalent westerly and northwesterly winds generate suitable waves over a comparatively long fetch. The first test (test 1) was on December 20-21, 1989, and the second (test 2) on March 28, 1990. The duration of test 1 was from 1700 hr on December 20 to 0100 hr on December 21. The duration of test 2 was from 1730 hr to 2130 hr on March 28.

The aluminum field tower frame assembly was designed for providing bottom stability and to hold a 4.2 cm diameter aluminum shaft within a concentric pipe of 5.8 cm o.d. as shown. The tower had a total height of 2.45 m. The size at the base was 1.5 m by 1.0 m, tapering to 0.25 m by 0.15 m at the top. The slanted members were braced together in order to give adequate strength to the tower against buckling and torsion during installation and retrieval operations. A wooden plank (base) of 0.8 m by 0.8 m size was firmly fixed at the top of the tower for mounting the data acquisition equipment. The tips (pins) of all the four legs of the tower were made conical so that they could easily penetrate the soft mud layer and provide stability. Horizontal braces were provided at the bottom of the tower at an elevation of 8 cm above the ends of legs. In addition to providing strength to the tower, these braces arrested the excessive downward movement of the tower, bringing it to rest over relatively hard bottom.

At the lower end of the central shaft a holder was provided to carry the accelerometer mounted in a plexiglass "boat", consisting essentially of a horizontal oval disc with vertical guide vanes (see Appendix B). With the accelerometer embedded in the disc, the boat was made neutrally buoyant at a density of about 1.07 g/cm^3. This arrangement allowed the accelerometer to be loosely suspended at a desired elevation below the shaft, constrained only by the vertical play of the shaft in a fluid mud of 1.07 g/cm^3 density. The accelerometer could be rotated by rotating the shaft itself to orient the device in the desired direction.

The pressure gage and the EM meter were clamped on to the concentric pipe (Fig. 7). In test 1 the EM meter was oriented in such a way as to allow it to record the two horizontal components of the wave velocities, u_1 and v_1. In test 2, u_1 and the vertical component, w_1, were measured. The accelerometer was mounted in such a way as to enable it to record the horizontal component of acceleration in the dominant wave direction, $\dot{u}_2$, and the vertical

component, $\dot{v}_2$. Data bursting for all the three transducers was at the rate of 4 Hz for 10 min every hour in test 1, and 5 min every 1/2 hour in test 2. This digitization frequency and record lengths may be considered to be minimally adequate based on previous studies (see Mehta and Dyer, 1990). The transducers were connected to a data acquisition system (Tattletale, Model 6) mounted on the wooden plank (Fig. 8).

Mean water depth, mud thickness and the depths below still water level at which the pressure sensor, the EM meter and the accelerometer were deployed in the two tests are given in Table 1.

Table 1. Test parameters (depths and elevations)

Test No.	Water depth (m)	Mud thickness (m)	Depth below still water level (m)		
			Pressure	Velocities	Accelerations
1	1.43	0.55	0.54	0.87	1.63
2	1.64	0.35	0.58	1.22	1.69

V. BOTTOM MUD CHARACTERISTICS

In consonance with the nature of the problem and the two-layered formulation shown in Fig. 2, the bulk density and the dynamic viscosity can be considered to be the two important parameters characterizing the mud bottom. Vertical density profiles in the mud were obtained by a simple bottom coring procedure (Srivastava, 1983), using a hand-held corer that yielded approximate variation of density with depth below the mud-water interface. It should be noted that in the lake environment this interface is quite well defined during calm conditions (Fig. 9).

Mud viscosity was measured in a laboratory viscometer at different mud bulk densities (see Appendix C). The relationship between the dynamic viscosity and mud density shown in Fig. 10

(see also Fig. C.6 in Appendix C) will be considered to be adequate in characterizing the wave energy dissipation property of the mud at different densities. Note that due to limitations in the apparatus, mud suspensions of densities higher than 1.12 g/cm^3 could not be tested. It was therefore assumed that at higher (up to 1.18 g/cm^3) densities, the viscosity could be obtained by linearly extrapolating the curve shown in Fig. 10.

Mud bulk density profiles (one from test 1 and two from test 2) are shown in Figs. 11a,b. The substrate underneath the mud layer may be considered as "hard"; the transition to hardness being here defined as the level at which the field tower rested on its own account, rather than in terms of hardness related to bottom composition. The mud layer thickness shown in the figures and given in Table 1 is based on this consideration.

It is interesting to note that in the second test the tower seemingly rested on a hard, approximately 7 cm thick "lens", with softer material both above and below this thin lens. The occurrence of such a lens can be due to peculiarities associated with episodic accumulation arising from locally resuspended and allothegenous sediment. Also shown in the figures is the level at which the accelerometer (AC) was embedded. In test 1 it was 0.2 m below the mud-water interface and in test 2 it was 0.05 m below the interface. The corresponding densities were 1.18 and 1.15 g/cm^3. Considering that the boat with the accelerometer was neutrally buoyant at 1.07 g/cm^3, the placement of the device at a somewhat higher density imparted buoyancy which was undesirable. The problem occurred because of the difficulty in determining mud density *in situ* when the acceleometer was deployed. Mechanistically the problem is somewhat analogous to the wave-induced motion of a submerged buoy tethered by a rope to the bottom, with the rope held taut by the buoyancy of the buoy. It can be shown easily that given physical parameters relevant to the present problem, the effect of buoyancy on measured accelerations would be minor.

VI. WATER AND MUD MOTIONS

The time-series of pressure, water velocities and mud accelerations were analyzed in terms of their spectral properties and central tendencies. Water pressures were converted to wave heights via the pressure response factor based on the linear theory. For a description of the linear theory and wave spectra see Dean and Dalrymple (1984). In what follows, data from test 1 are discussed, followed briefly by those from test 2.

With reference to test 1, Fig. 12a shows the variation of the significant wave height, $H_{1/3}$, with time over the seven hour test duration (data from the first data block at 1700 hr were found to be spurious due to lack of adequate time for electronic system warm-up, and therefore are not included). Zero hour corresponds to 1800 hr on December 20, 1989. Note that each hourly data point represents a 10 min average value; 10 min being the record length for each hourly data block. Under gentle to moderate breeze, $H_{1/3}$, is observed to have been rather small, peaking to 10 cm at 3 hr. In Fig. 12b the corresponding variation of the dominant (modal) surface wave frequency, f_m, defined as the frequency at the peak of the wave energy density spectrum, is shown. An example of the spectrum itself is shown in Fig. 13a. This and all other spectra represent ensemble averages obtained by selecting a band width of 10 sampling points, the sampling interval being 0.25 s. The modal frequency variation is compared with the same determined from the water velocity spectrum (see for example Fig. 13b). As observed the dominant wind-wave frequency was comparatively constant, varying between 0.38 and 0.50 Hz, with a mean value of 0.42 Hz over the test duration.

The relative constancy of the wave frequency throughout test duration suggests that the wind fetch was likely to have been more or less constant, notwithstanding the fact that the wave height did vary somewhat more significantly than frequency. In Fig. 14 the angular direction of the horizontal water velocity (resultant of the two measured components, u and v) relative to an arbitrarily selected coordinate (direction) is plotted. This plot does indicate a comparatively constant direction of wave

approach throughout the test (the angle varied between 35^0 and 47^0, with a mean of 42^0). The direction was approximately westerly. This direction corresponds to a lake fetch on the order of 50 km with a mean depth of around 3 m (Fig. 3a). Selecting a wave period of 2.5 s corresponds to a wind of 20 km/hr (moderate breeze), using shallow water forecasting curves for wave generation over a rigid bottom (Coastal Engineering Research Center, 1977). However, the forecasted wave height under these conditions is 40 cm. It can be surmised that, notwithstanding the approximations (e.g. constant water depth) involved in these calculations, the discrepancy is likely to be due to significant wave damping over the mud bottom which stretches over 30 km, so that only the first 20 km distance can be considered to be over a rigid bottom.

In Fig. 15, the variance of the resultant velocity (amplitude) is plotted. Comparing this observed time-variation with the corresponding variation of wave height in Fig. 12a shows expected similarities in time-trends.

In Fig. 16a the variances of the horizontal and vertical components of mud acceleration are plotted over the duration of test 1. These indicate the latter to be expectedly smaller in comparison with the former a part of the time, but during the early (except at 0 hr) and later phases of the test their magnitudes were generally of the same order. This implies that the shallow water condition was not quite met, and that wave orbital motion in the mud varied from practically horizontal (e.g. at 0 hr when the vertical acceleration was negligibly small) to circular (e.g. at 1 and 5 hrs). In fact, it can be easily shown that the shallow water condition was only appropriate for waves having frequencies less than around 0.2 Hz.

In Fig. 16b the modal frequencies corresponding to the spectral peaks arising from wind wave action are plotted. An example of the horizontal acceleration spectrum itself is given in Fig. 16c. Note that the spectrum shows a marked peak at a very low frequency corresponding to a long period oscillation distinct from direct wind forcing. Commensurate peaks also appear in the

wave and velocity spectra of Figs. 13a,b. Vertical acceleration measurements did not exhibit these low frequency, long wave signatures for evident reasons, and the corresponding spectra are not considered further in what follows. The long wave signature is further discussed later.

Note that the modal frequencies in Fig. 16b correspond to the portion of the horizontal acceleration spectrum exclusive of the low frequency signature. The modal frequencies of vertical acceleration generally coincided (range: 0.42 to 0.48 Hz; mean = 0.40 Hz), given the limits of likely errors due measurement and analysis procedures, with those of the surface wave and water velocity given in Fig. 12b, while those of the horizontal acceleration are observed to be slightly higher (range: 0.40 to 0.62 Hz; mean = 0.51 Hz). This shift may reflect the fact that for the higher frequencies encountered the shallow water assumption did not quite hold, and as a consequence there was greater damping at lower frequencies than at the higher ones. It is also possible to attribute this frequency shift to likely limitations in the measurement of accelerations with the "boat", noting that difficulties with the laboratory setup precluded a detailed investigation of the motion of the boat in the range of the very small amplitude motion that was encountered within the mud during the field tests.

VII. RESPONSE OF LINEARIZED FLUID MUD-WATER SYSTEM

Given the surface wave spectrum such as in Fig. 13a, which characterizes the measured wave amplitude (A) variation with wave frequency, Eq. D-15c can be used to calculate the water velocity, and the time-derivative of Eq. D-15d to calculate mud acceleration.

An evident difficulty in adapting the simple model to measurement involves the selection of a representative (constant) mud density, since as seen from Figs. 11a,b the density characteristically increased quite rapidly with depth below the interface in the top ~10 cm. The matter of selecting mud density of course bears critically on the rate of energy dissipation, due to the rather drastic dependence of the mud viscosity on density

(Fig. 10). In order to account for this problem, Maa and Mehta (1987)and others (e.g. Shibayama et al.,1989) have developed layered bed models in which the mud density and viscosity can vary arbitrarily with depth. It was felt that the use of such models for the present case would essentially amount to an over-specification of the physical system, whose understanding was constrained by the rather limited data collection effort. Furthermore, from the perspective of lake dynamics the important point to be made for the present case is to show that, even under relatively weak wave action, mud down to a significant depth below the interface moves in the shallow parts of the lake, thereby presumably influencing constituent (e.g. nutrient) fluxes in a measurable way. In that context, the purpose of the simple model used here may be considered to be for corroborating the observation of mud motion through basic physical principles.

For calculating the velocity and acceleration spectra from the wave energy spectra, the following transfer functions based on Eqs. D-15a, D-15c and D-15d were used:

From wave energy spectrum to water velocity spectrum:

$$S_{u_1u_1} = K_{u_1}^2 S_{\eta\eta} \tag{11a}$$

where

$$K_{u_1} = \text{Real}\left(\frac{k\sigma}{F_r^2}\right) \tag{11b}$$

From wave energy spectrum to mud acceleration spectrum:

$$S_{\dot{u}_2\dot{u}_2} = K_{\dot{u}_2}^2 S_{\eta\eta} \tag{12a}$$

where

$$K_{\dot{u}_2} = \text{Real}\left\{\frac{-igk}{H_1}\left(1 - \frac{rk^2}{F_r^2}\right)[1 - \cosh(mH_1z) + \sinh(mH_1z) \cdot \tanh(1-i)\chi]\right\} \tag{12b}$$

Model application can be illustrated by considering data from test 1. Water depth H_1 is given in Table 1. The choice of appropriate mud thickness, H_2, was obviously difficult in the same sense as choosing a representative mud density. With regard to density, a value of 1.18 g/cm^3 was selected, corresponding to the position (AC) of the accelerometer shown in Fig. 11a. The computations were found to be particularly sensitive to the choice of H_2 by virtue of the effect of χ (see Appendix D) on the kinematics, which in turn signifies the interrelationship between the mud boundary layer and energy dissipation. Furthermore, as a rule mud becomes rather immobile at densities exceeding around 1.2 g/cm^3. Therefore, it would be unreasonable to select the entire mud thickness of 0.55 m for computational purposes. It was decided to select H_2 = 0.283 m (corresponding to a density of 1.22 g/cm^3). This selection seemed to give the best results by way of agreement with data, for the cases examined.

Given the surface wave data represented in Fig. 13a, the calculated (simulated) and measured water velocity and mud horizontal acceleration spectra are shown in Figs. 17a,b. Note that the velocity measurement was 0.87 m below the still water level (Table 1), an elevation that was likely to have been above the wave boundary layer, since the total water depth was 1.43 m; hence the interface was well below the position of the current meter. Therefore, the model assumption of inviscid upper layer, when comparing simulated values with data essentially in the upper portion of the water column, may not be overly limiting. Data and simulation generally show the same trends. Note that by virtue of the assumptions of linearity and inviscid upper layer, the calculated velocity spectrum is closely self-similar to the wave energy spectrum. Since in the field the measurement of pressure under non-breaking waves is usually more reliable than water velocity, the general similarity between the measured wave energy and water velocity spectra, as well as the general agreement between the simulated and measured velocity spectra, can be considered, in a sense, to attest to the reliability of the water velocity data from the field.

Comparing the simulated and measured horizontal mud accelerations in Fig. 17b indicates that while the model generally agrees with the data, the latter show the occurrence of accelerations at high frequencies which can not be accounted for by the shallow water model. As noted before, these high frequency waves were proportionately less damped most probably due to these being outside the shallow water domain, in intermediate depth. This type of selective damping of shallow water wave components relative to those in intermediate depth has been quite well documented, for example, by Wells and Kemp (1986) in their study on wave propagation over a large mud flat off Surinam.

In Figs. 18a,b,c measurements and model calculations are shown for the data block at 5 hr, similar to those for the block at 1. Once again the interpretations relative to the data, as well as comparison between data and model calculations, remain the same. All measured spectra (wave energy, water velocity and horizontal mud acceleration) for test 1 are given in Appendix E. With reference to mud acceleration spectra, seemingly exaggerated peaks corresponding to the long wave spectral signal occasionally appeared, e.g. at 0, 2 and 6 hrs in test 1. We are uncertain about the cause of this type of a response; it is not clear for instance if this was due to a problem in the acceleration measurement, or if there was a physical cause. Granting no data error, the large peak would mean much less damping of the low frequency than that of the wind wave. While this implication seems to be borne out by theory as noted later, the implied dependence of the damping coefficient on wave frequency is greater than what the theory indicates. A further look at this phenomenon in future will be necessary.

Data from test 2 were found to be somewhat unsatisfactory in the sense that wave action was very weak throughout the test duration, with the result that the wind induced wave spectra contained very little energy. For illustrative purposes, spectra obtained from the first block (at 1800 hr on March 28, 1990) are shown in Figs. E.7 through E.11.

The low energy content of wind waves during the second test is evidenced by a comparison, for example, between Figs. 13a and

E.7. Somewhat surprisingly, however, the low frequency peak is quite prominent (relative to wind wave peak) in Fig. E.7. We further note that: 1) The forcing wave and the low frequency occur at about the same frequencies (0.57 Hz and 0.05 Hz) as in test 1, which in turn suggests that the general nature of the phenomena at the test site are likely to be persistent. (Note that test 1 was conducted at the inception of the winter period while test 2 was at the end of this period.) In other words, the conclusions derived from the examination of test 1 data are likely to be applicable to events in the study area on more than a mere isolated basis. 2) The persistence of the low frequency peak, even in the absence of significant wind energy, is noteworthy in that the occurrence of this peak is somewhat enigmatic insofar as the causative mechanism is concerned.

With regard to the water velocity spectra is Figs. E.8 and E.9, recall that the first is the horizontal component and the second vertical. Thus the horizontal component may not precisely reflect the velocity in the wave direction (which, unlike in test 1, could not be determined). On the other hand, the general features in Fig. E.8 are commensurate with those in Fig. E.7. Here again a strong low frequency, long wave signature is observed. Vertical velocities (Fig. E.9) were expectedly smaller and did not show the low frequency signature.

Comparing Figs. E.10 and E.11 for the horizontal and vertical mud accelerations it is seen that the wind-induced signature was too small to be recorded. Furthermore, the horizontal acceleration was more important than vertical at the low frequency.

An interesting application of the model relates to wave damping in the lake. Thus, for example, at a frequency of 0.4 Hz, the wave damping coefficient calculated by the model is 0.0034 m^{-1}. Over rigid beds on the other hand, shallow water waves attenuate much more slowly; the damping coefficients are only on the order of 10^{-5} m^{-1} (Ippen and Harleman, 1966). Thus, wind generated waves will be smaller over a compliant bottom. As noted, during the experiment, waves at the site were only a

quarter as high as those that would be generated over a rigid bed.

VIII. LOW FREQUENCY SIGNATURE

The dominant frequency of the low frequency spectral signature is plotted in Fig. 19 for test 1 from wave energy, water velocity and horizontal mud acceleration spectra. It is observed that all the spectra yield rather consistent values ranging from 0.029 Hz to 0.049 Hz, with a mean of 0.043 Hz. In practical terms the frequency was seemingly unaffected by changes in the wave conditions during the test. Referring to Figs. 13a,b and 16c (data block at 1 hr, test 1), it is seen that the low frequency peak relative to the forcing wave (modal) peak was enhanced in the mud (Fig. 16c) relative to that in water (Figs. 13a,b). Model results for the same data block in Figs. 17a,b show similar trends, and indicate that this type of a response for shallow water waves is due to frequency dependent wave damping as can be gleaned from the attenuation coefficient characterized in Fig. D.2. Thus for example, selecting 0.4 Hz and 0.04 Hz as representative frequencies for the forcing wave and the low frequency, respectively, the corresponding damping coefficients are 0.0034 m^{-1} and 0.0013 m^{-1}, which indicates relatively much less damping at the lower frequency. It is also noteworthy that by integrating the acceleration twice, the horizontal displacement of mud can be shown to increase with decreasing frequency. Maximum displacements on the order of 2 mm can be shown to have occurred at ~0.03 Hz in both tests.

Some comments on the causative mechanism for the low frequency signature are in order. In that context it must be noted that the dominant period of seiching in Lake Okeechobee is in the range of 5 to 6 hr (Ahn, 1989), i.e. a frequency on the order of 10^{-4} Hz, which is considerably smaller than the observed low frequency peak. It seems plausible that the low frequency wave is in fact a second order effect resulting from wind induced wave forcing leading to surf beat. This effect, in which short period wind-waves are modulated by a longer period wave of very

low amplitude, commonly observed along the open coast having a hard or sandy bottom with mild slopes and having a frequency range of $3x10^{-3}$ to $8x10^{-3}$ Hz (Wiegel, 1964), may be modified by a compliant bottom as in the present case, but it serves the purpose to examine this mechanism assuming a rigid bottom, at least for arriving at a qualitative explanation for the occurrence of the long wave signature.

We consider two waves, $\eta_1(0,t)$ and $\eta_2(0,t)$, of respective frequencies σ_1 and $\sigma_2 = \sigma_1 + \Delta\sigma$, where $\Delta\sigma$ is a small difference:

$$\eta_1 = a_1\cos(\sigma_1 t - \varepsilon_1) \tag{13a}$$

$$\eta_2 = a_2\cos(\sigma_2 t - \varepsilon_2) \tag{13b}$$

Here, ε_1 and ε_2 are the phase lags. Assuming further that the amplitude $a = a_1 = a_2$, the resultant (forcing) wave, $\eta_r = \eta_1 + \eta_2$ can be shown to be

$$\eta_r = 2a\cos(\sigma t - \varepsilon)\cdot\cos\left[\frac{\Delta\sigma\cdot t - \Delta\varepsilon}{2}\right] \tag{14}$$

where $\sigma = (\sigma_1 + \sigma_2)/2$, $\varepsilon = (\varepsilon_1 + \varepsilon_2)/2$, and $\Delta\varepsilon = \varepsilon_1 - \varepsilon_2$. It is thus seen that the sinusoidal wave term, $2a\cos(\sigma t - \varepsilon)$, is modulated by $\cos[(\Delta\sigma\cdot t - \Delta\varepsilon)/2]$, which causes the well known "beat effect" due to wave groupiness.

The fact that real waves have finite amplitudes means that higher (than first) order effects arising from changes in water surface elevation and associated kinematics cannot always be ignored. An effect germane to the present case is the setting up of a long wave which modulates the wave given by Eq. 14. This forced long wave follows from inclusion of the kinetic head term in the dynamic free surface boundary condition (DFSBC), and evaluation of the mean (relative to σ) water surface profile by carrying out the computations to second order (Longuet-Higgins and Stewart, 1962; Dean and Dalrymple, 1984). Without restricting the problem to shallow water, the wave-averaged DFSBC is:

$$\bar{\eta} = -\frac{1}{2g}\,\overline{(u^2 + w^2)} + \overline{\frac{\eta}{g}\,\frac{\partial\phi}{\partial z \partial t}} \qquad (15)$$

where the overbar represents short period ($2\pi/\sigma$) averaging, u and w are the horizontal and vertical velocity components, and ϕ, the well known form of the potential function which satisfies the boundary value problem (assuming a rigid bottom for this simplified case), is given by

$$\phi = -\frac{ag}{\sigma}\,\frac{\cosh k(H + z)}{\cosh kH}\,\sin\sigma t \qquad (16)$$

where H is the water depth. Noting that $u = -\partial\phi/\partial x$ and $w = -\partial\phi/\partial z$, it can be easily shown that

$$\bar{\eta} = -\frac{a^2 k}{\sinh kH}\,[1 + \cos(\Delta\sigma \cdot t - \varepsilon)] \qquad (17)$$

where $k = (k_1 + k_2)/2$. The first term on the right hand side represents a steady set down, and the second is the forced long wave. The energy spectrum (or the energy density spectrum) thus obtained is shown in Fig. 20, which shows that the long wave, corresponding to two forcing waves at frequencies $f_1 = \sigma_1/2\pi$ and $f_2 = \sigma_2/2\pi$ and amplitude a, has a frequency $f_\ell = \Delta\sigma/2\pi$ and amplitude $a^2k/\sinh kH$. It is important to note that, comparing Eq. 17 with Eq. 14 indicates that the long wave is π radians (180^0) out of phase with the wave group envelope of the forcing wave.

When forcing is represented by a continuous spectrum, the treatment for determining the forced long wave spectrum becomes involved (Sharma and Dean, 1979). Here a very approximate approach is selected. Consider for example the double peaked velocity spectrum corresponding to the forcing wave in Fig. 13b. Assuming the two peak frequencies to be the primary contributors to the corresponding long wave peak, we have the following parameters (obtained from the Fourier series of the corresponding surface wave record): $a_1 = 2.4$ cm, $a_2 = 2.6$ cm, long wave

amplitude a_ℓ = 0.30 cm, f_1 = 0.38 Hz, f_2 = 0.42 Hz, f_ℓ = 0.049 Hz, $\varepsilon_1 = 191^0$, $\varepsilon_2 = 171^0$, and $\varepsilon_\ell = -65^0$. Note that $\Delta f = f_2 - f_1$ = 0.04, which is reasonably close to f_ℓ. The forcing wave (η_r) and the forced wave, η_ℓ, are plotted against $\psi = \Delta\sigma \cdot t - \Delta\varepsilon$ in Fig. 21. It is evident that the forced wave is almost π radians out of phase with the short period wave envelope as the theory would require. If we assume shallow water condition, the forced wave amplitude (from Eq. 17) would be a^2/H. Given $a = 0.5(a_1 + a_2)$ = 2.50 cm and H = 143 cm, a^2/H = 0.044 cm. Thus the theory underpredicts the amplitude significantly, which might be due to inherent theoretical limitations as well as the rather gross assumptions made in applying the theory to the present case.

IX. CONCLUDING REMARKS

Notwithstanding the limited nature of the data obtained, the complexities in modeling mud motion and the rather obvious constraint in simulation arising from the shallow water assumption as well as others (e.g. inviscid water layer, linearized response, particularly of the mud layer), it is seen from the data and simulation that measurable mud accelerations can occur tens of centimeter below the mud-water interface, under wave action that is mild enough to preclude any measurable erosion of the interface. It can be easily shown that corresponding maximum horizontal displacements on the order of 2 mm occurred at the low frequency end (~0.03 Hz) of the spectrum in both tests. The displacement spectrum, S_{dd}, is obtained from the wave spectrum, $S_{\eta\eta}$, as follows:

$$S_{dd} = K_d^2 S_{\eta\eta} \tag{18a}$$

where

$$K_d = \text{Real}\left\{ i \frac{kH_1}{F_r^2} \left(1 - \frac{rk^2 H_1^2}{F_r^2}\right)\left[1 - \cosh\left(\frac{mz}{H_1}\right) + \tanh\left(\frac{mH_2}{H_1}\right) \sinh\left(\frac{mz}{H_1}\right)\right]\right\} \tag{18b}$$

Although bioturbation does not seem to be a significant factor in Lake Okeechobee (Kirby et al., 1989), the effect of persistent mud oscillation, even though very small, can be germane to likely changes in the rates of exchange of phosphorus and other water quality influencing chemical constituents. Similarly, there may be an effect on the formation and upward transport of gas bubbles which occur abundantly in the muddy area of the lake (Kirby et al., 1989). It is believed that gas bubbles contribute measurably to nutrient dynamics in the lake.

The "openness" of the particulate matrix of the bottom mud in this lake seems to be greatly controlled by the presence of a significant fraction of floral organic matter, so that persistent mud motion may effectively increase pore water transport, and associated constituent exchange. While this issue does not quite fall within the rubric of the present scope of work, we recommend that it be examined in the light of these findings.

We wish to point out a further issue that is related to the constitutive behavior of bottom mud. While in this study we considered mud up to a density of about 1.2 g/cm^3 to be a highly viscous fluid, careful measurements (e.g. Sills and Elder, 1981) indicate that, at least under quiescent conditions, at densities exceeding about 1.1 g/cm^3, clayey mud typically exists as porous solid rather than a fluid. The organics-rich Lake Okeechobee mud is prone to remain in a fluidized state at densities at least up to about 1.065 g/cm^3 (Hwang, 1989). It is therefore unclear if at 1.18 g/cm^3 density this mud is normally (i.e. in the absence of episodic wave action) fluidized. Hence the chosen model description may be approximate in this respect. Nonetheless, since the model calculated mud accelerations compare favorably with the measured ones at least in order of magnitude, the description of mud as a fluid seems acceptable, although a better physical description, which recognizes the transition from the fluid phase to the solid phase, would indeed constitute a worthwhile improvement.

X. REFERENCES

Ahn K. (1989). Wind-wave hindcasting and estimation of bottom shear stress in Lake Okeechobee. M.S. Thesis, Univ. of Florida, Gainesville.

Coastal Engineering Research Center (1977). Shore Protection Manual, Vol. 1, U.S. Army Engineer Waterways Experiment Station, Vicksburg, MS.

Dean R.G. and Dalrymple R.A. (1984). Water Wave Mechanics for Engineers and Scientists. Prentice-Hall, Englewood Cliffs, NJ.

Dixit J.G. (1982). Resuspension potential of deposited kaolinite beds. M.S. thesis, Univ. of Florida, Gainesville.

Foda M.A. (1989). Sideband damping of water waves over a soft bed. Journal of Fluid Mechanics, 201, 189-201.

Gade H.G. (1958). Effects of non-rigid, impermeable bottom on plane surface waves in shallow water. Journal of Marine Research, 16(2), 61-82.

Hwang K.-N. (1989). Erodibility of fine sediment in wave-dominated environments. Rept. UFL/COEL-89/017, Coastal and Oceanographic Engineering Dept., Univ. of Florida, Gainesville.

Ippen A.T. and Harleman D.R.F. (1966). Tidal dynamics in estuaries. In: A.T. Ippen ed., Estuary and Coastline Hydrodynamics, McGraw-Hill, New York, 493-545.

Jonsson I.G. (1966). Wave boundary layer and friction factors. Proceedings of the 10th Coastal Engineering Conference, Vol. 1, American Society of Civil Engineers, New York, 127-148.

Kendrick M.P. and Derbyshire B.V. (1985). Monitoring of a near-bed turbid layer. Rept. SR 44, Hydraulics Research, Wallingford, U.K.

Kirby R.R., Hobbs C.H. and Mehta A.J. (1989). Fine sediment regime of Lake Okeechobee, Florida. Rept. UFL/COEL-89/009, Coastal and Oceanographic Engineering Dept., Univ. of Florida, Gainesville.

Longuet-Higgins M.S. and Stewart R.W. (1962). Radiation stress and mass transport in gravity waves, with application to 'surf beat'. Journal of Fluid Mechanics, 13, 481-504.

Maa P.-Y. (1986). Erosion of soft muds by waves. Rept. UFL/COEL-TR/059, Coastal and Oceanographic Engineering Dept., Univ. of Florida, Gainesville.

Maa P.-Y. and Mehta A.J. (1987). Mud erosion by waves: a laboratory study. Continental Shelf Research, 7(11/12), 1269-1284.

Mehta A.J. (1989). On estuarine cohesive sediment suspension behavior. Journal of Geophysical Research, 94(C10), 14303-14314.

Mehta, A.J. and Dyer K.R. (1990). Cohesive sediment transport in estuarine and coastal waters. In: The Sea, Vol. 9: Ocean Engineering Science, Part B. LeMehaute and D.M. Hanes eds., Wiley, New York, 815-839.

Ross M.A. (1988). Vertical structure of estuarine fine sediment suspensions. Ph.D. Dissertation, Univ. of Florida, Gainesville.

Ross M.A. and Mehta A.J. (1990). Fluidization of soft estuarine muds by waves. In: The Microstructure of Fine-Grained Sediments: From Mud to Shale, Ch. 19, R.H. Bennett ed., Springer-Verlag, New York, 185-191.

Sharma J.N. and Dean R.G. (1979). Development and evaluation of a procedure for simulating a random directional second order sea surface and associated wave forces. Ocean Engrg. Rept. No. 20, Dept. of Civil Engrg., Univ. of Delaware, Newark.

Shibayama T., Aoki T. and Sato S. (1989). Mud mass transport due to waves: a visco-elastic model. Proceedings of the 23rd Congress of I.A.H.R., Ottawa, Canada, B567-B574.

Sills G.C. and Elder D. McG. (1986). The transition from sediment suspension to settling bed. In: Estuarine Cohesive Sediment Dynamics, A.J. Mehta ed., Springer-Verlag, Berlin, 192-205.

Srivastava M. (1983). Sediment deposition in a coastal marina. Rept. UFL/COEL/MP-83/1, Coastal and Oceanographic Engineering Dept., Univ. of Florida, Gainesville.

Suhayda J.N. (1986). Interaction between surface waves and muddy bottom sediments. In: Estuarine Cohesive Sediment Dynamics, A.J. Mehta ed., Springer-Verlag, Berlin, 401-428.

Tubman M.W. and Suhayda J.N. (1976). Wave action and bottom movements in fine sediments. Proceedings of the 15th Coastal Engineering Conference, Vol. 3, American Society of Civil Engineers, New York, 1168-1183.

van Rijn L.C. (1985). The effect of waves on kaolinite/sand beds. Rept. M2060, Delft Hydraulics, Delft, The Netherlands.

Wells J.T. and Kemp G.P. (1986). Interaction of surface waves and cohesive sediments: field observations and geologic significance. In: Estuarine Cohesive Sediment Dynamics, A.J. Mehta ed., Springer-Verlag, Berlin, 43-65.

Wiegel R.L. (1964). Oceanographical Engineering, Prentice-Hall, Englewood Cliffs, NJ.

Williams D.J.A. and Williams P.R. (1989a). Rheology of concentrated cohesive sediments. Journal of Coastal Research, Special Issue No. 5, 165-173.

Williams P.R. and Williams D.J.A. (1989b). Rheometry for concentrated cohesive suspensions. Journal of Coastal Research, Special Issue No. 5, 151-164.

APPENDIX A

INFLUENCE OF WATER LEVEL ON MUD AREA SUBJECT TO RESUSPENSION

The area of mud zone in Lake Okeechobee subject to wave resuspension was calculated as a function of the lake water level. A rectangular computational domain was selected including the entire lake (Fig 3a). The domain was divided into 58 by 64 square grid cells of sides dx = dy = 1 km. Depth values at grid intersections were obtained from a survey taken in the summer of 1989 (Ahn, 1989). A representative depth for each cell was computed as the average of the depths at the four intersection points of the cell.

Mud thickness in the lake is highly variable (Fig. 3b). For the present purpose the muddy zone was considered to be that zone having mud thickness in excess of 10 cm, assuming the area over which mud thickness is between 0 and 10 cm to be too thin and patchy to contribute measurably to resuspended sediment mass. The total effective mud area of this lake under this assumption is 528 km^2.

The critical erosional depth, H_c, over mud bottom in the lake was considered to be 3.4 m. In other words, that portion of the mud bottom over which the actual depth at a given water level is greater than H_c, no erosion can be considered to take place. The value of H_c of course depends on the wave characteristics (height and period), the bed resistance coefficient and the critical bed shear stress for erosion. Since in general wave characteristics vary with wind speed and direction, and with bottom conditions, a unique value of H_c can not be considered to exist for the lake. In addition, the bottom resistance coefficient and the critical bed shear stress also depend on the composition and form of the mud surface. For the present limited purposes however, it was considered sufficient to select representative values of wave and bottom related parameters in order to obtain a single representative value of H_c. Therefore, a wave height of 0.6 m, period of 3 s (Ahn, 1989), Manning's bed resistance coefficient n = 0.011 corresponding to a smooth

cohesive bed (Dixit, 1982), and a critical bed shear stress of 0.5 N/m^2 (Hwang, 1989) were selected. The selected wave height and period may be considered to represent moderately strong storm wave conditions in the lake. The value of H_c = 3.4 m was derived using linear wave theory following standard approach (Jonsson, 1966).

The number N of mud bottom cells whose depths were less than H_c was obtained at different water levels in increments of 0.5 m between +1.5 m and -1.0 m relative to NGVD datum. The total erosional area of muddy zone was then approximated as N·dx·dy. Results are given in the following table:

Table A.1 Variation of erodible mud area with relative water level.

Relative water level (m)	Erosional mud area (km^2)
-1.0	528
-0.5	528
0.0	471
0.5	237
1.0	97
1.5	48

APPENDIX B
OPERATION OF THE ACCELEROMETER

It was required to calibrate the Entran (Model EGA2-C-5DY) biaxial accelerometer and to provide a suitable mount for deploying the device. Calibration was carried out with a static arrangement followed by a dynamic check, as briefly noted below.

The accelerometer uses a Wheatstone bridge arrangement consisting of semiconductor strain gages. These gages are bonded (two on each side) to a simple cantilever beam which is end loaded with a small mass. Under acceleration, a "g" force is created by the mass, which in turn causes a bending moment to the beam. The strain due to the moment results in a bridge imbalance. With an applied voltage, this imbalance produces a millivolt (mV) deviation at the bridge output, which is proportional to the acceleration vector. The x- and y-channels have an acceleration range from -5g to 5g.

The static calibration procedure consisted of tilting the accelerometer at different angles in the -90 to 90 degree range with respect to the vertical, unstrained position (0 degree) of the mass below the beam. The voltage was set equal to zero in the unstrained position, and the millivolt output (mV) at other angles, θ, was measured. The calibration plot consisted of the relationship between the acceleration component $g\sin\theta$ and the corresponding mV for both the channels. The responses were found to be linear, and can be described by the equations:

$$a_x = -1.98976\ \text{mV} + 4.9745 \qquad \text{(B-1)}$$

$$a_y = 2.0772\ \text{mV} - 5.2401 \qquad \text{(B-2)}$$

where a_x and a_y are the accelerations in m/s^2.

The dynamic check involved testing the device in a wave flume in the Coastal Engineering Laboratory. The accelerometer was embedded in a plexiglass "boat" shown in Fig. B.1. By gluing a styrofoam block of suitable size underneath the boat together with the accelerometer, the device was made practically neutrally

buoyant in water, and the boat was tethered between two metal frame supports via two rather loose strings running horizontally between the supports so as to allow a free play (heave and surge) of the boat in the vertical plane. On the other hand, yawing and rolling were restricted by this arrangement. Since the longitudinal axis of the boat was set in the direction of the wave motion, there was not much swaying motion, and the largely irrotational particle motion under waves did not cause too much pitching.

The actual test consisted of recording the a_x and a_y components of the acceleration of the boat orbiting under wave motion, simultaneously with the boat's orbital amplitudes visually, using vertical and horizontal scales mounted on the glass side wall of the flume (see Dixit, 1982, for a description of the flume). A series of tests were carried out at different wave frequencies. The measured horizontal displacement of the boat orbit was compared with the same quantity obtained by twice time-integrating the corresponding components of acceleration. The vertical motions were found to be too small to measure accurately.

The comparison is shown in Fig. B.2. The deviations from the 45^0 line may not indicate random error. The response of the boat may have been dependent on the wave frequency and hence on the magnitude of water displacement, although any basis for such a dependence could not be identified. Overall there seems to be an agreement between measurement and calculation. Hence Eq. B-1 was considered to be reasonable. The same was assumed to be the case with respect to Eq. B-2 in the absence of direct evidence (for or against such an assumption).

APPENDIX C
MEASUREMENT OF MUD VISCOSITY

Mud viscosity was measured using a Brookfield (Model LVT) viscometer and miniature vanes; see for example Maa (1986) for a description of the measurement procedure. The measured relationships between the applied stress and the rate of strain (shearing rate) are shown in Figs. C.1 through C.5 for five different densities of the lake mud. Within the range of shearing rates considered, all the samples indicated a distinctly pseudoplastic (shear thinning) behavior. For shearing rates exceeding around 2 to 4 s^{-1}, the linear part of the relationship implies a constant viscosity. Conveniently referring to this viscosity as μ_H at "high" shearing rates, these viscosities (relative to the viscosity of water at 22 ^{0}C) are plotted against the mud density, ρ_2, in Fig. C.6. Note the two orders of magnitude increase in the relative viscosity over a small increase in density from 1 to about 1.02 g/cm^3. Over the subsequent range of density up to 1.1 g/cm^3 the increase in relative viscosity is observed to have been less significant.

Any interpretation of data obtained using vanes, in terms of a relationship between viscosity and the structure of the sediment aggregate matrix must be treated with circumspection, since vanes, by their very presence, break up the sediment matrix at the cylindrical surface determined by the vane dimensions (Williams and Williams, 1989b). Furthermore, viscosity is not characterized by density in a unique sense, insofar as viscosity and density are independent physical properties of fluids. Nevertheless the observed trend does seem to suggest a rather significant influence of sediment packing, as reflected by the bulk density, on the dynamic viscosity. At densities less than about 1.02 g/cm^3 the aggregate structure rapidly became tightly packed with increasing density. However, further increase in density apparently did not drastically alter the compact arrangement attained at 1.02 g/cm^3. Since the "granular" density of the sediment was 2.14 g/cm^3, the sediment concentration

corresponding to 1.02 g/cm^3 would be 37.5 g/l. The corresponding volume fraction would be 0.014. It is conceivable that this volume fraction approximates the so-called critical volume fraction above which the rigidity of the aggregate matrix, as reflected by the shear modulus of elasticity, increases rapidly (Williams and Williams, 1989a).

Typical rates of shearing in mud are lower than that for which the viscosity-density relationship at "high" rate of shearing in Fig. C.6 (Maa and Mehta, 1987). In fact in the present application the rate of shearing averaged over mud thickness (considering it to be representative of local rate of shearing) was well below 1 s^{-1}, closer to 0.1-0.2 s^{-1}. In order to estimate the viscosity, μ_L, at such low rates of shearing, a tangent was drawn through the data points at low shearing rates as illustrated in Fig. C.3. Viscosities calculated in this way from the tangent slope are also plotted against the corresponding mud density in Fig. C.6. In general these viscosities are an order higher in magnitude than μ_H values at the same value of density, but show the same general trend with respect to density change as μ_H. This similarity in trend reinforces the earlier surmised influence of density in governing the packing arrangement of the sediment aggregates.

APPENDIX D
INVISCID-VISCID FLOW PROBLEM SOLUTION

The solution to Eqs. 6 through 9, given boundary conditions 10a through 10d proceeds as follows:

We begin by assuming the following harmonic solutions for $\tilde{\eta}_1$, $\tilde{u}_1$, $\tilde{\eta}_2$ and $\tilde{u}_2$ according to:

$$\tilde{\eta}_1 = A \exp[i(\tilde{k}\tilde{x} - \tilde{t})] \tag{D-1a}$$

$$\tilde{u}_1 = B \exp[i(\tilde{k}\tilde{x} - \tilde{t})] \tag{D-1b}$$

$$\tilde{\eta}_2 = C \exp[i(\tilde{k}\tilde{x} - \tilde{t})] \tag{D-1c}$$

$$\tilde{u}_2 = D \cdot E(z) \exp[i(\tilde{k}\tilde{x} - \tilde{t})] \tag{D-1d}$$

where $\tilde{k} = kH_1$ is the dimensionless wave number, and B, C, D and E(z) are unknown coefficients representing the amplitudes of $\tilde{u}_1$, $\tilde{\eta}_2$ and $\tilde{u}_2$, respectively. The amplitude of $\tilde{u}_2$ is treated as having a z-independent part, D, and a z-dependent part, E. These coefficients are evaluated by substitution in Eqs. 6 through 9 together with the boundary conditions, Eq. 10.

From Eqs. 6, D-1a, b we obtain

$$B = A \frac{\tilde{k}}{F_r^2} \tag{D-2}$$

Eqs. 7, D-1a, b, c and D-2 yield

$$C = A \left(1 - \frac{\tilde{k}^2}{F_r^2}\right) \tag{D-3}$$

From Eqs. 8, D-1a, b, c, d, D-2, and D-3 we obtain

$$D \left(\frac{1}{Re} \tilde{E}'' + i \tilde{E}\right) = iA \frac{\tilde{k}}{F_r^2} \left(1 - r \frac{\tilde{k}^2}{F_r^2}\right) \tag{D-4}$$

where $\tilde{E}'' = \partial^2\tilde{E}/\partial\tilde{z}^2$. Next we let

$$G = iA\frac{\tilde{k}}{F_r{}^2}\left(1-r\,\frac{\tilde{k}^2}{F_r{}^2}\right) \tag{D-5}$$

and further let

$$D = Re\ G \tag{D-6}$$

Hence

$$\tilde{E}'' + iRe\ \tilde{E} = 1 \tag{D-7}$$

which can be readily solved to yield

$$\tilde{E} = -\frac{i}{Re} + M_1\cosh(m\tilde{z}) + M_2\sinh(m\tilde{z}) \tag{D-8}$$

where

$$m = (1-i)\left(\frac{Re}{2}\right)^{1/2} = \left(\frac{Re}{i}\right)^{1/2} \tag{D-9}$$

Now the conditions 10c and 10d, respectively, yield

$$M_1 = \frac{i}{Re} \tag{D-9a}$$

$$M_2 = -M_1\tanh(m\tilde{H}_2) \tag{D-9b}$$

Hence D-8a becomes

$$\tilde{E} = -\frac{i}{Re}\left[1-\cosh(m\tilde{z}) + \tanh(m\tilde{H}_2)\cdot\sinh(m\tilde{z})\right] \tag{D-10}$$

Next, from Eq. 9,

$$\frac{1}{\tilde{k}} = \frac{D}{C}\int_0^{\tilde{h}} \tilde{E}\ d\tilde{z} \tag{D-11}$$

Substituting D-10 into D-11 and carrying out the integration yields

$$\frac{1}{\tilde{k}} = -\frac{D}{C}\frac{i}{Re}\left\{\tilde{h} + \frac{\tanh(m\tilde{H})[\cosh(m\tilde{h})-1] - \sin(m\tilde{h})}{m}\right\} \tag{D-12}$$

Next we introduce the linearizing approximation $\tilde{h} \simeq \tilde{H}_2$, since $\tilde{\eta}_2$ is small. Then, simplifying D-12 and substituting for C and D from D-3 and D-6 gives

$$\left(\frac{1}{\tilde{k}}\right)^2 = \frac{\tilde{H}_2}{F_r^2} \frac{\left(1-r\,\frac{\tilde{k}^2}{F_r^2}\right)}{\left(1-\frac{\tilde{k}^2}{F_r^2}\right)} \cdot \Gamma \qquad \text{(D-13a)}$$

where

$$\Gamma = 1 - \frac{\tanh(m\tilde{H}_2)}{m\tilde{H}_2} \qquad \text{(D-13b)}$$

Solving for $\tilde{k}/F_r$

$$\frac{\tilde{k}}{F_r} = \left\{\frac{1 + \tilde{H}_2\Gamma \pm [(1 + \tilde{H}_2\Gamma)^2 - 4r\tilde{H}_2\Gamma]^{1/2}}{2r\tilde{H}_2\Gamma}\right\}^{1/2} \qquad \text{(D-14a)}$$

Thus

$$\frac{\tilde{k}}{F_r} = f(\tilde{H}_2, r, Re) \qquad \text{(D-14b)}$$

i.e. $\tilde{k}$ depends on H_2, r, Re and F_r and, further, the wave number, k, also varies with water depth H_1. The two solutions for the dimensionless wave number $\tilde{k}$ from Eq. D-14a correspond to the + and - signs; + sign corresponding to a larger amplitude at the interface relative to that at the surface, and - sign corresponding to the opposite case. We proceed with the latter, since selection of the former would violate conservation of energy. For this situation, coefficients B, C and D are obtained from D-2, D-3, D-5 and D-6; hence $\tilde{\eta}_1$, $\tilde{\eta}_2$, $\tilde{u}_1$ and $\tilde{u}_2$ can now be written as

$$\tilde{\eta}_1 = A \exp[i(\tilde{k}\tilde{x} - \tilde{t})] \qquad \text{(D-15a)}$$

$$\tilde{\eta}_2 = A[1 - (\frac{\tilde{k}}{F_r})^2]\exp[i(\tilde{k}\tilde{x} - \tilde{t})] \qquad \text{(D-15b)}$$

$$\tilde{u}_1 = A \frac{\tilde{k}}{F_r^2} \exp[i(\tilde{k}\tilde{x} - \tilde{t})] \qquad \text{(D-15c)}$$

$$\tilde{u}_2 = A \frac{\tilde{k}}{F_r^2} [1-r(\frac{\tilde{k}}{F_r})^2][1 - \cosh(m\tilde{z}) + \tanh(m\tilde{H}_2)$$

$$\sinh(m\tilde{z})]\exp[i(\tilde{k}\tilde{x} - \tilde{t})] \qquad \text{(D-15d)}$$

As observed $\tilde{\eta}_2$ is damped relative to $\tilde{\eta}_1$ by the multiplier $1-(\tilde{k}/F_r)^2$. Likewise, $\tilde{u}_2$ is damped relative to $\tilde{u}_1$ by the two multipliers of $A\tilde{k}/F_r^2$ (amplitude of $\tilde{u}_1$) in D-15d.

Next we seek the dispersion relationship from the real part, k_r, of the wave number k, and an expression for the wave attenuation coefficient k_i, the imaginary part of k. Surface wave attenuation is then specified as $a_x = a_0\exp(-k_i x)$, where $a_0 = AH_1$, and a_x is the amplitude at a distance x. Note that with this interpretation of A, Eqs. D-15a through D-15d satisfy the boundary conditions 10b, as the wave amplitudes and corresponding velocities vanish at infinite distance (from x=0, where $a_x = a_0$). We have, by definition,

$$\tilde{k} = \tilde{k}_r + i\tilde{k}_i \qquad \text{(D-16a)}$$

and let

$$Y = (\frac{\tilde{k}}{F_r})^2 = Y_R + iY_I \qquad \text{(D-16b)}$$

and

$$\tilde{H}_2\Gamma = R + iI \tag{D-16c}$$

Hence D-14a (with - sign) becomes

$$Y = \frac{1 + R + iI - [(1 + R + iI)^2 - 4r(R + iI)]^{1/2}}{2r(R + iI)} \tag{D-17}$$

From which

$$Y_R = \frac{1}{2r(R^2 + I^2)}\{R[1+R-\cos\tfrac{\theta}{2}(p^2+q^2)^{1/4}]+ I[I-\sin\tfrac{\theta}{2}(p^2+q^2)^{1/4}]\} \tag{D-18a}$$

$$Y_I = \frac{1}{2r(R^2 + I^2)}\{R[I-\sin\tfrac{\theta}{2}(p^2+q^2)^{1/4}]- I[1+R-\cos\tfrac{\theta}{2}(p^2+q^2)^{1/4}]\} \tag{D-18b}$$

where

$$p = (1+R)^2 - 4rR - I^2 \tag{D-19a}$$

$$q = 2I(1+R - 2r) \tag{D-19b}$$

$$R = \tilde{H}_2\left[1 - \frac{\exp(4\chi) - 1 + 2\sin(2\chi)\cdot\exp(2\chi)}{2\chi[\exp(4\chi) + 1 + 2\cos(2\chi)\cdot\exp(2\chi)}\right] \tag{D-19c}$$

$$I = \tilde{H}_2\left[1 - \frac{\exp(4\chi) - 1 - 2\sin(2\chi)\cdot\exp(2\chi)}{2\chi[\exp(4\chi) + 1 + 2\cos(2\chi)\cdot\exp(2\chi)}\right] \tag{D-19d}$$

where

$$\chi = \tilde{H}_2\left(\frac{Re}{2}\right)^{1/2} = H_2\left(\frac{\sigma}{2\nu}\right)^{1/2} \tag{D-19e}$$

Then, from D-16a, D-16b, D-18a and D-18b we obtain

$$\tilde{k}_r = \{\tfrac{1}{2} F_r^2[(Y_R + Y_I)^{1/2}] - Y_R\}^{1/2} \tag{D-20}$$

which is the desired dispersion relationship, and

$$\tilde{k}_i = \{\frac{1}{2} F_r^2[(Y_R + Y_I)^{1/2}] - Y_R\}^{1/2} \qquad (D\text{-}21)$$

which is the desired expression for the wave attenuation coefficient.

It can be readily shown (see also D-14b) that $\tilde{k}_r/F_r$ depends on $\tilde{H}_2$, r and χ. Note that χ is mud layer thickness normalized by $(2\nu/\sigma)^{1/2}$, which is twice the thickness of the laminar, wave-induced (mud) bottom boundary layer (Dean and Dalrymple, 1984). For a selected value of r = 0.15 (e.g. corresponding to test 1), this dependence is shown in Fig. D.1 for $\tilde{H}_2$ ranging from 0.1 to 1. It is observed that for a given $\tilde{H}_2$, $\tilde{K}_r/F_r$ decreases from 1 at χ = 0, becoming practically constant above a certain χ. This trend can be easily examined, for example, for a given two layered system (H_1, H_2 fixed) subject to a wave train of given frequency (σ fixed). At χ = 0, the bottom is rigid, hence $\tilde{k}_r = F_r$ means $\sigma/k = (gH_1)^{1/2}$, which is the well known shallow water dispersion relationship. Increasing χ implies decreasing viscosity ν, hence decreasing μ, since r and, therefore, ρ_2 are held constant in this problem. Note that $\tilde{k}_r/F_r = C_0/C$, where C_0 is the rigid bottom surface wave celerity and C is celerity at any $\chi>0$. Initially, therefore, as the bottom becomes soft, the wave speed increases over that due to rigid bottom. As $\chi\to\infty$, the lower layer becomes inviscid, and the wave speed equals $[g(H_1 + H_2)]^{1/2} = [gH_1(1 + \tilde{H}_2)]^{1/2}$.

Thus, for example, given $\tilde{H}_2$ = 0.2, the ratio C_0/C will approach 0.913 as χ increases. For practical purposes, the lower layer becomes "watery" for values of χ exceeding 2 to 3, and the celerity does not change too rapidly with further increase in χ as seen from Fig. D.1.

In Fig. D.2 the normalized attenuation coefficient, $\tilde{k}_i/F_r$, is plotted against χ for values of $\tilde{H}_2$ ranging from 0.1 to 1. As before, considering a given system in which only μ is allowed to vary, we note that since $\tilde{k}_i/F_r = k_iC_0/\sigma$, Fig. D.2 essentially

shows how k_1 changes with increasing χ, starting with $\chi=0$ at which $k_1=0$ (rigid bottom case). An interesting feature of the observed variation in k_1 is the occurrence of resonance as χ approaches unity. In other words, wave damping is greatest when the mud layer thickness (H_2) equals twice the boundary layer thickness. Note that the rate of wave energy dissipation is $\rho_1 g C k_1 a_0^2 = \rho_1 g C k_1 a_0^2 \exp(-2k_1 x)$ (Dean and Dalrymple, 1984; Maa, 1986). As χ increases beyond this value, k_1 decreases and approaches zero as $\chi \to \infty$ as the lower layer also becomes inviscid. Characteristic values of χ in the present experiment were high. For example, representative parameters for test 1 are: H_2 = 0.28 m, σ = 2.51 rad/s and $\nu = 1.76 \times 10^{-3}$ m^2/s. This gives χ = 7.5, which essentially means that the mud was very soft and resonance effect was largely absent at the dominant wind wave frequency.

In Fig. D.3, the depth-variation of the velocity amplitude, u_m, is plotted corresponding to parameters from test 1, a_0 = 8 cm (a somewhat higher than typical value), and χ ranging from 0.1 to 1.5 (illustrative range). Notice the heavy damping of oscillation with decreasing χ in the fluid mud layer. By virtue of the model assumptions, no boundary layer is found in the water layer, even though the oscillation is damped with decreasing χ by virtue of the momentum coupling of the two layers. Besides the absence of boundary layer effect particularly just above the interface, the absence of velocity equality at the interface is yet another manifestation (limitation) of the assumed inviscid-viscid behavior. The outcome is suggestion of steeper gradients and hence rotationality at the interface than in reality, although laboratory measurements (Maa and Mehta, 1987) do indicate a rather drastic reduction in the mud velocity relative to that in water across a thin interfacial layer.

In Fig. D.4, the phase of u_m relative to the surface wave, η_1, is shown for χ ranging from 0.1 to 1.5. As with u_m in Fig. D.3, phase lags are significant mainly in the mud. A sharp phase discontinuity is evident at the interface due to the model assumption which leads to a corresponding discontinuity in the velocity.

APPENDIX E
MEASURED SPECTRA IN TESTS 1 AND 2

Relevant spectra for test 1 include those for wave energy (Figs. E.1 and E.2), water velocity (Figs. E.3 and E.4) and mud acceleration (Figs. E.5 and E.6). These correspond to eight data blocks (0 hr to 7 hr).

For test 2, measured spectra from data block at 1800 hr are shown only for illustration. These include wave energy (Fig. E.7), water velocities (Figs. E.8 and E.9) and mud accelerations (E.10 and E.11).

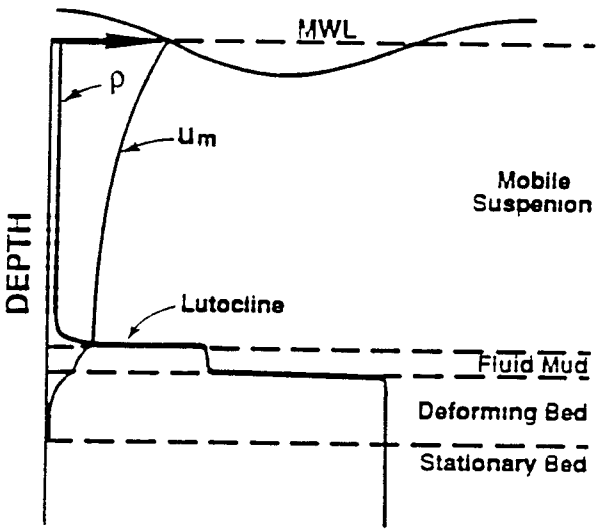

Fig. 1. Schematic of mud bottom response to waves in terms of vertical sediment density and velocity profiles (after Mehta, 1989).

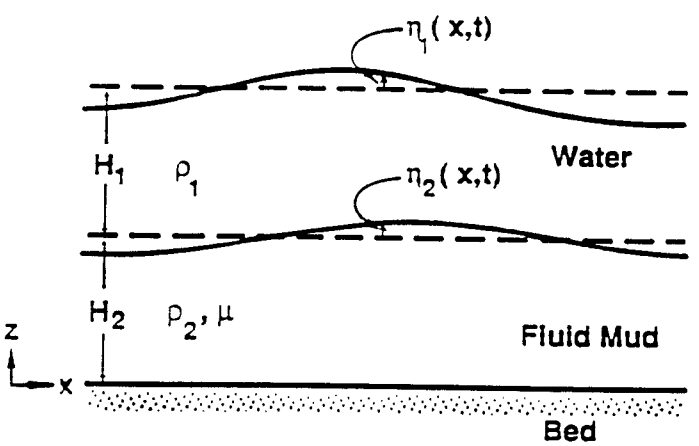

Fig. 2. Two-layered water-fluid mud system subject to progressive wave action.

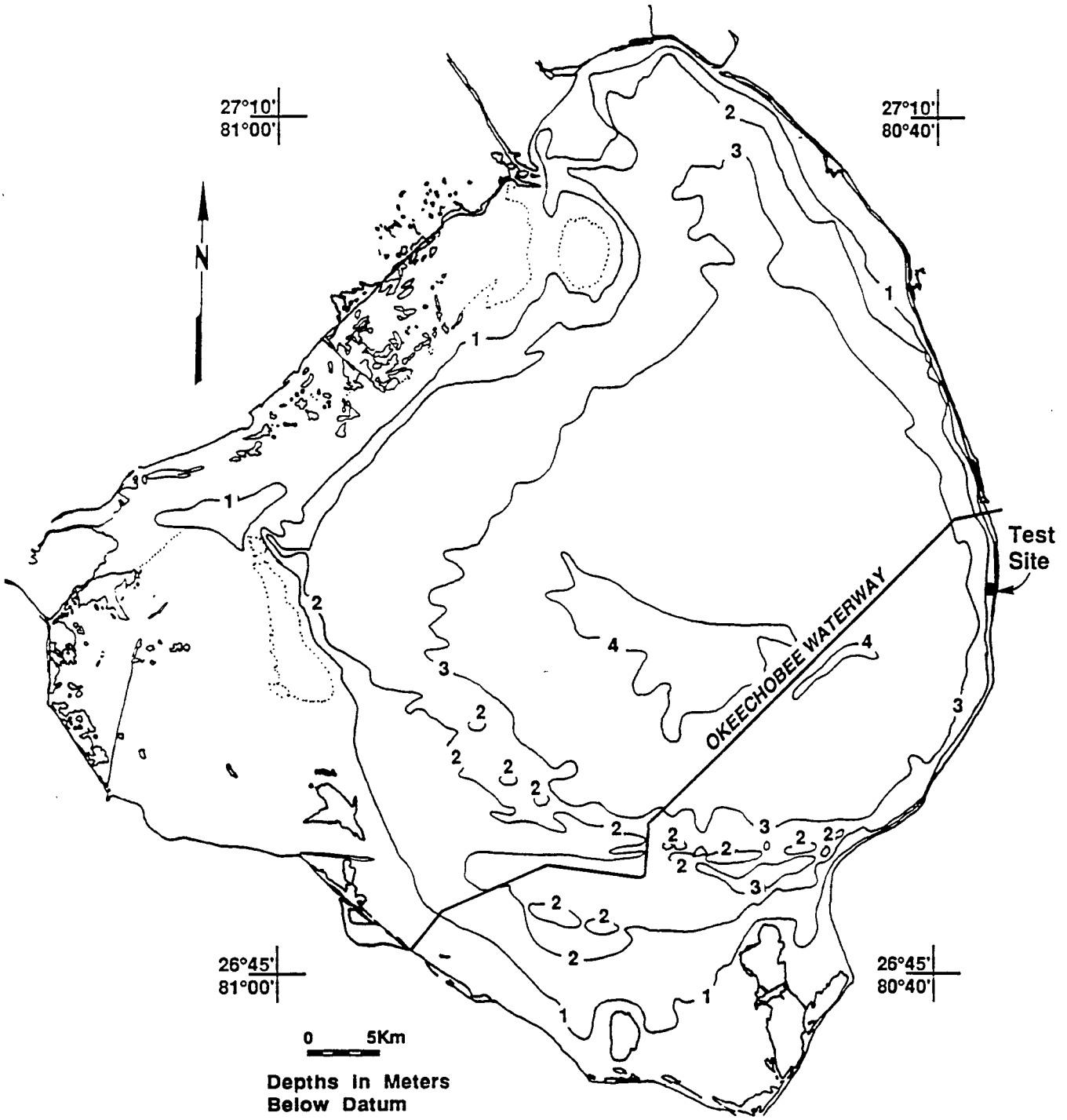

Fig. 3a. Bathymetric map of Lake Okeechobee. Depths are relative to a datum which is 3.81 m above msl (NGVD).

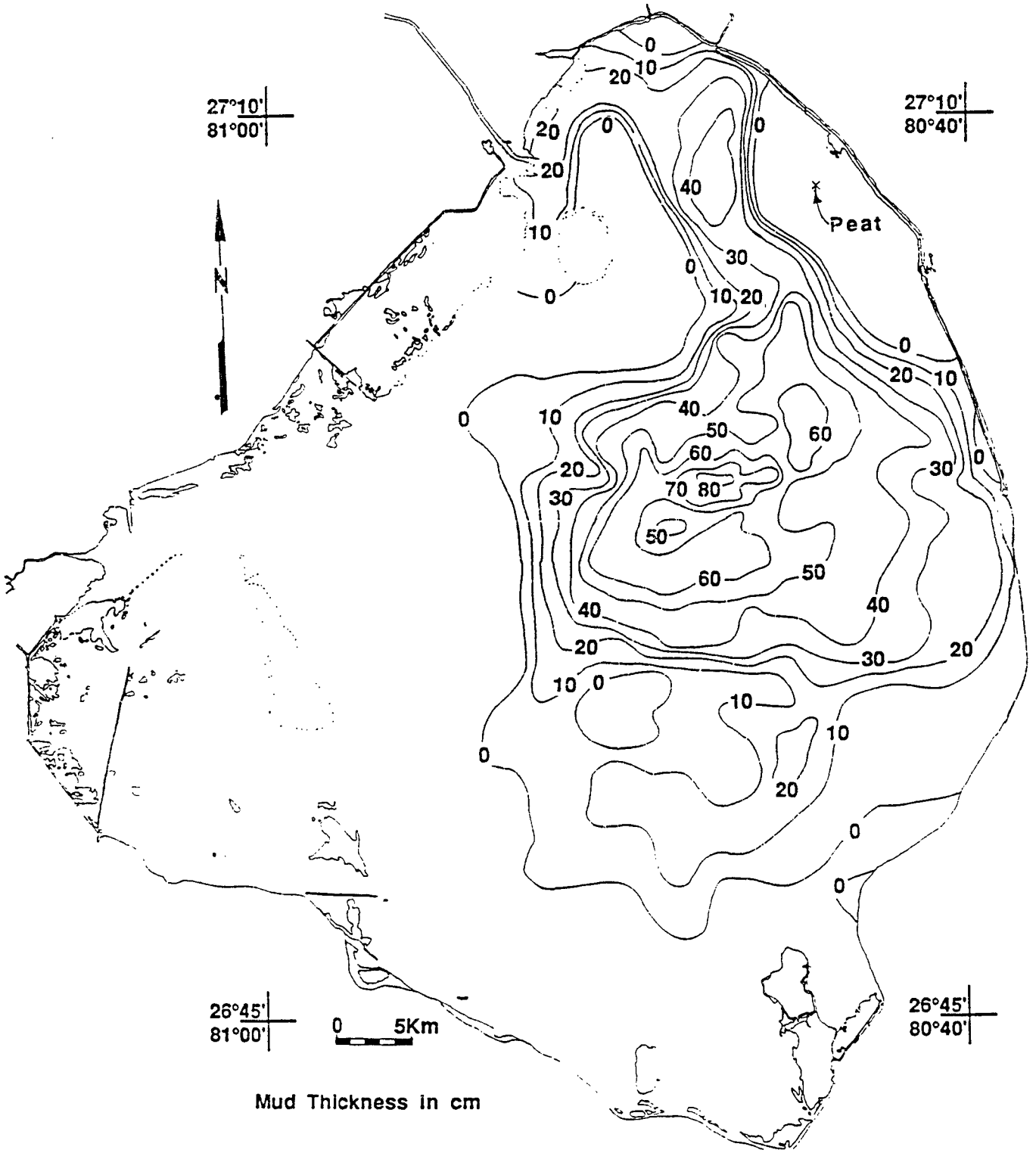

Fig. 3b. Mud thickness contour map of Lake Okeechobee (after Kirby et al., 1989).

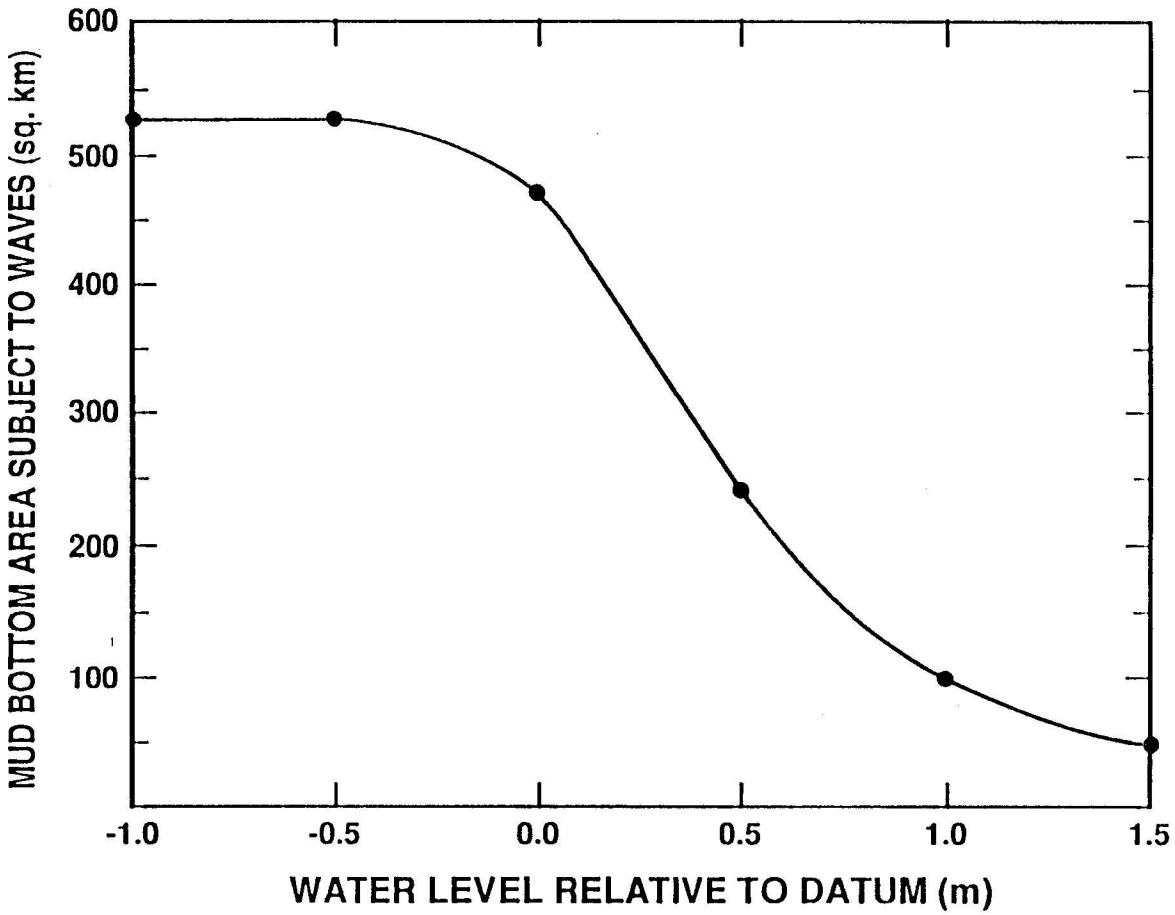

Fig. 4. Lake area with mud bottom subject to wave action as a function of water level relative to datum.

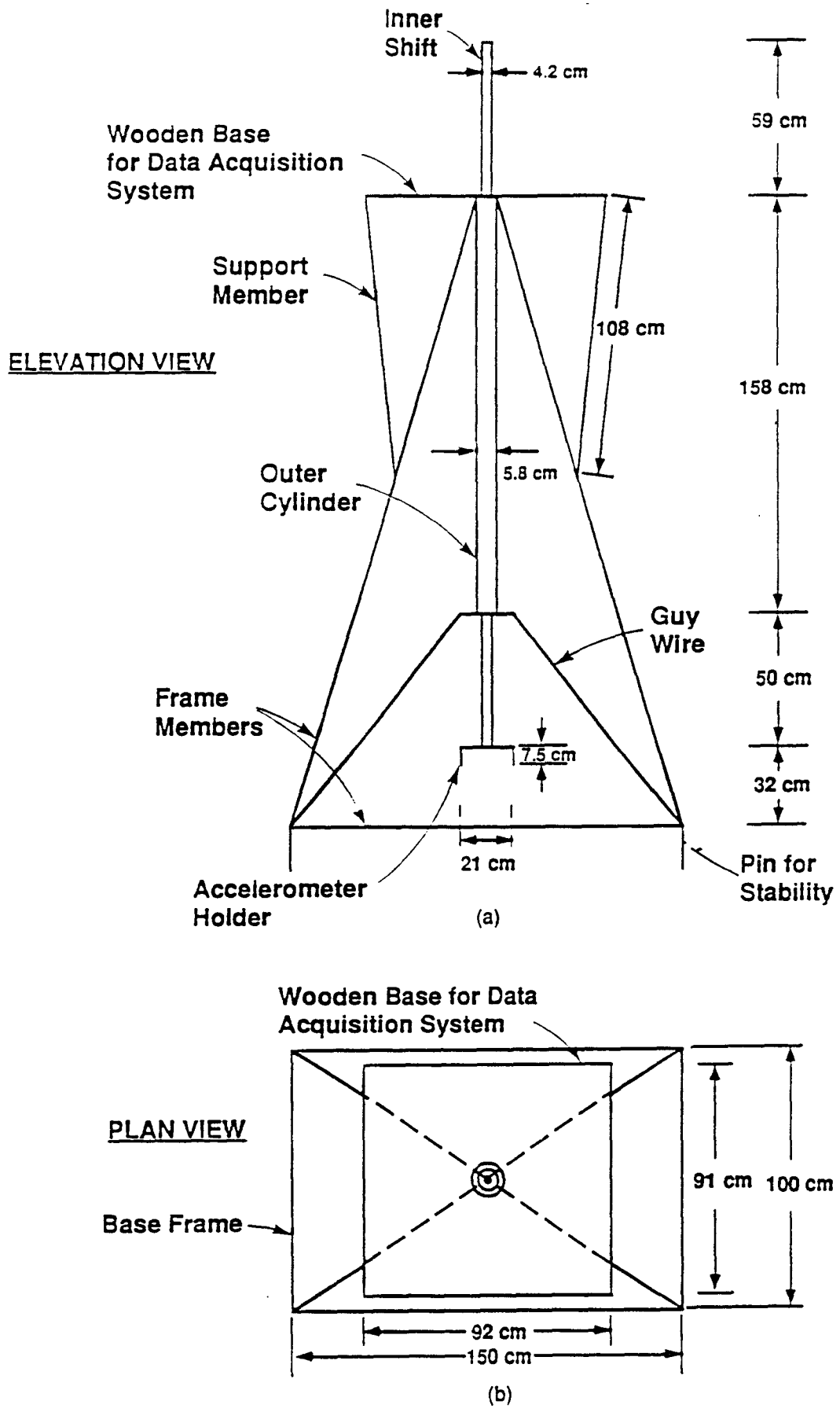

Fig. 5. Tower used in field tests: a) elevation view, b) plan view.

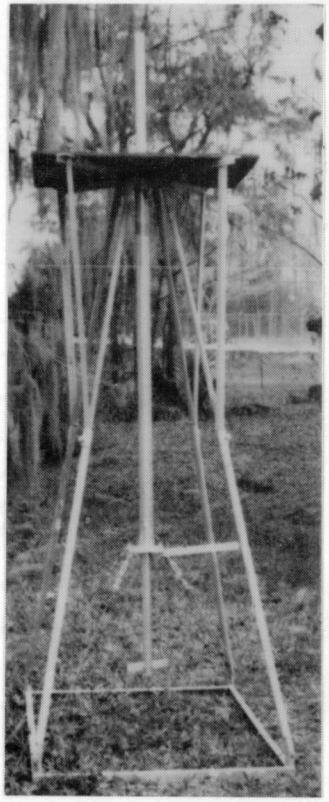

Fig. 6. A view of the field tower.

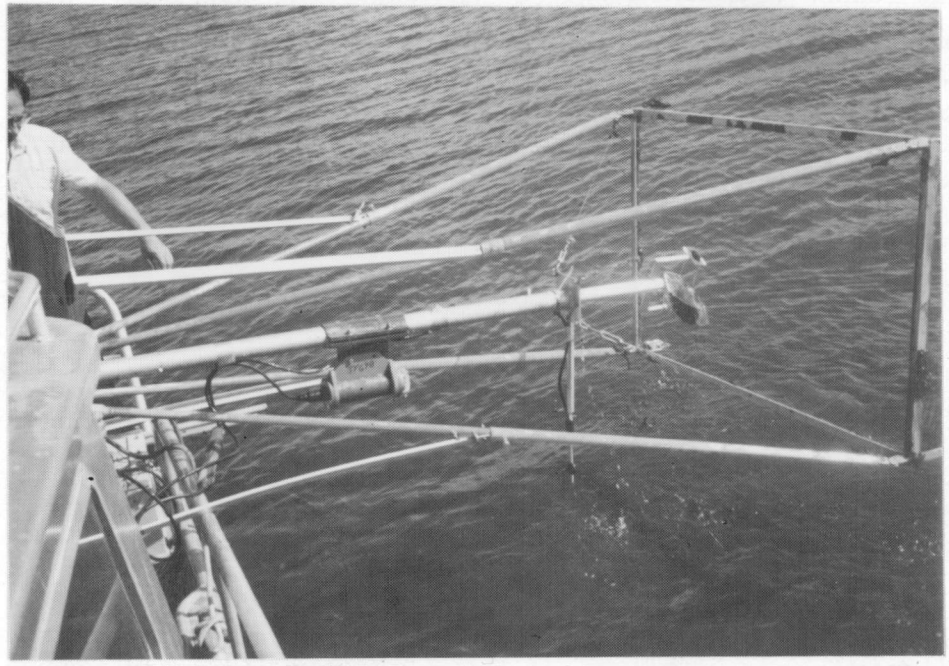

Fig. 7. Tower and instrumentation assembly begin deployed at the site.

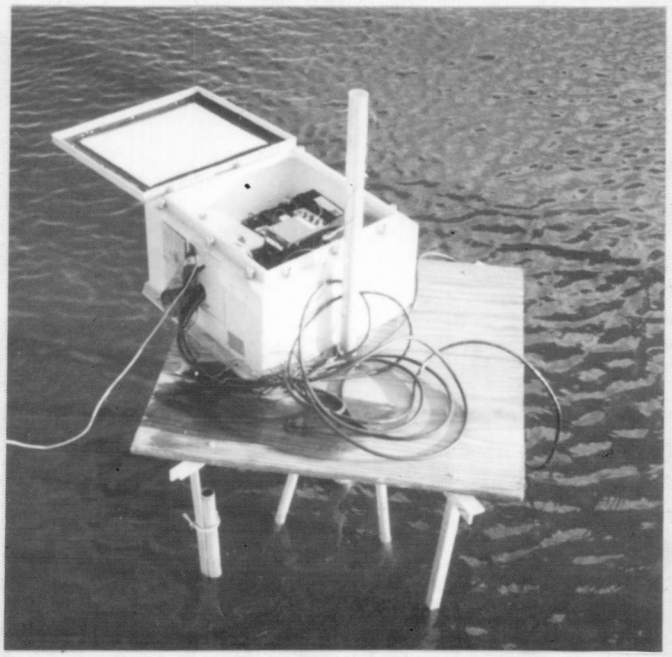

Fig. 8. Measurement system in place together with data acquisition system.

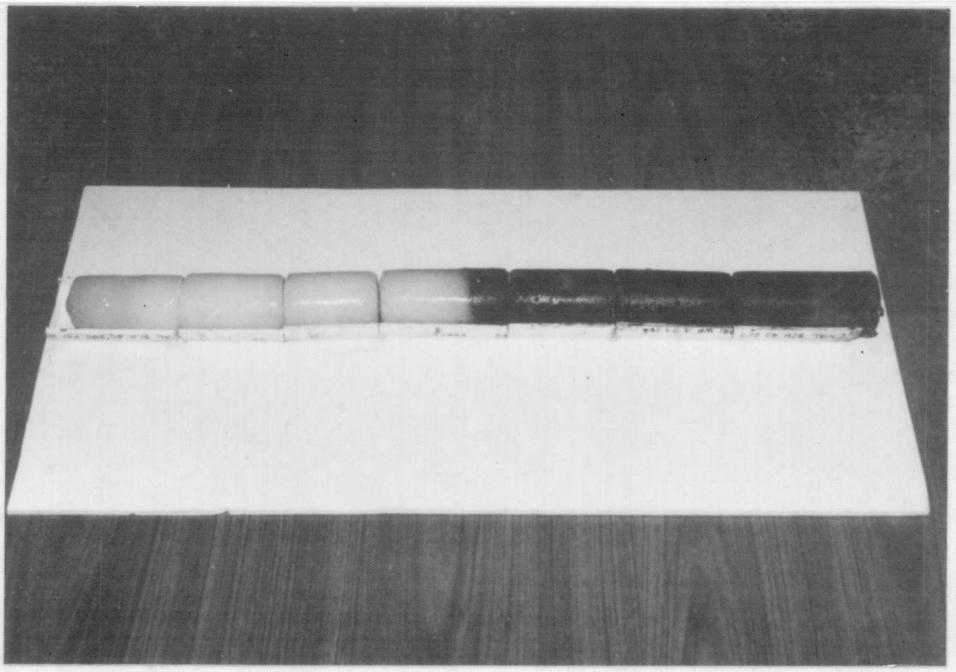

Fig. 9. Bottom core from test 1 is frozen in a mixture of dry ice and alcohol and cut into 6-8 cm long pieces. Note the clearly defined mud-water interface.

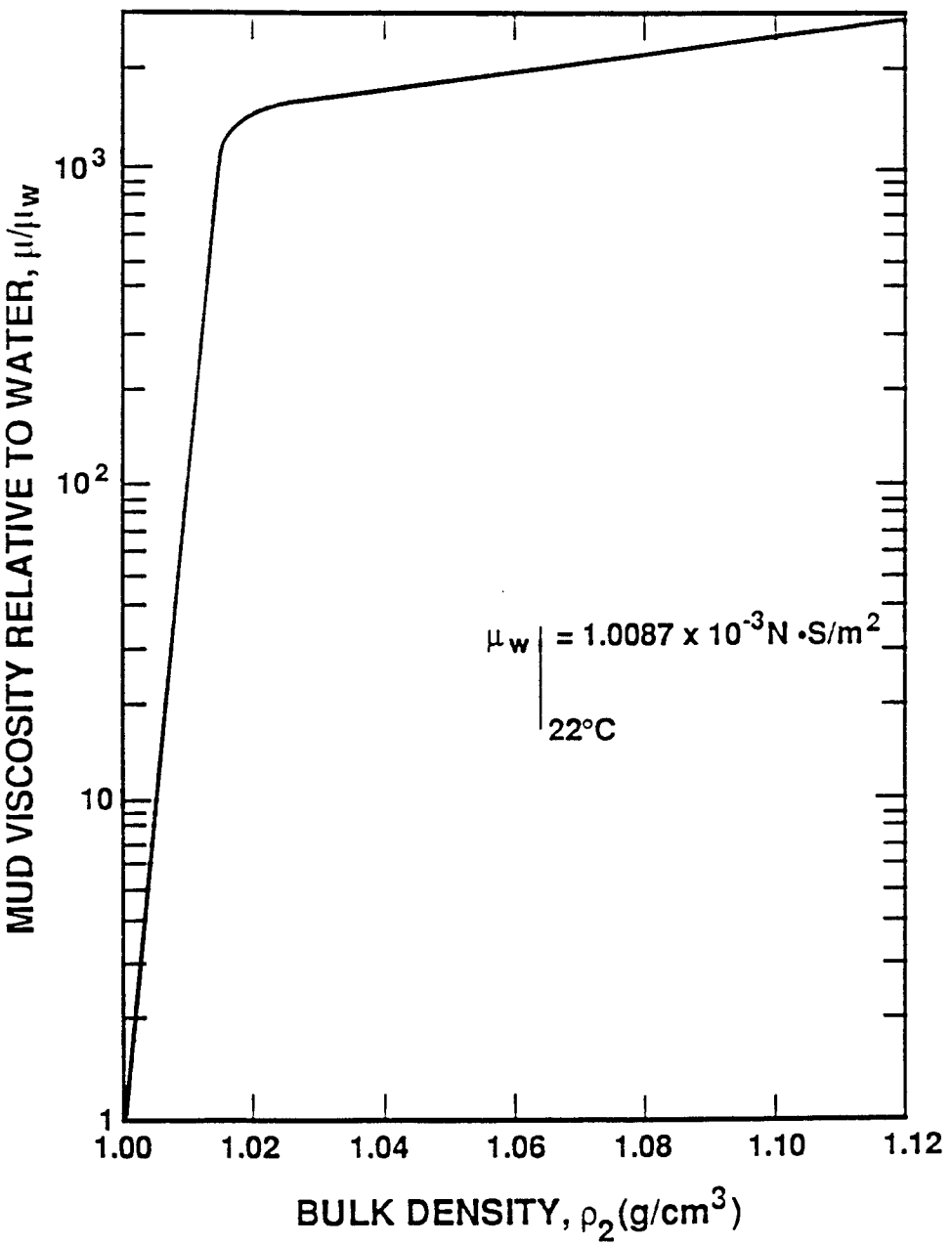

Fig. 10. Relationship between dynamic viscosity and density for Okeechobee mud.

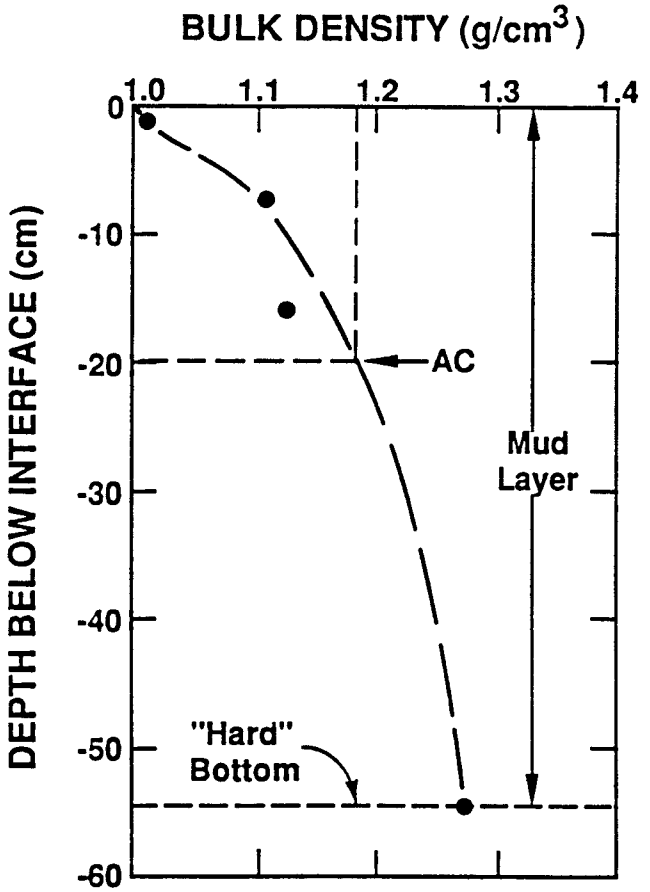

Fig. 11a. Mud density profile at the site during test 1.

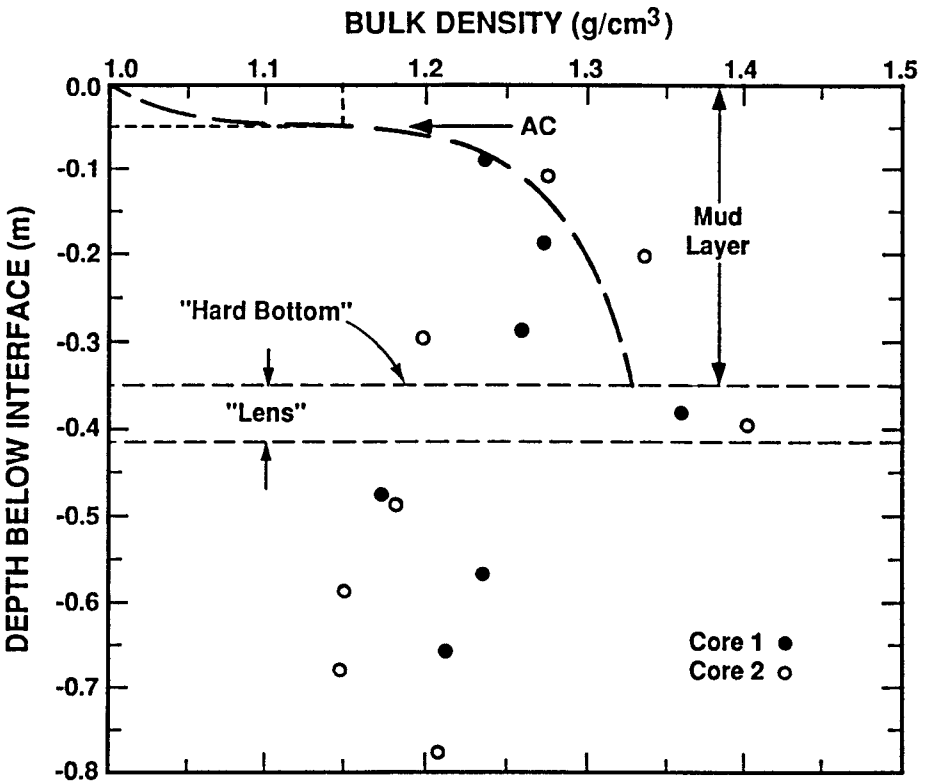

Fig. 11b. Mud density profiles at the site during test 2.

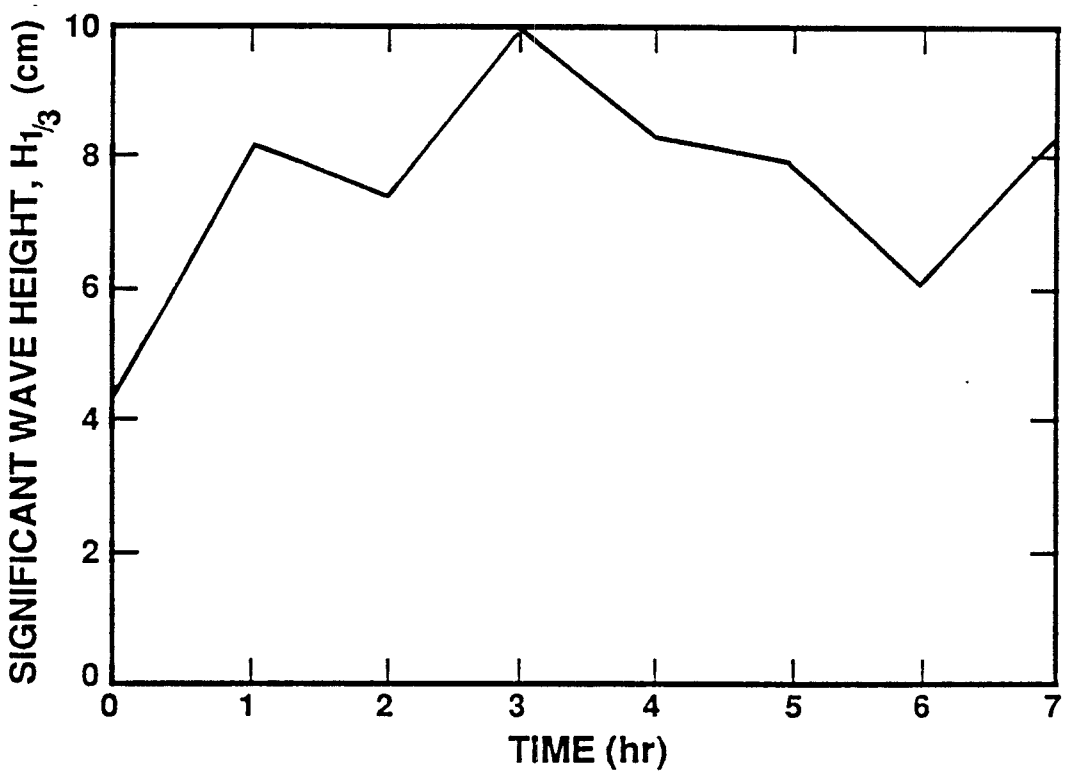

Fig. 12a. Variation of significant wave height during test 1.

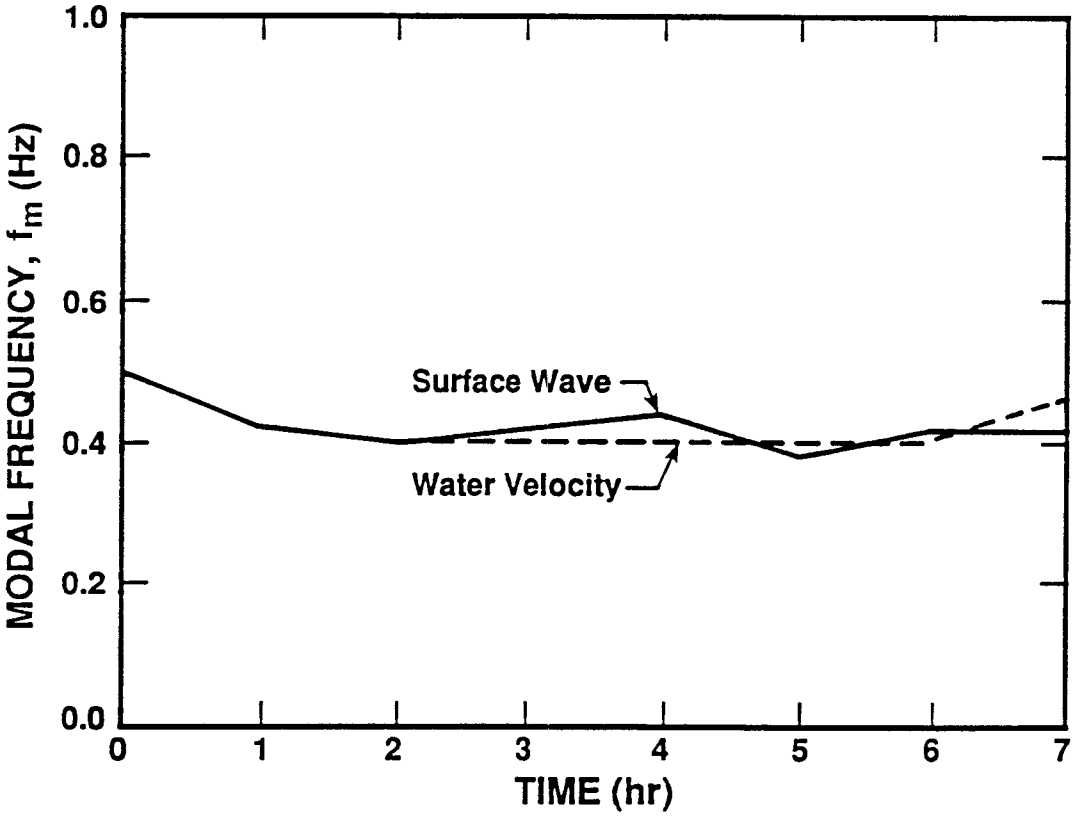

Fig. 12b. Variation of modal wave frequency during test 1.

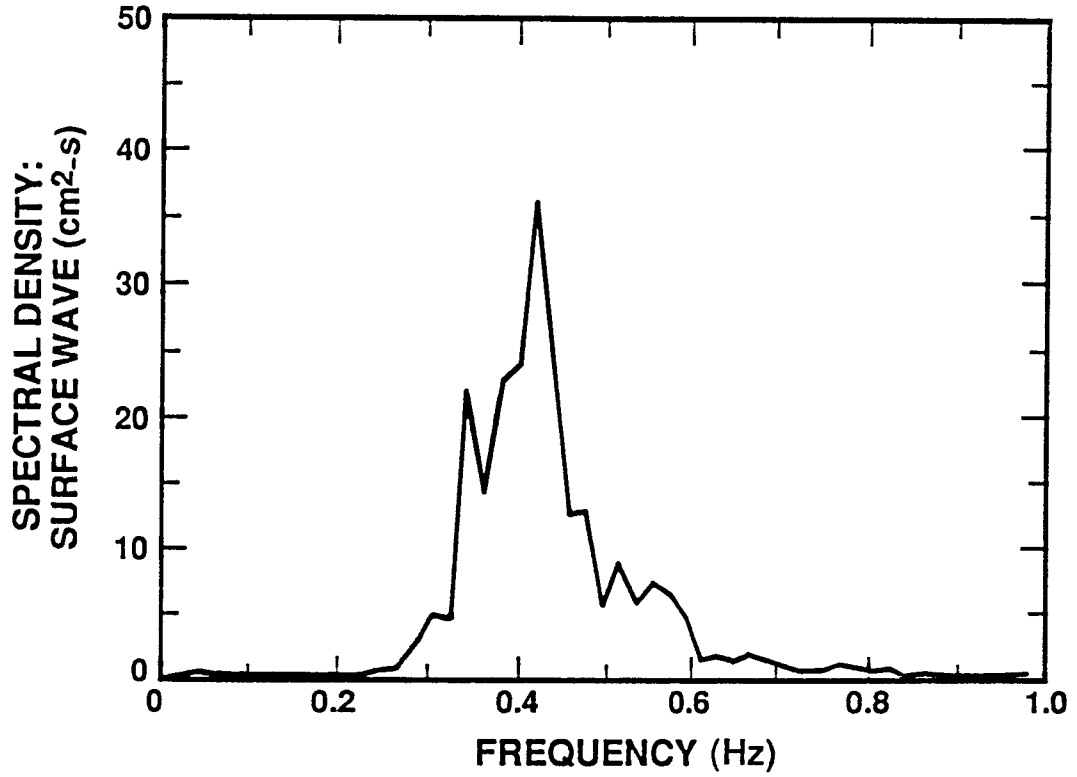

Fig. 13a. Wave energy spectrum at 1 hr, test 1.

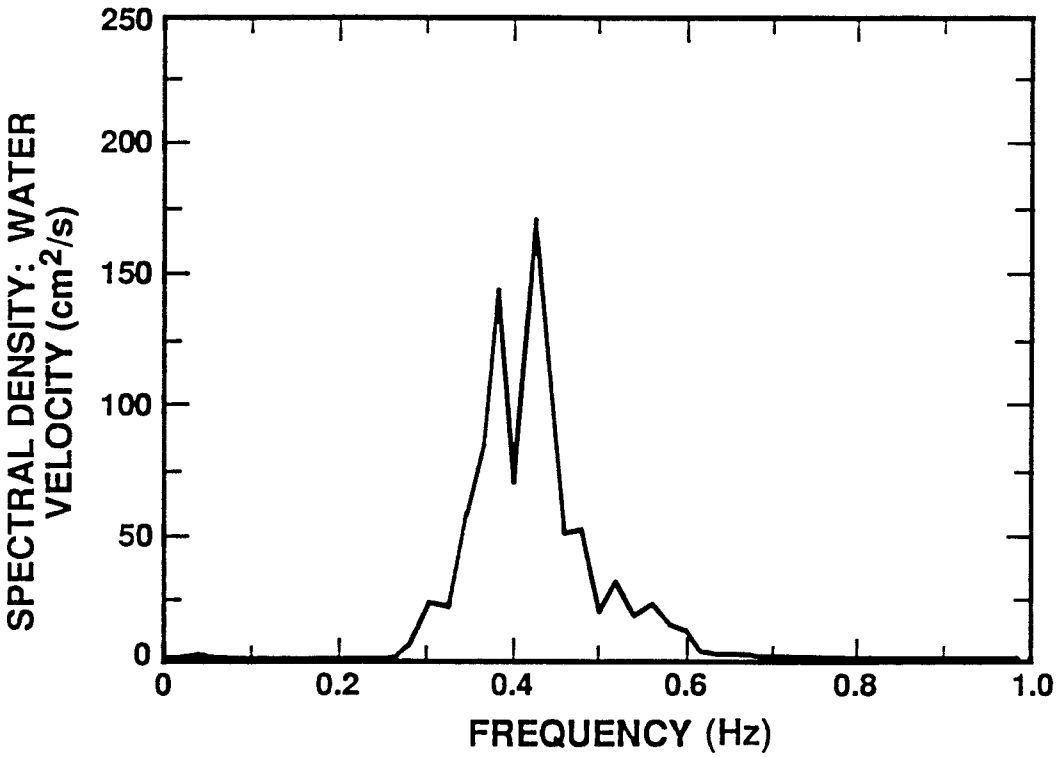

Fig. 13b. Water velocity spectrum at 1 hr, test 1.

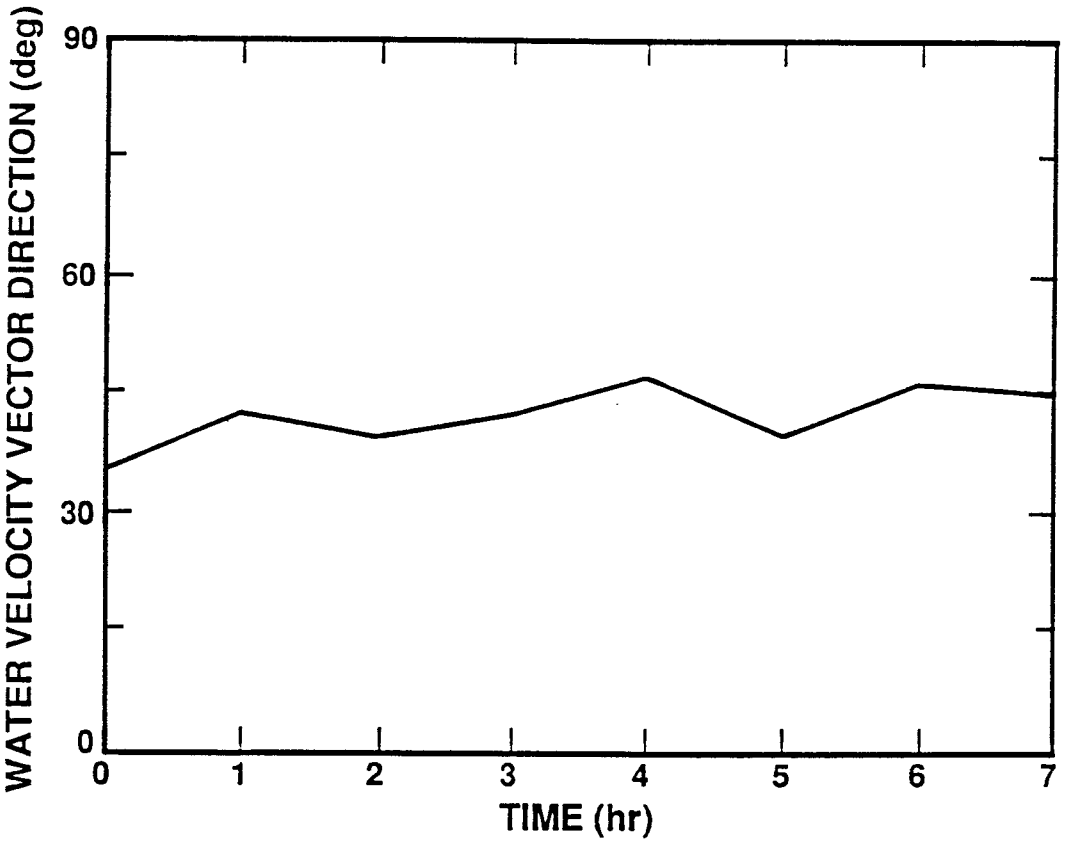

Fig. 14. Variation of relative direction of water velocity during test 1.

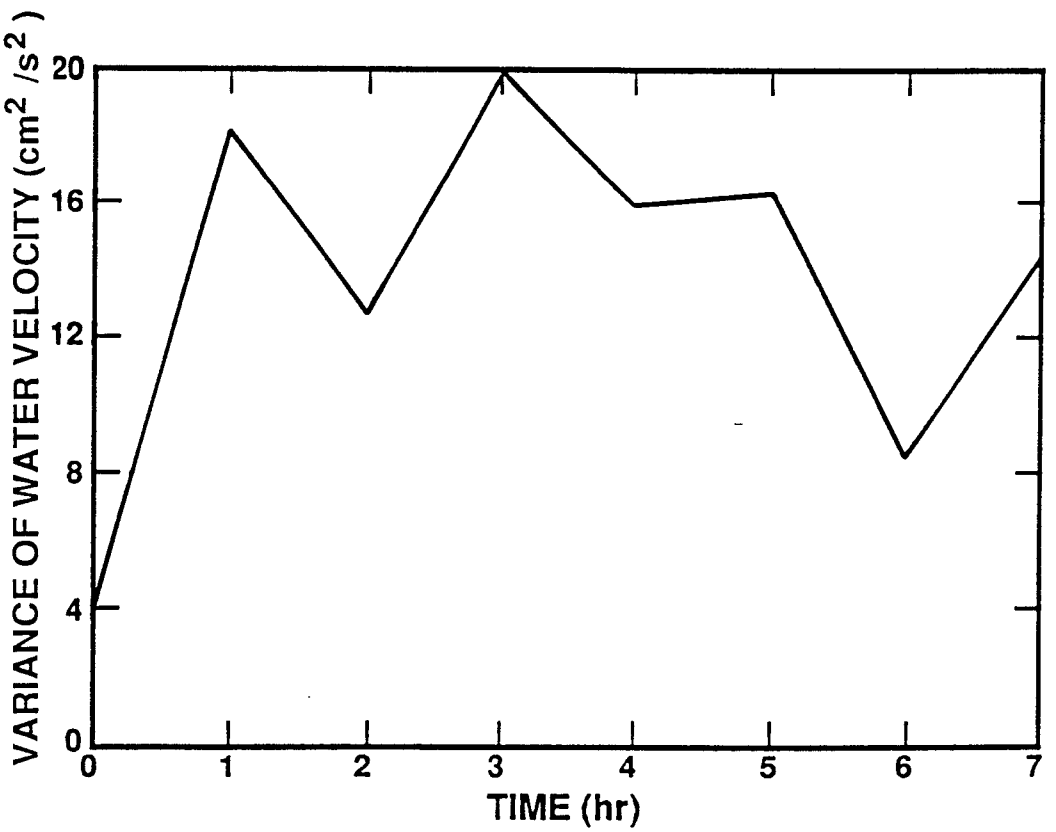

Fig. 15. Time-variation of water velocity amplitude variance during test 1.

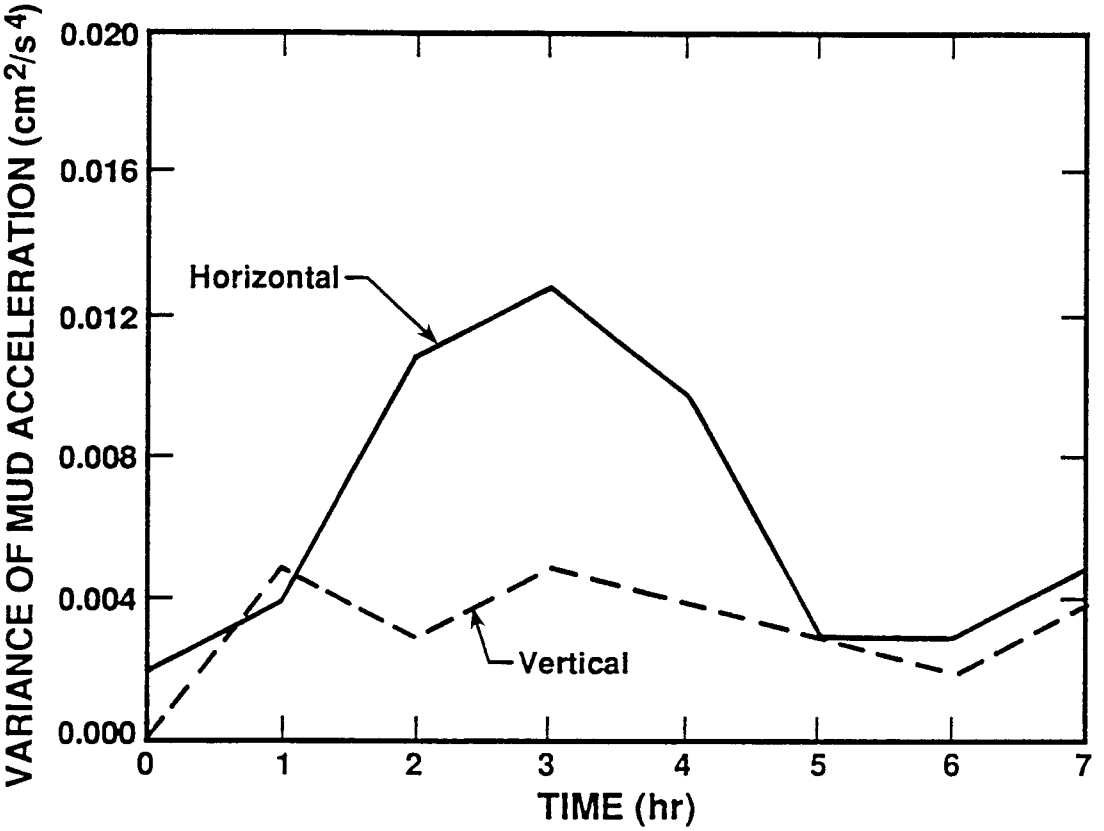

Fig. 16a. Time-variations of the variances of horizontal and vertical mud accelerations during test 1.

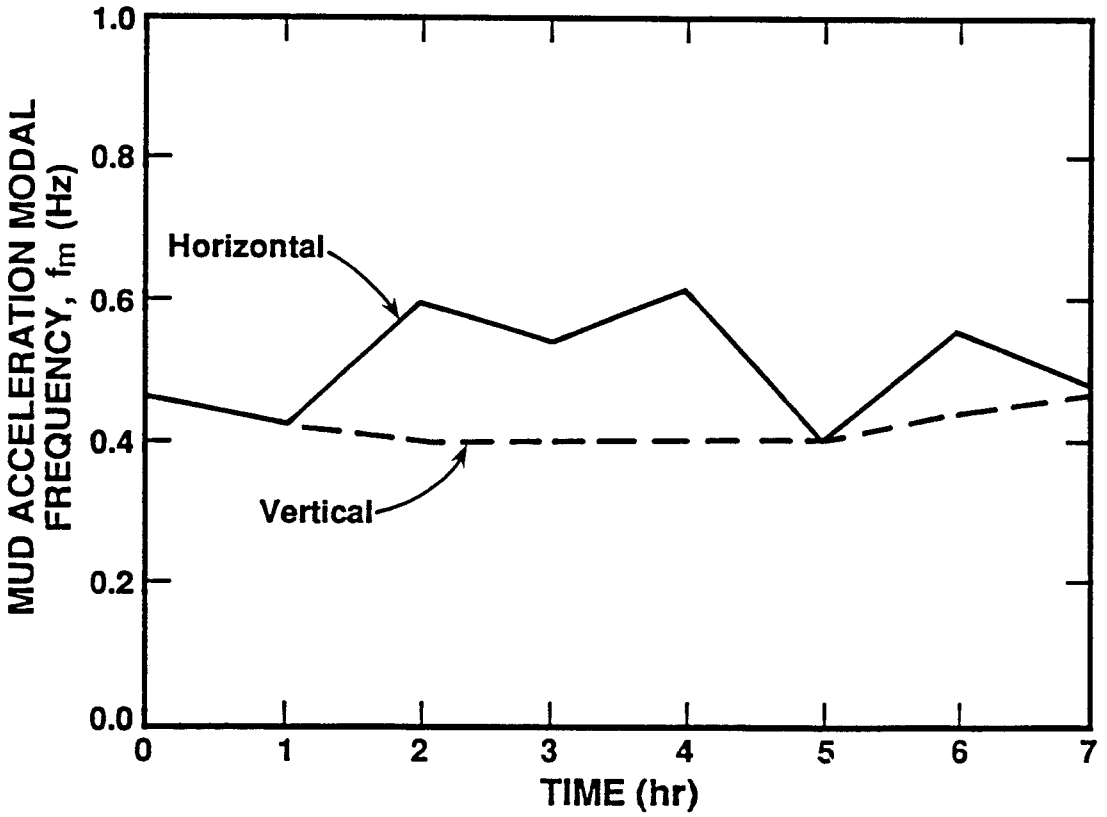

Fig. 16b. Variations of modal frequencies of horizontal and vertical mud accelerations during test 1.

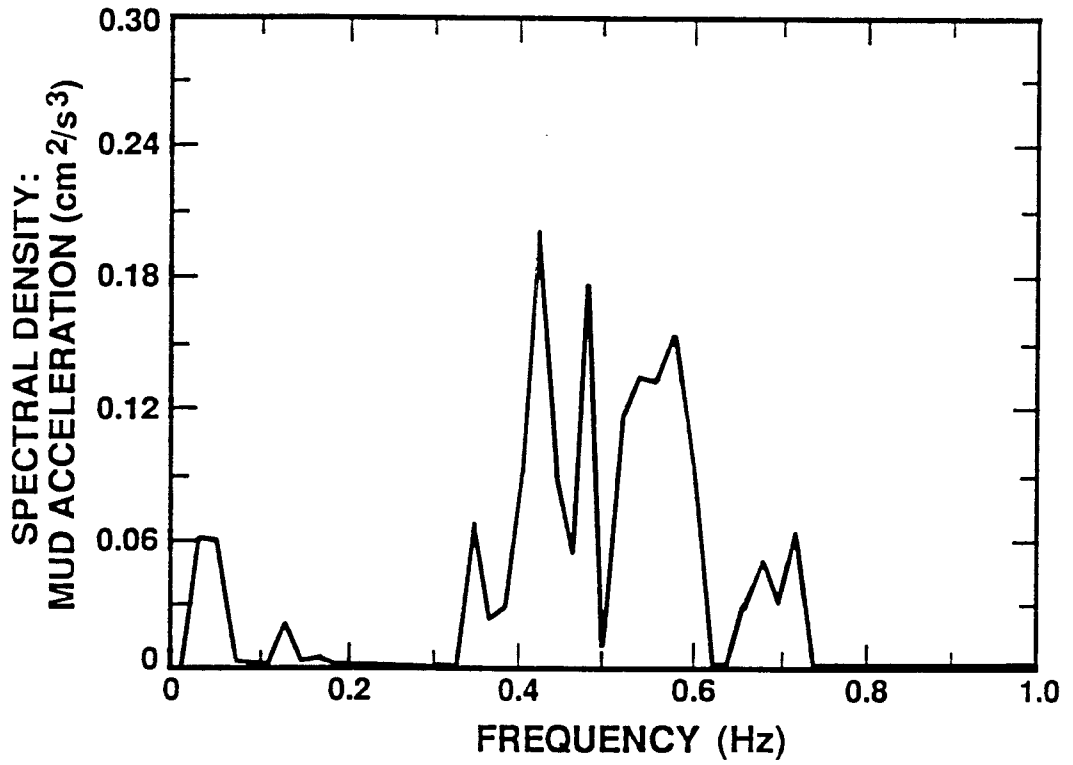

Fig. 16c. Horizontal mud acceleration spectrum at 1 hr, test 1.

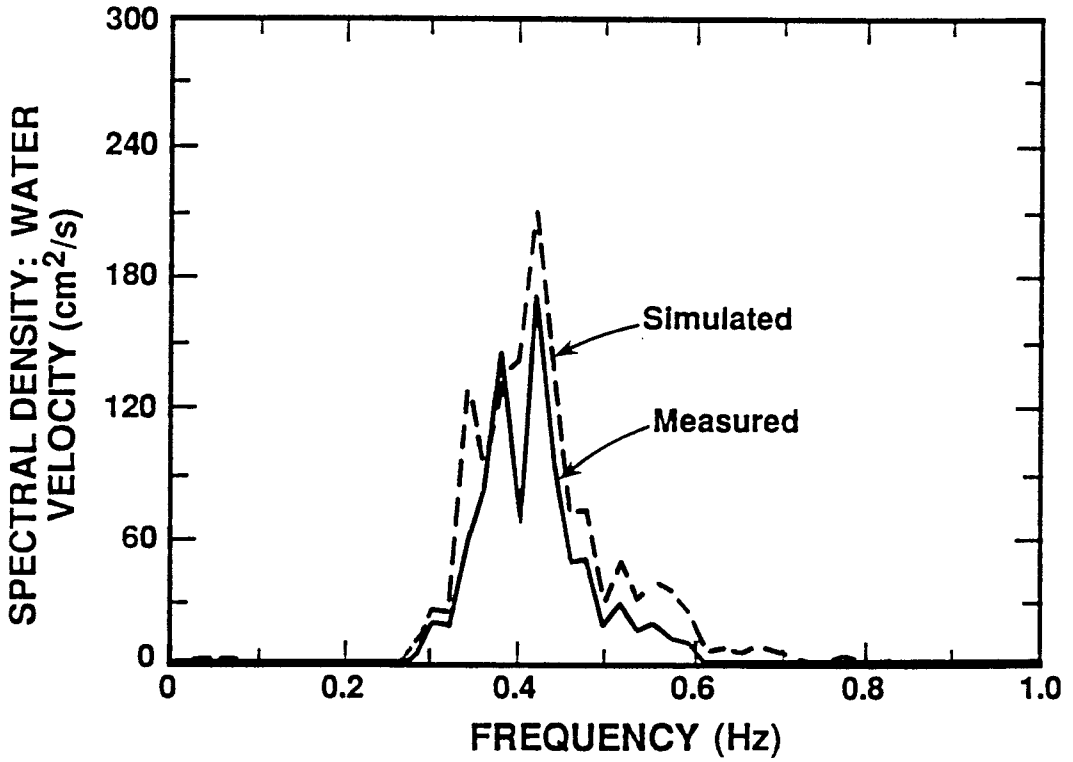

Fig. 17a. Model calculated and measured water velocity spectra at 1 hr, test 1.

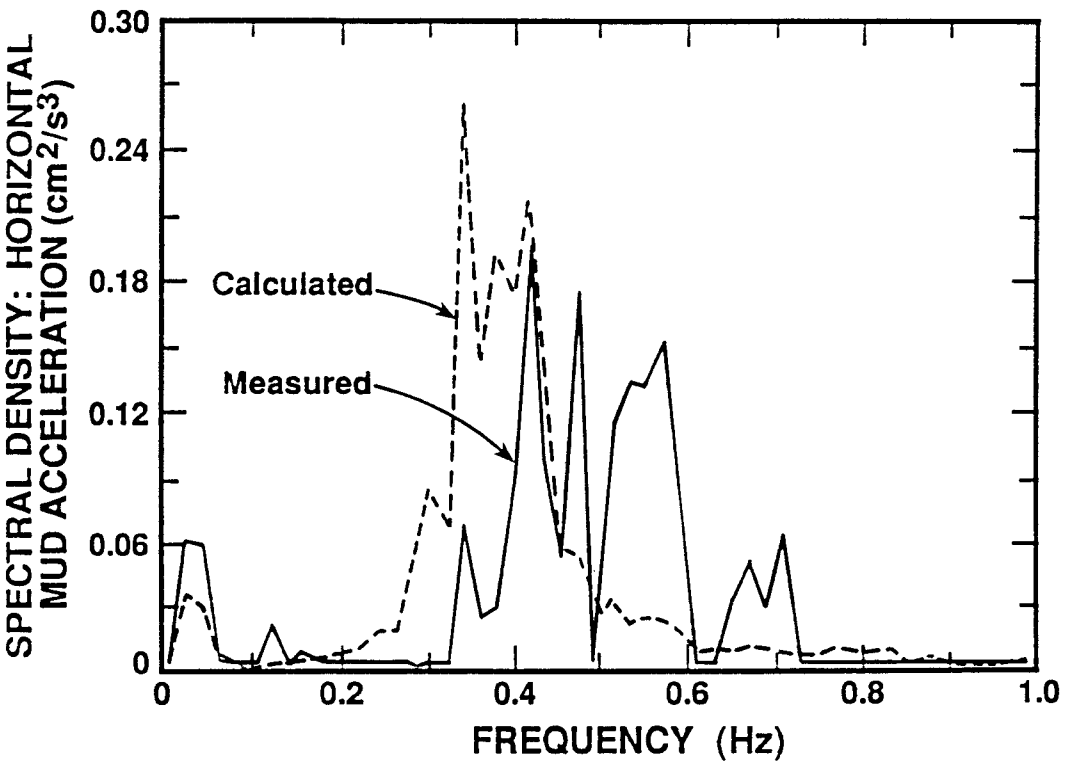

Fig. 17b. Model calculated and measured mud acceleration spectra at 1 hr, test 1.

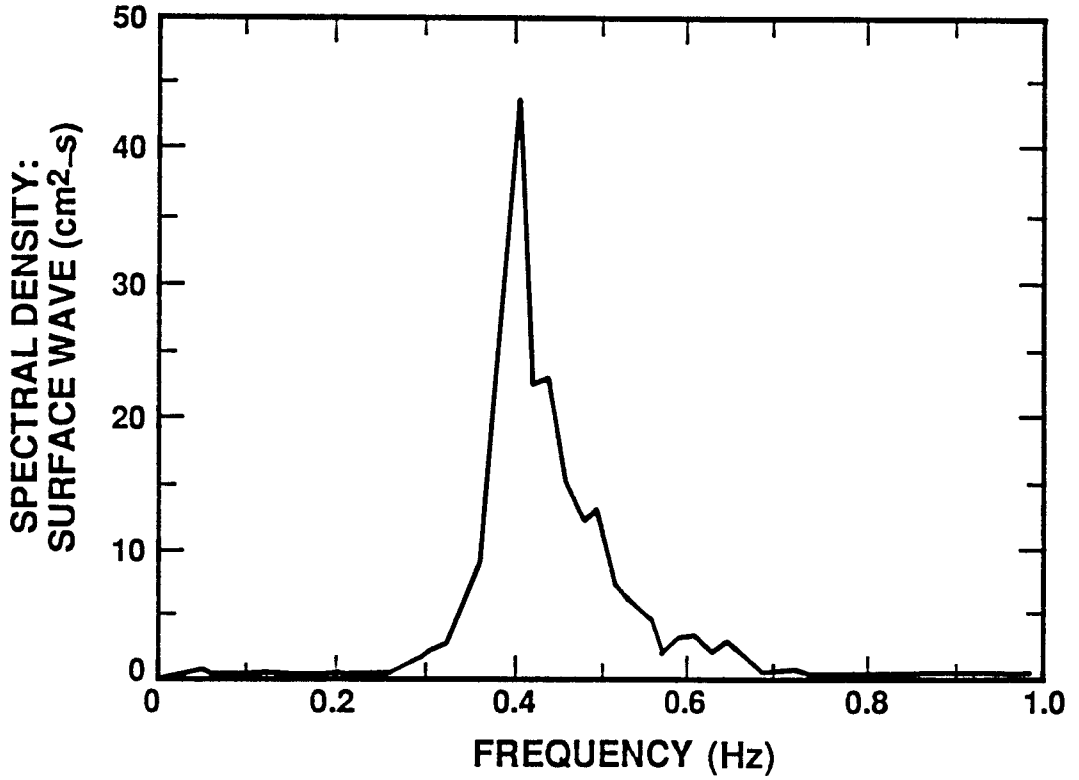

Fig. 18a. Wave energy density spectrum at 5 hr, test 1.

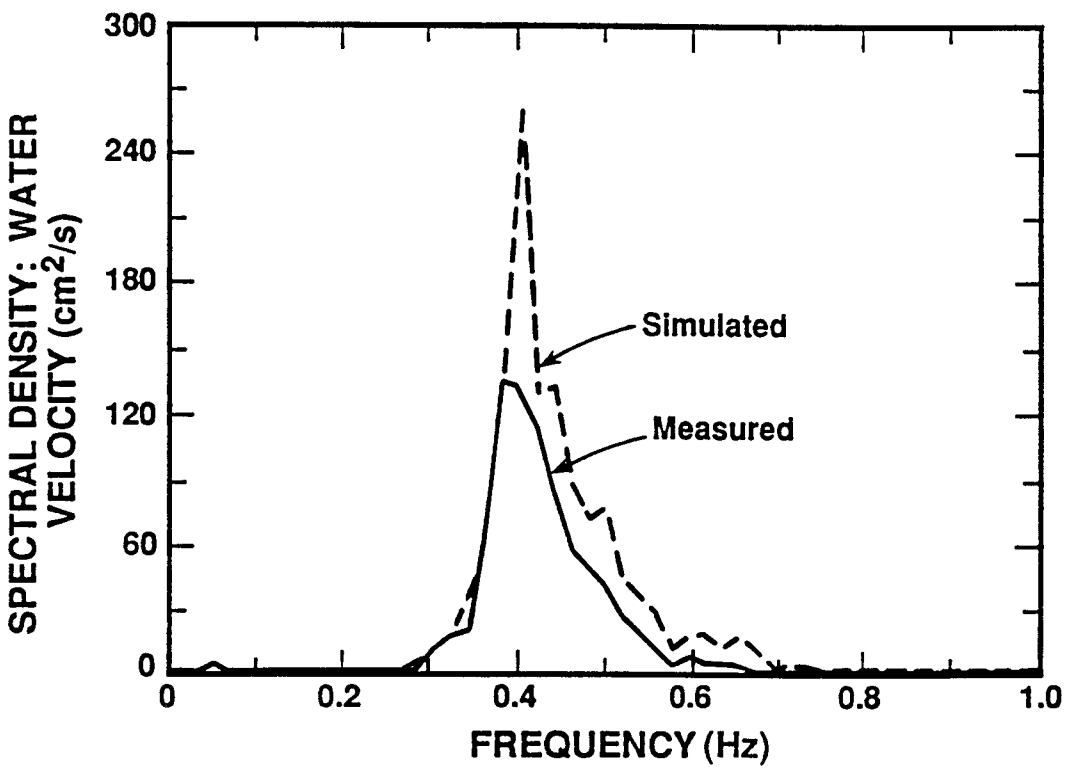

Fig. 18b. Model calculated and measured water velocity spectra at 5 hr, test 1.

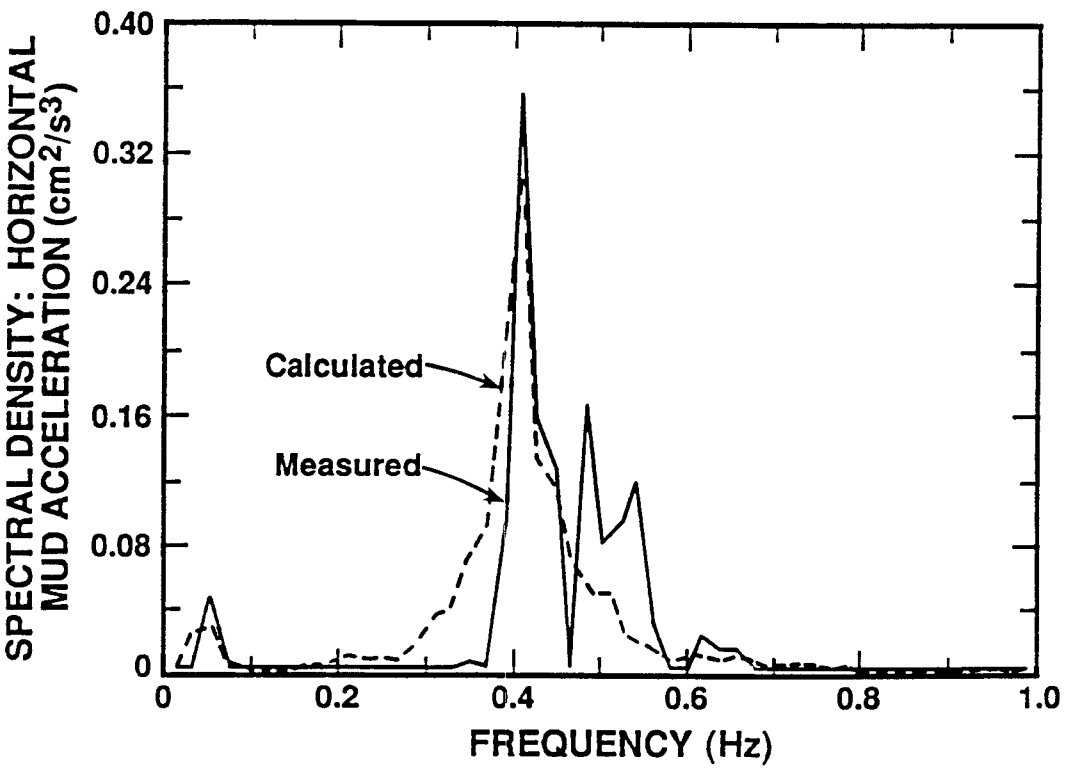

Fig. 18c. Model calculated and measured horizontal mud acceleration spectra at 5 hr, test 1.

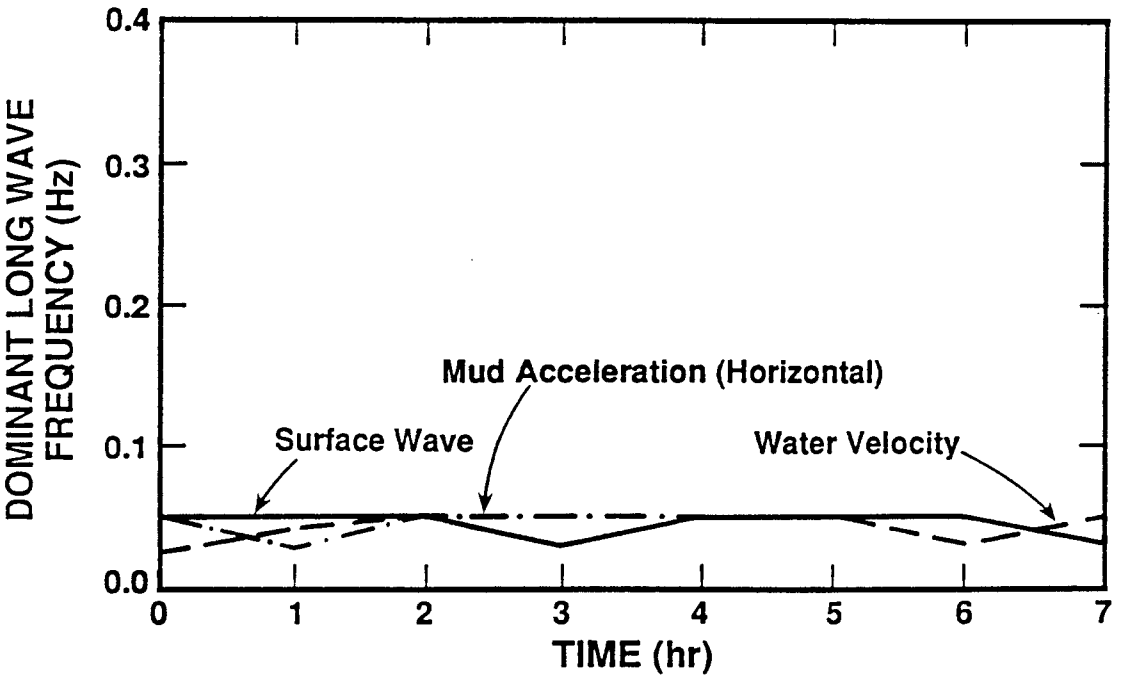

Fig. 19. Dominant long wave frequency variation during test 1.

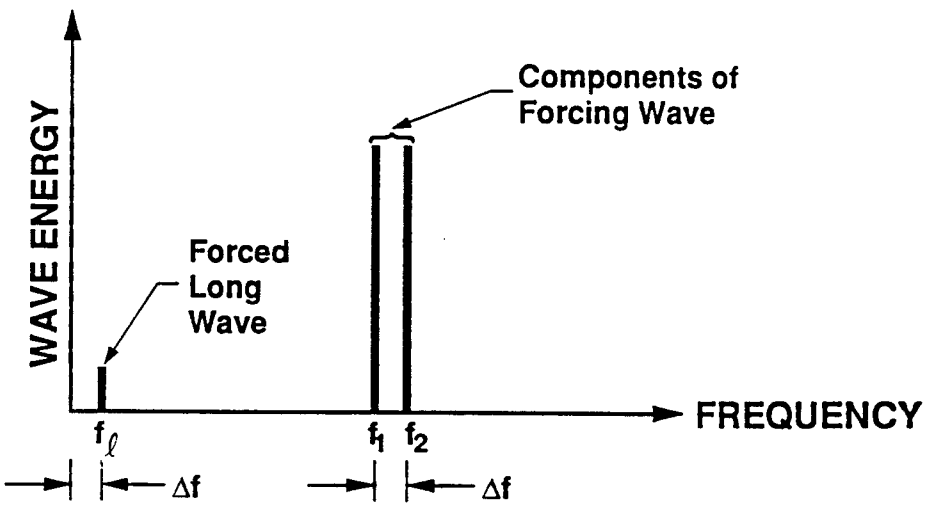

Fig. 20. Wave energy spectrum showing short period forcing at two frequencies and forced long wave.

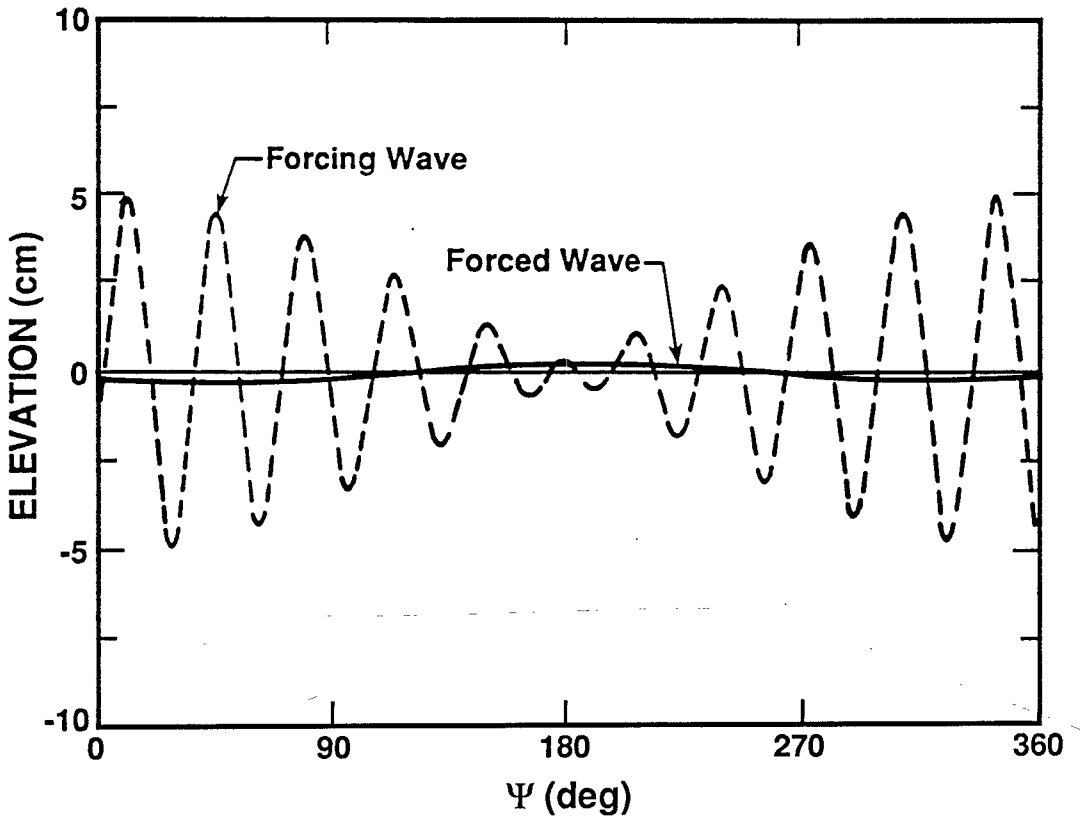

Fig. 21. Short period forcing wave and forced long wave derived from water level measurement at 1 hr, test 1.

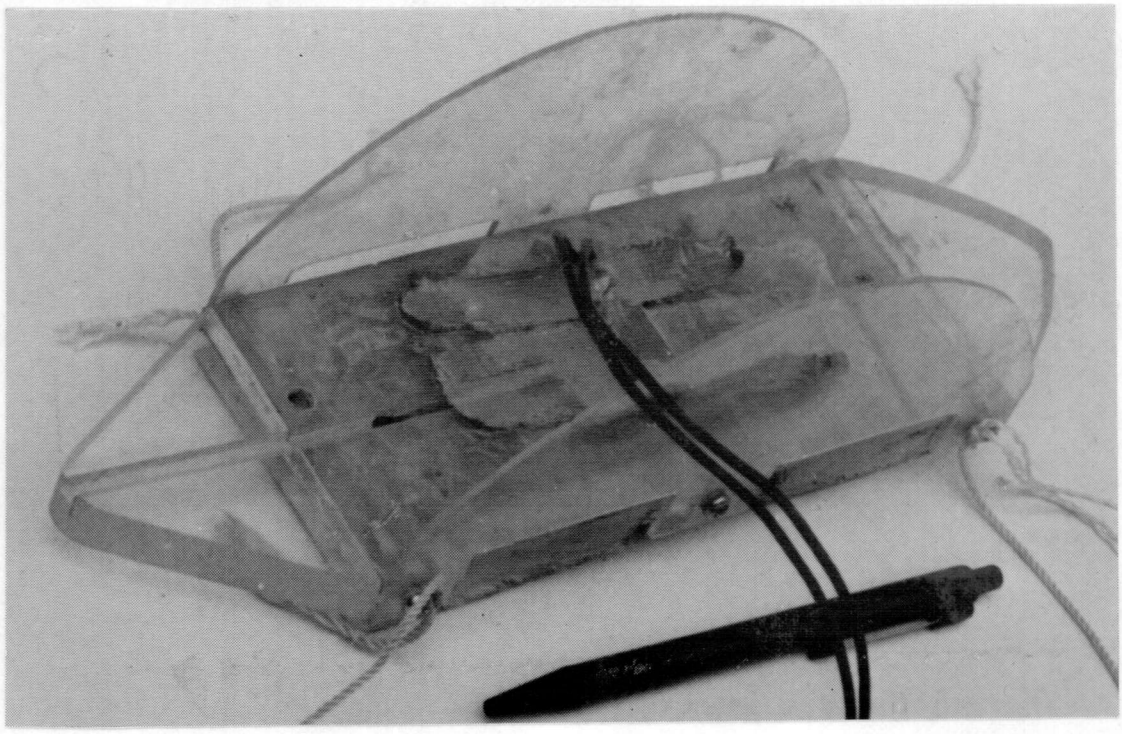

Fig. B.1 A view of the plexiglass "boat" together with the accelerometer (not visible). The boat length is 26 cm. Pen is for length reference only.

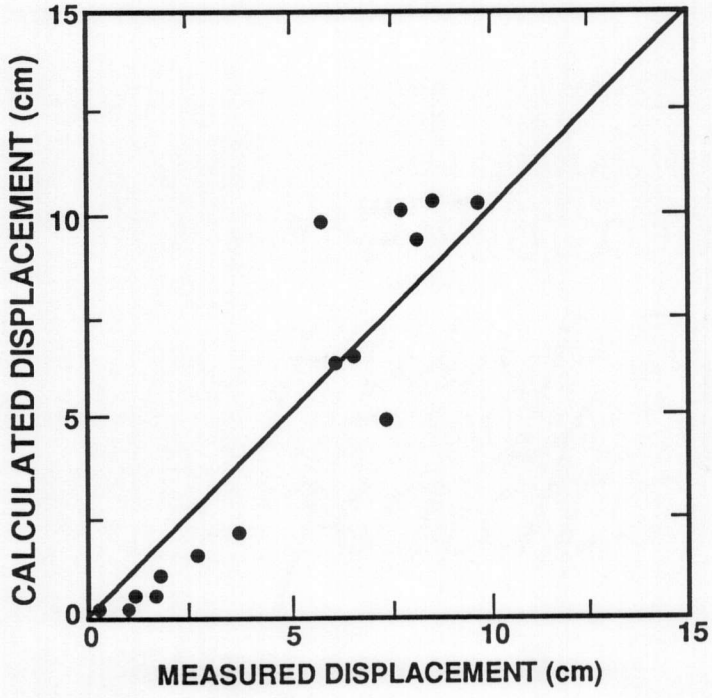

Fig. B.2 Scale measured versus calculated (from acceleration) wave orbtibal displacements (amplitudes) based on dynamic testing of accelerometer.

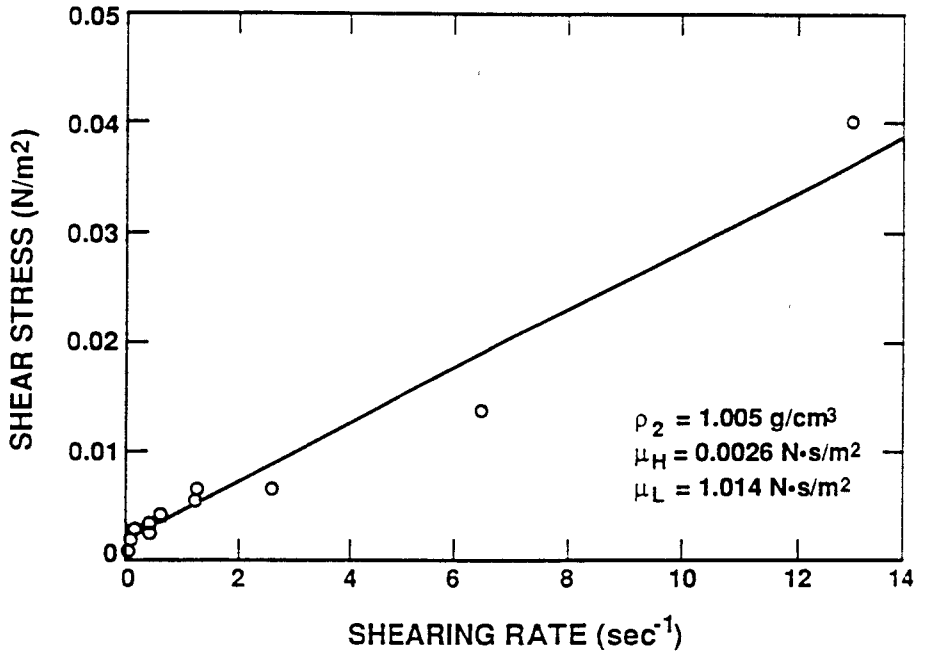

Fig. C.1 Relationship between applied stress and rate of shearing for Okeechobee mud; data for a mud density of 1.005 g/cm^3.

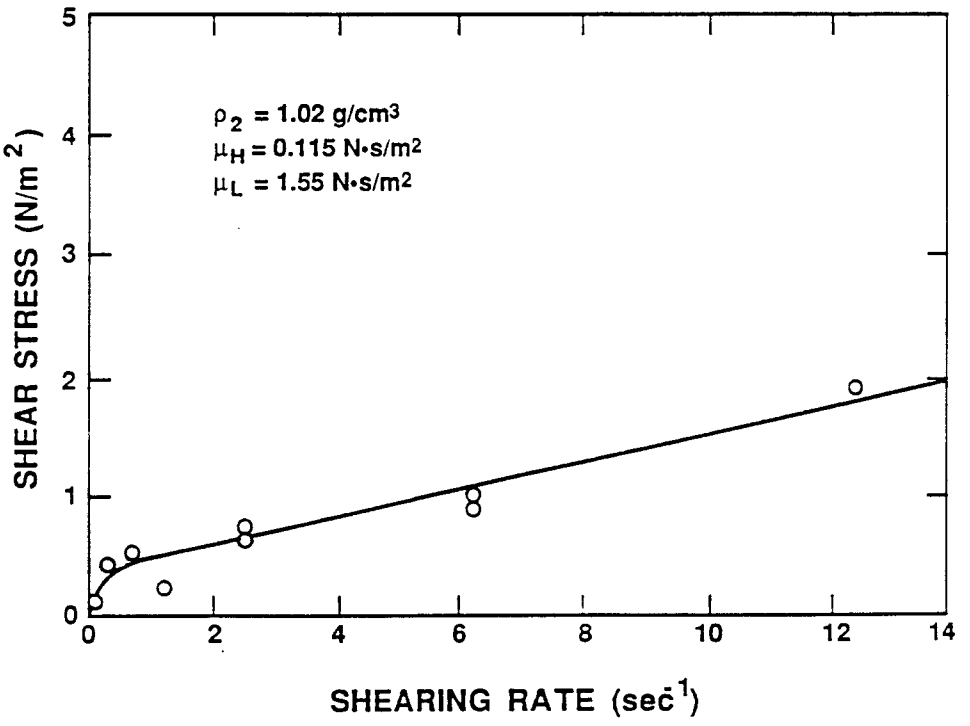

Fig. C.2 Relationship between applied stress and rate of shearing for Okeechobee mud; data for a mud density of 1.02 g/cm^3.

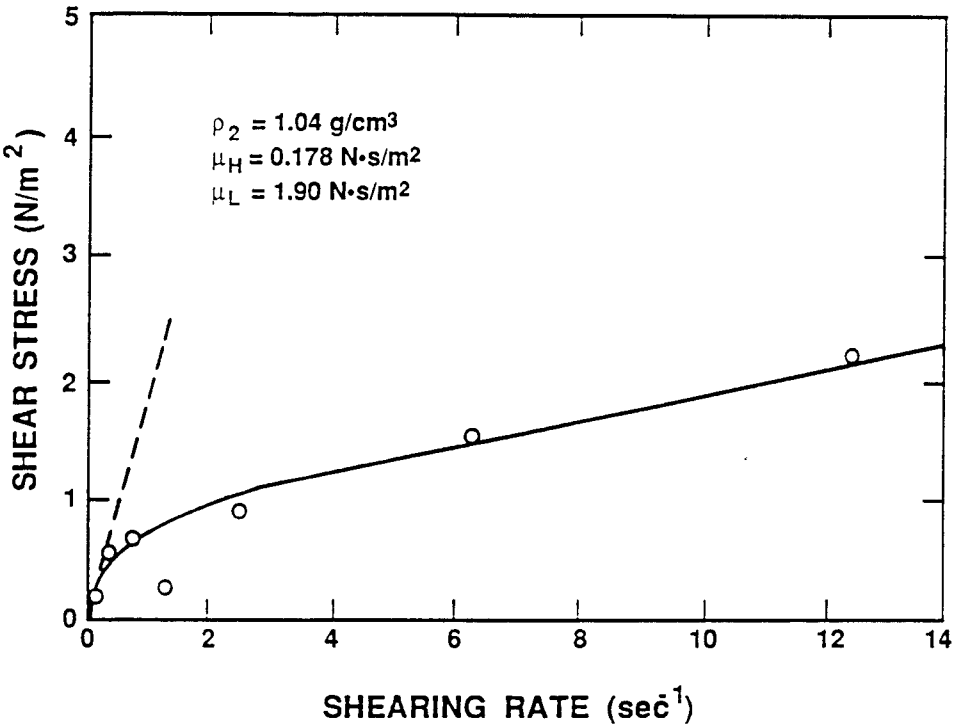

Fig. C.3 Relationship between applied stress and rate of shearing for Okeechobee mud; data for a mud density of 1.04 g/cm^3.

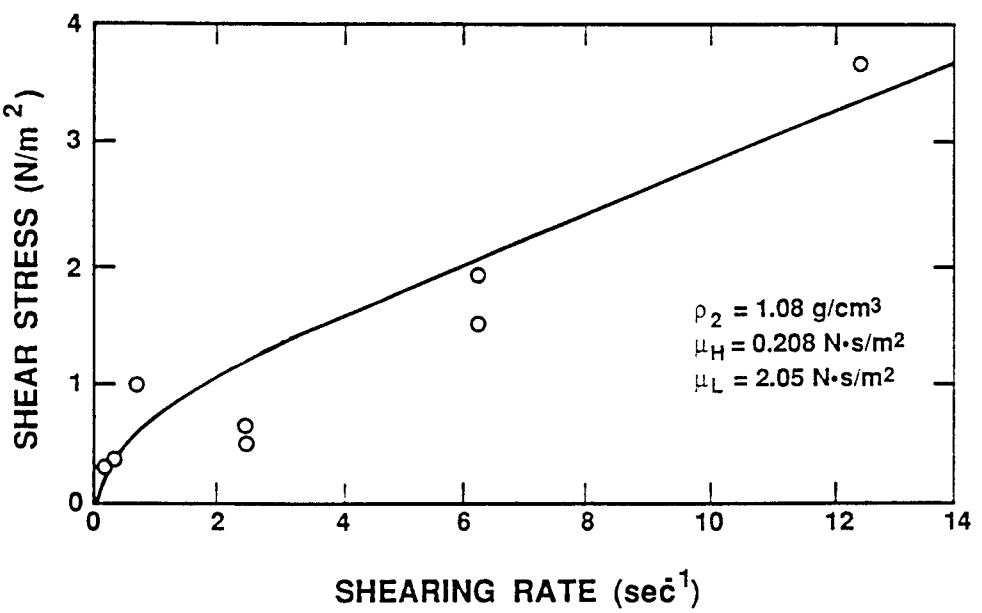

Fig. C.4 Relationship between applied stress and rate of shearing for Okeechobee mud; data for a mud density of 1.08 g/cm^3.

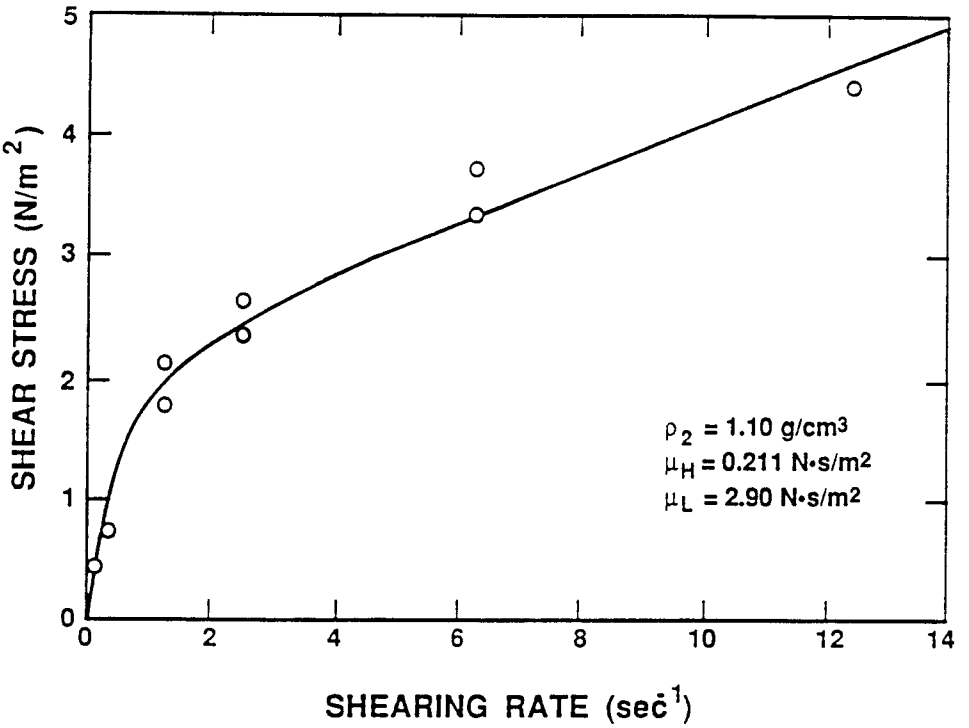

Fig. C.5 Relationship between applied stress and rate of shearing for Okeechobee mud; data for a mud density of 1.1 g/cm^3.

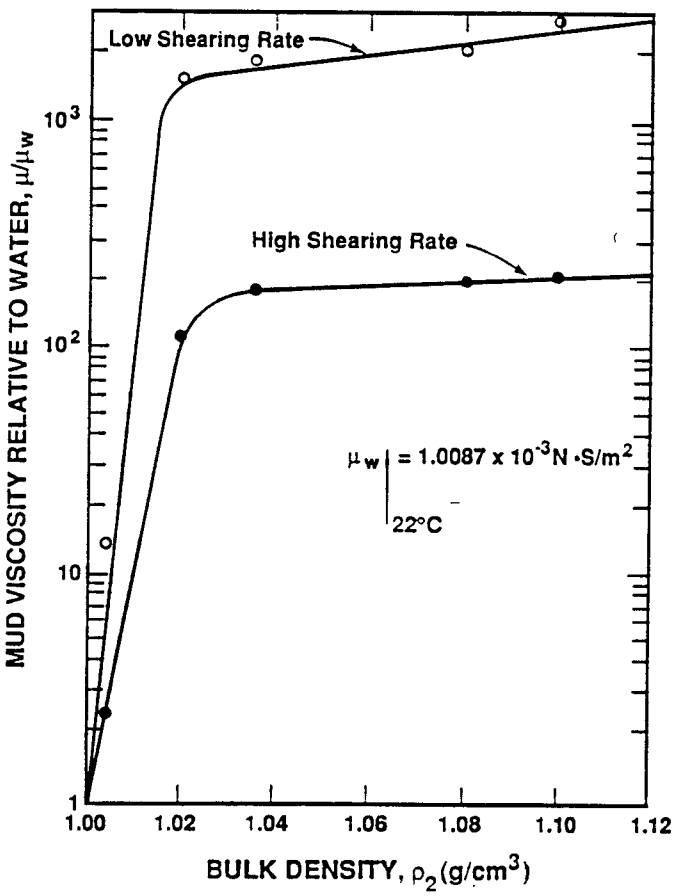

Fig. C.6 Relationship between mud viscosity (relative to water) and density at "high" and "low" rates of shearing.

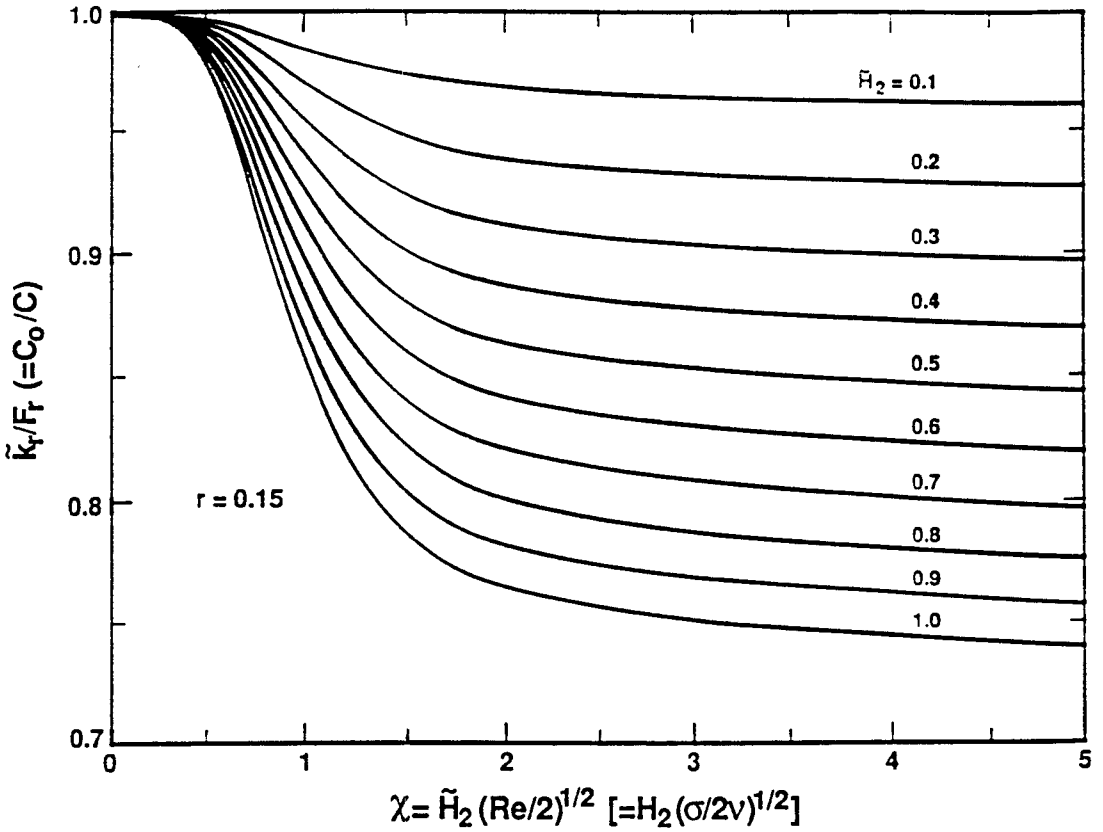

Fig. D.1 Dispersion relationship based on the inviscid-viscid model.

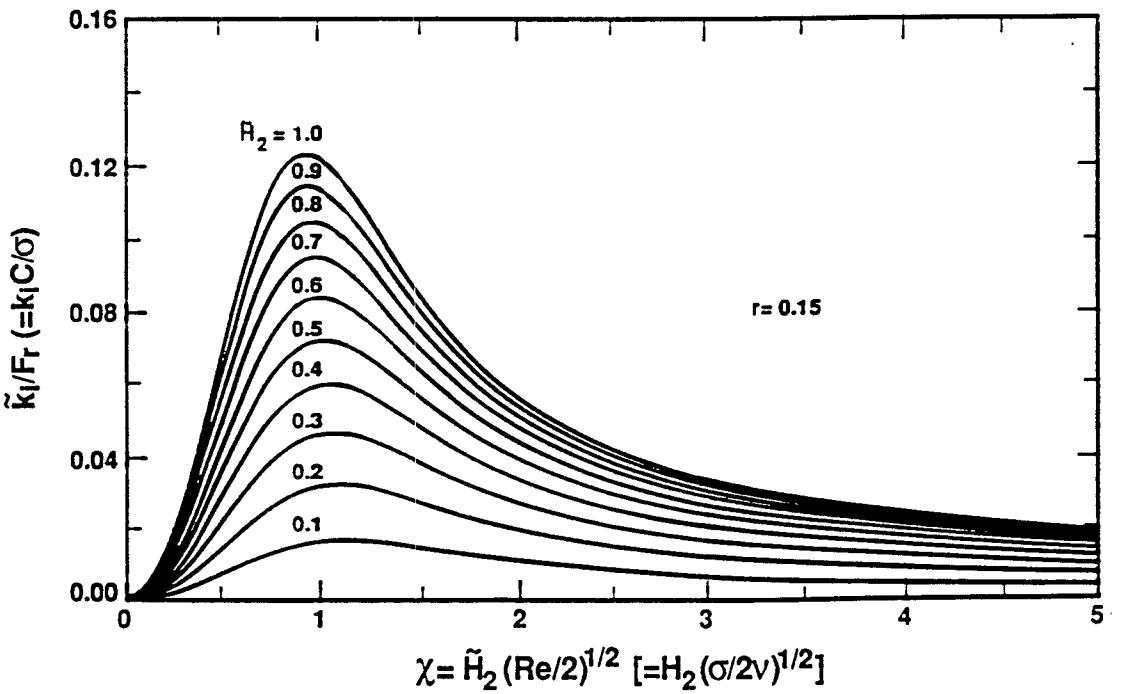

Fig. D.2 Wave attenuation relationship based on the inviscid-viscid model.

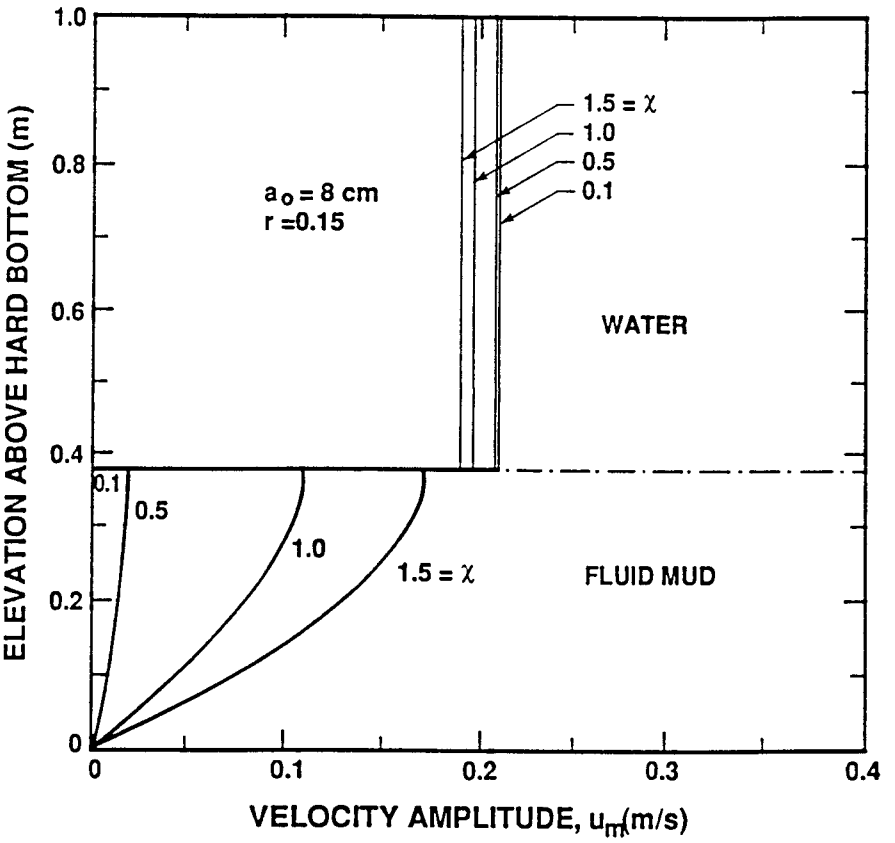

Fig. D.3 Simulated profiles of velocity amplitude, u_m for different values of χ using parameters from test 1.

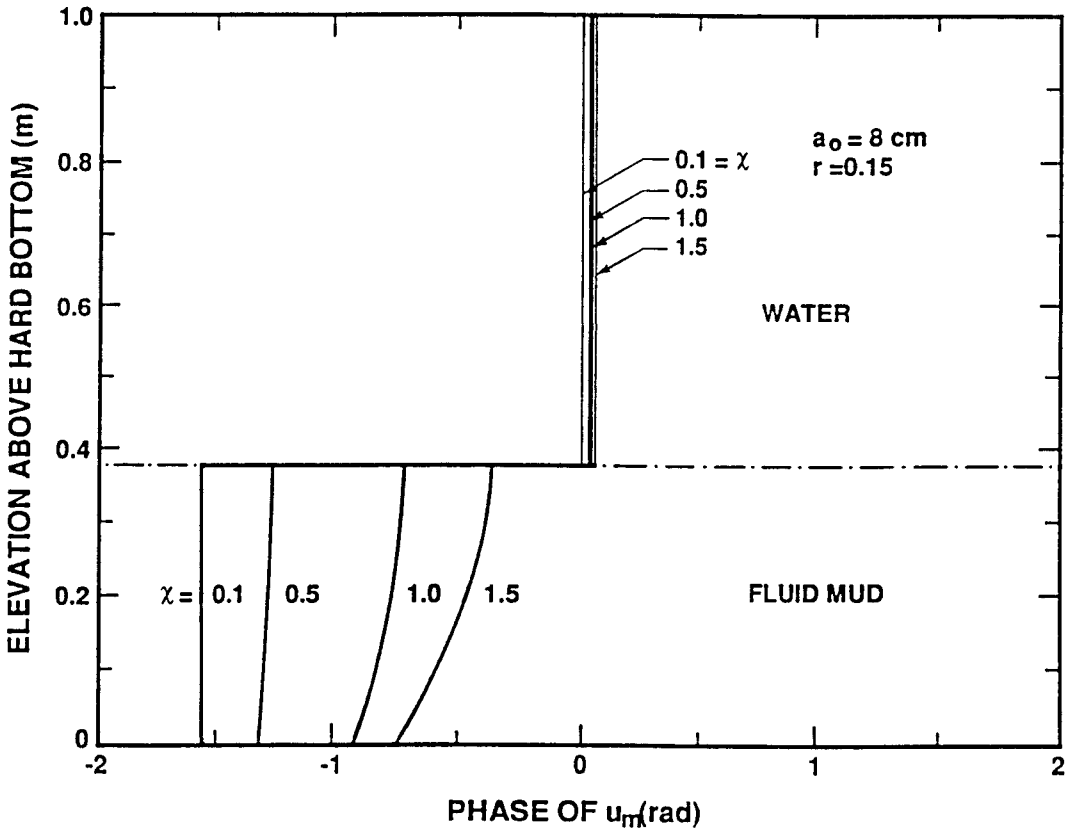

Fig. D.4 Simulated profiles of the phase of u_m corresponding to Fig. D.3

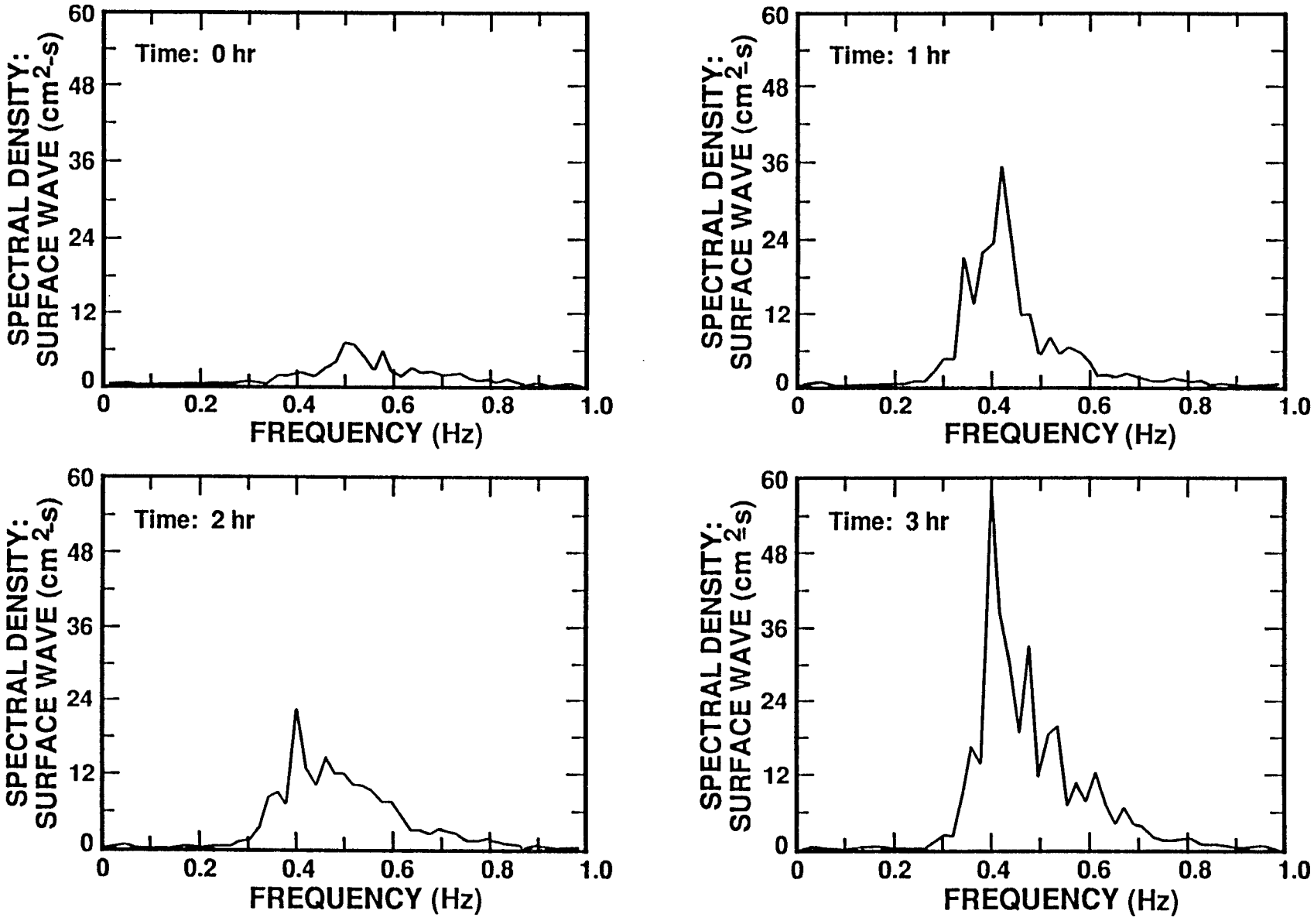

Fig. E.1 Wave energy spectra, test 1, 0-3 hrs.

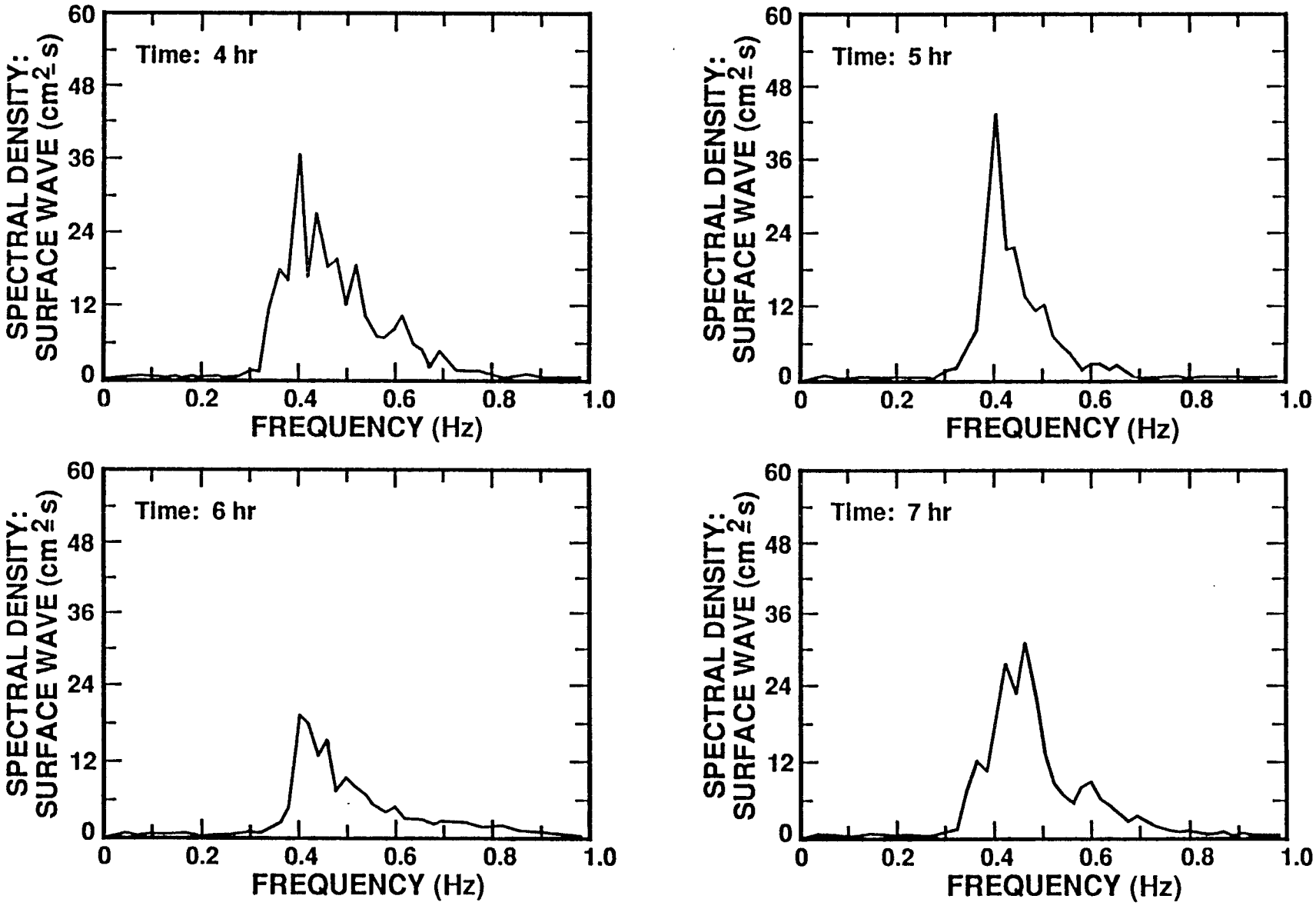

Fig. E.2 Wave energy spectra, test 1, 4-7 hrs.

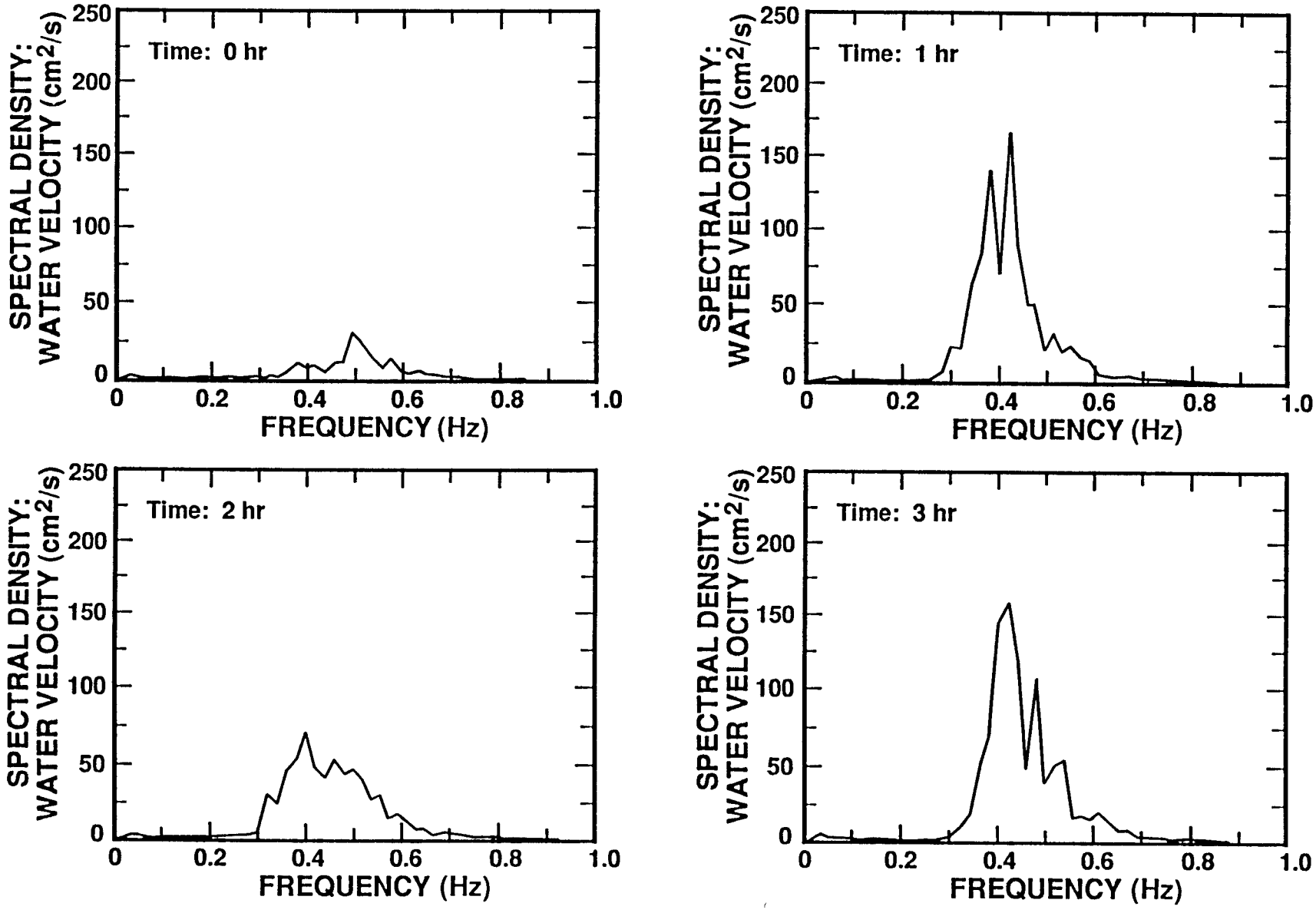

Fig. E.3 Water velocity spectra, test 1, 0-3 hrs.

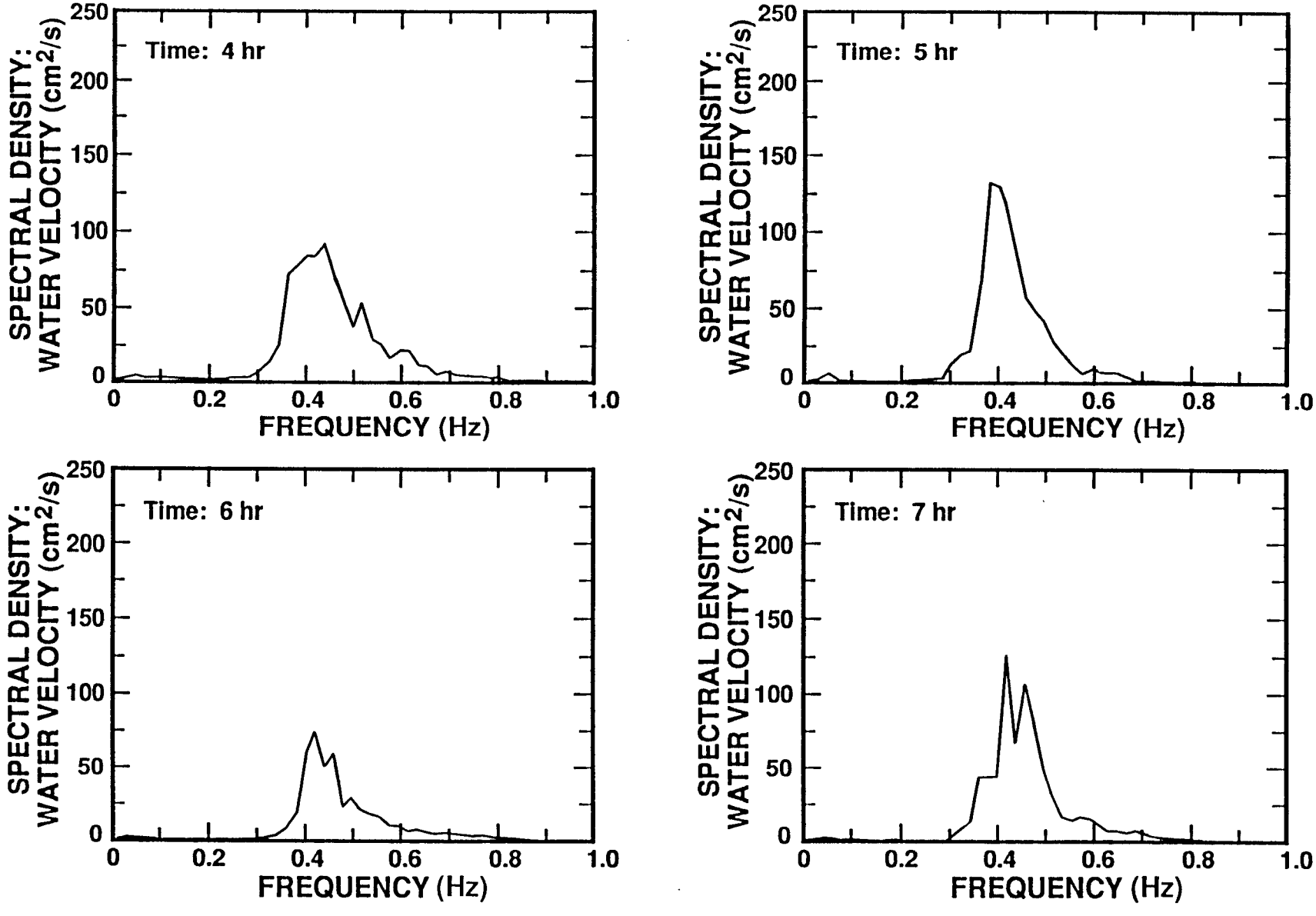

Fig. E.4 Water velocity spectra, test 1, 4-7 hrs.

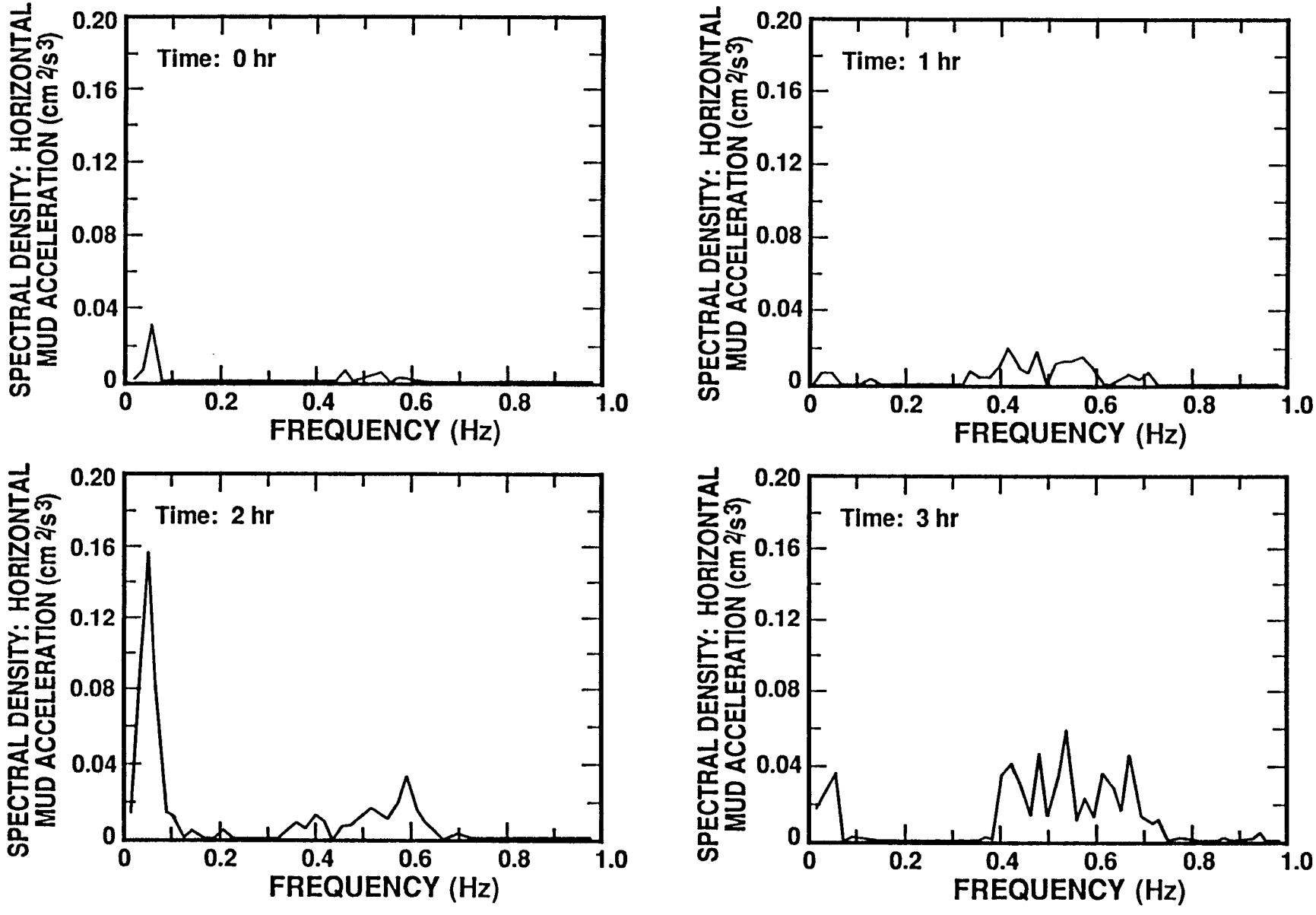

Fig. E.5 Mud acceleration spectra, test 1, 0-3 hrs.

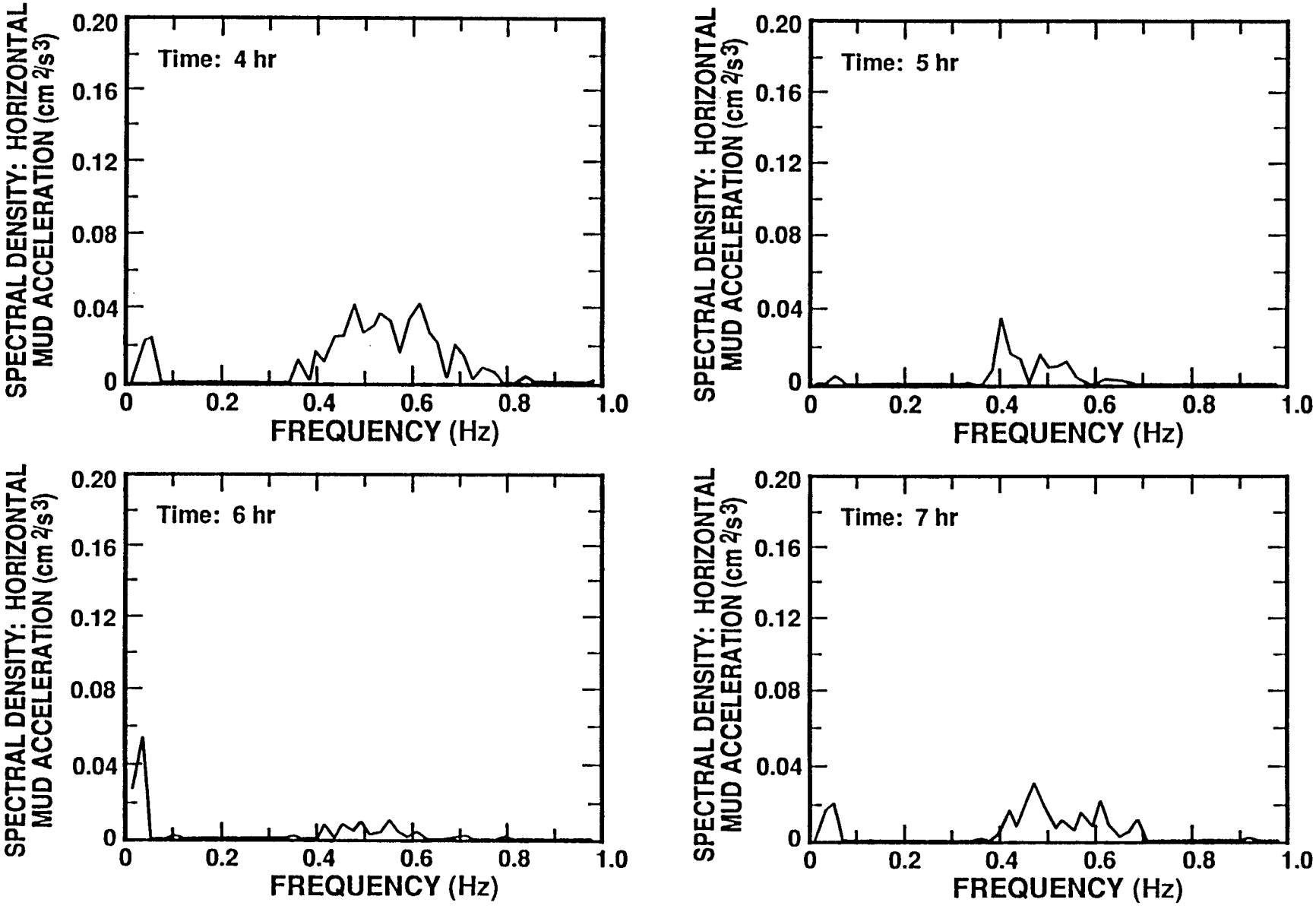

Fig. E.6 Mud acceleration spectra, test 1, 4-7 hrs.

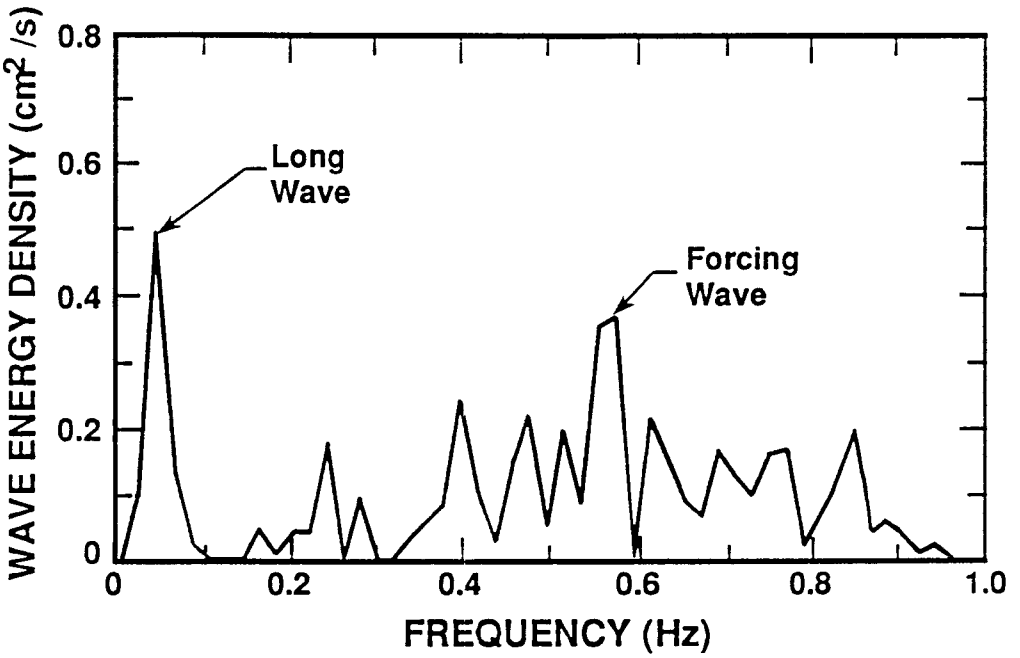

Fig. E.7 Wave energy spectrum at 1800 hr, test 2.

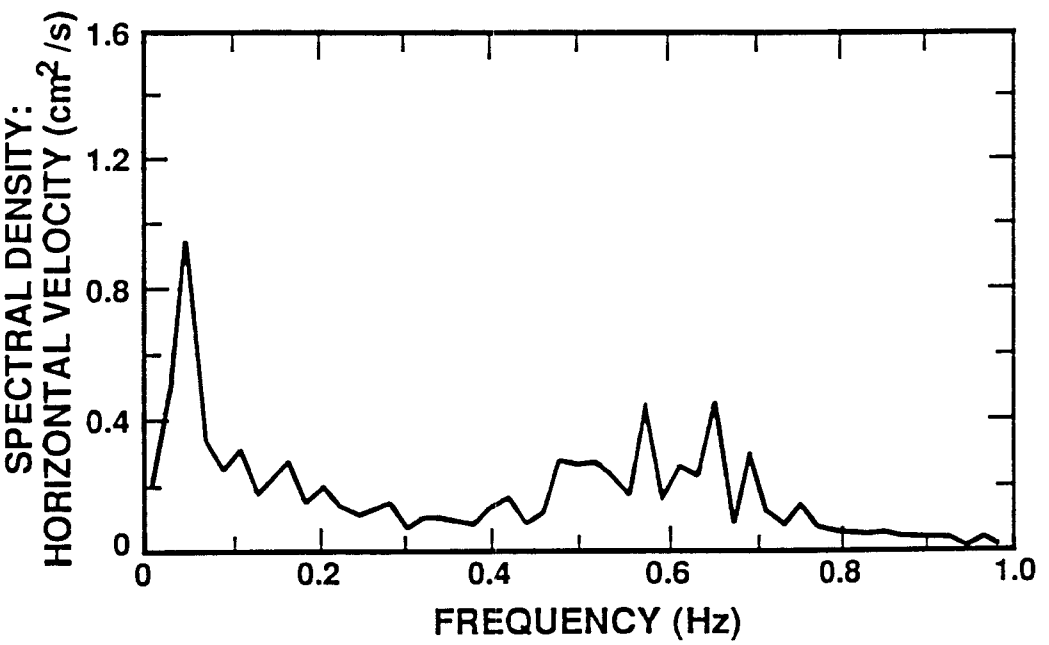

Fig. E.8 Horizontal velocity spectrum at 1800 hr, test 2.

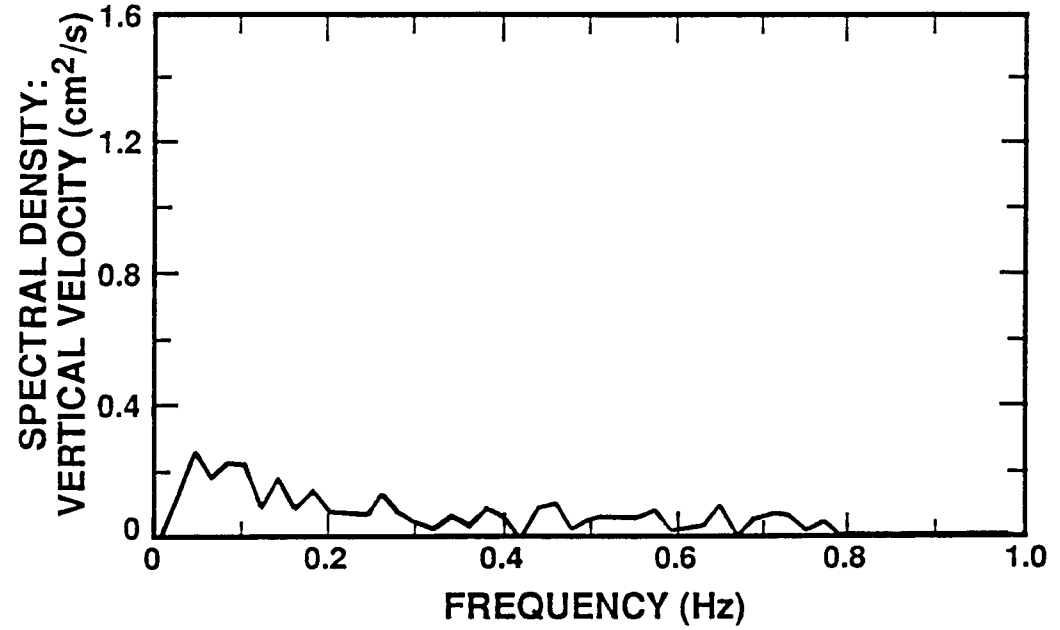

Fig. E.9 Vertical velocity spectrum at 1800 hr, test 2.

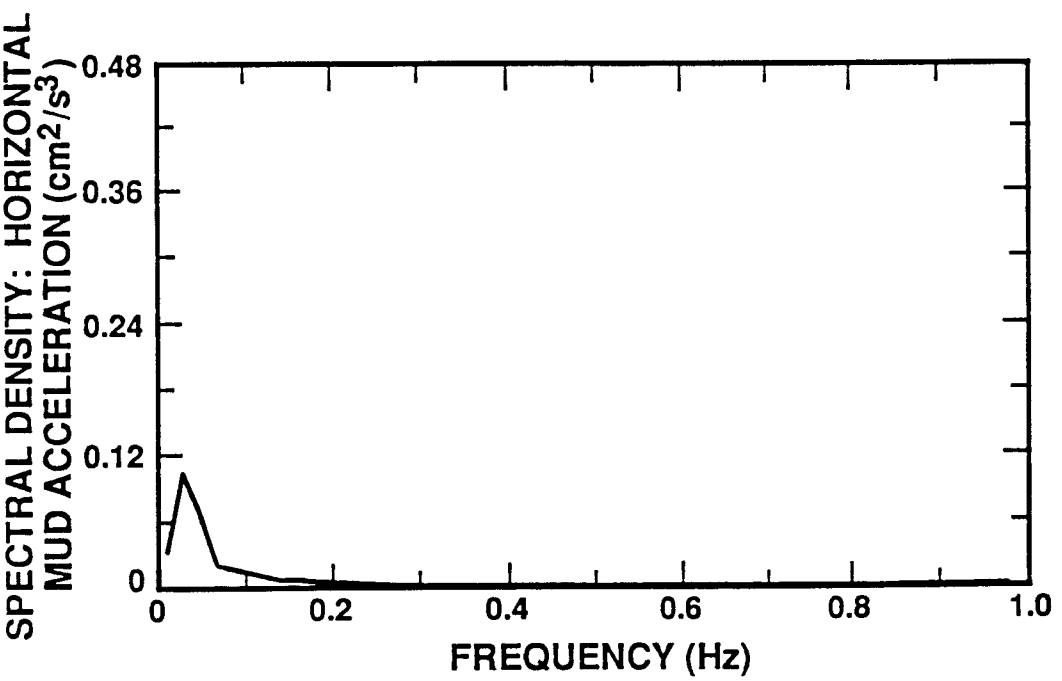

Fig. E.10 Horizontal acceleration spectrum at 1800 hr, test 2.

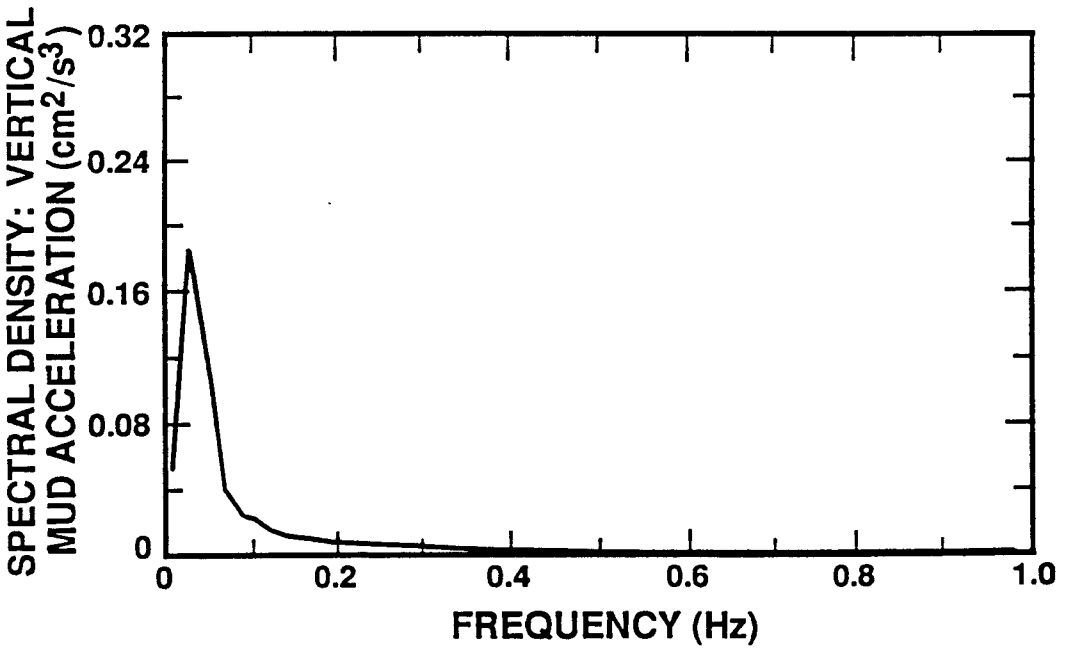

Fig. E.11 Vertical acceleration spectrum at 1800 hr, test 2.